VOLUME 110 NUMBER 1

THE ASTROPHYSICAL JOURNAL

AN INTERNATIONAL REVIEW OF SPECTROSCOPY AND ASTRONOMICAL PHYSICS

JULY 1949

THE UNIVERSITY OF CHICAGO PRESS
CHICAGO, ILLINOIS, U.S.A.

July 1949 Vol. 110, No. 1

THE ASTROPHYSICAL JOURNAL

AN INTERNATIONAL REVIEW OF SPECTROSCOPY AND ASTRONOMICAL PHYSICS

The Astrophysical Journal is published bimonthly by the University of Chicago at the University of Chicago Press, 5750 Ellis Avenue, Chicago, Illinois, during July, September, November, January, March, and May. ¶The subscription price is $12.00 a year; the price of single copies is $3.00. Orders for service of less than a full year will be charged at the single-copy rate. ¶Postage is prepaid by the publishers on all orders from the United States and its possessions, Argentina, Bolivia, Brazil, Chile, Colombia, Costa Rica, Cuba, Dominican Republic, Ecuador, Guatemala, Haiti, Republic of Honduras, Mexico, Morocco (Spanish Zone), Nicaragua, Panama, Paraguay, Peru, Rio de Oro, El Salvador, Spain (including Balearic Islands, Canary Islands, and the Spanish Offices in Northern Africa; Andorra), Spanish Guinea, Uruguay, and Venezuela. ¶Postage is charged extra as follows: for Canada and Newfoundland, 42 cents on annual subscriptions (total $12.42); on single copies, 7 cents (total $3.07); for all other countries in the Postal Union, 96 cents on annual subscriptions (total $12.96), on single copies 16 cents (total $3.16). ¶Patrons are requested to make all remittances payable to The University of Chicago Press, in United States currency or its equivalent by postal or express money orders or bank drafts.

The following is an authorized agent:

For the British Empire, except North America and Australasia: The Cambridge University Press, Bentley House, 200 Euston Road, London, N.W. 1, England. Prices of yearly subscriptions and of single copies may be had on application.

Claims for missing numbers should be made within the month following the regular month of publication. The publishers expect to supply missing numbers free only when losses have been sustained in transit, and when the reserve stock will permit.

Business correspondence should be addressed to The University of Chicago Press, Chicago 37, Illinois.

Communications for the editors and manuscripts should be addressed to: W. W. Morgan, Editor of The Astrophysical Journal, Yerkes Observatory, Williams Bay, Wisconsin.

Line drawings and photographs should be made by the author, and all marginal notes such as co-ordinates, wave lengths, etc., should be included in the cuts. It will not be possible to set up such material in type.

One copy of the corrected galley proof should be returned as soon as possible to the editor, Yerkes Observatory, Williams Bay, Wisconsin. Authors should take notice that the manuscript will not be sent to them with the proof.

The cable address is "Observatory, Williamsbay, Wisconsin."

The articles in this journal are indexed in the *International Index to Periodicals*, New York, N.Y.

Applications for permission to quote from this journal should be addressed to The University of Chicago Press, and will be freely granted.

Entered as second-class matter, July 31, 1940, at the Post-Office at Chicago, Ill., under the Act of March 3, 1879.

Acceptance for mailing at special rate of postage provided for in United States Postal Act of October 3, 1917, Section 1103, amended February 28, 1925.

[PRINTED IN U.S.A.]

THE ASTROPHYSICAL JOURNAL

AN INTERNATIONAL REVIEW OF SPECTROSCOPY AND ASTRONOMICAL PHYSICS

VOLUME 110 — JULY 1949 — NUMBER 1

TRANSFER OF RADIATION

Donald H. Menzel and Hari K. Sen

Harvard College Observatory

Received April 15, 1949

ABSTRACT

We have given below an operational method for solving the equation of radiative transfer in a "gray" plane-parallel atmosphere. We have assumed an expansion for the *Ergiebigkeit*, $B(\tau)$, of the form:

$$B(\tau) = a + b\tau + \sum_{0}^{\infty} A_j K_{j+2}(\tau) ,$$

where $K_n(\tau)$ is the exponential integral of the nth order, defined by

$$K_n(\tau) = \int_1^{\infty} \frac{e^{-x\tau}}{x^n} dx .$$

The coefficients, A_j, to any required degree of approximation, can be evaluated from a system of linear equations. We have obtained solutions according to various independent assumptions and find the operational method to be at once simple and capable of a high degree of accuracy. For instance, with four terms in the expansion above, we have reached an accuracy of two parts in a million. A comparison with Hopf's exact solution shows that our method gives consistent accuracy both near the boundary and in the deeper layers of the atmosphere, a feature not reached by any extant approximate method, with the possible exception of the Ambarzumian-Chandrasekhar method of solution by functional equation. The latter method has, however, so far been applied only to the emergent intensity at the boundary of the star.

We believe that our operational method is capable of extension to more complicated radiative transfer problems, e.g., to the case of nongray atmospheres.

The equations describing the distribution of thermal neutrons in a pile are identical with those that treat the intensity of radiation in a star. As a result of the rekindled interest in the problem, several new methods of attack have become available. The procedure given herewith has the double advantage of simplicity and high accuracy.

The basic equation of radiative transfer, for material stratified in planes, is

$$\mu \frac{\partial I}{\partial \tau} = I - B , \qquad (1)$$

where τ is the optical depth, μ the cosine of the angle between the ray and the outward normal, I the specific intensity, and B the emission function. I is a function of τ and μ;

B depends only on τ. For radiative equilibrium, the absorbed and emitted radiations must be equal, or

$$2\pi \int_{-1}^{1} I\, d\mu = 2\pi \int_{-1}^{1} B\, d\mu = 4\pi B\,. \tag{2}$$

From equations (1) and (2) and certain boundary conditions we are to determine both I and B. The chief boundary condition is that the intensity of the ingoing beam vanish for $\tau = 0$, at the outer surface of the slab. Introducing the symbolic operator

$$D = \frac{\partial}{\partial \tau}\,, \tag{3}$$

we obtain the symbolic linear equation,

$$(1 - \mu D)\, I = B\,, \tag{4}$$

whose symbolic solution, by the ordinary methods of differential equations, is

$$I = A\, e^{\tau/\mu} + \frac{1}{1 - \mu D} B\,. \tag{5}$$

The first term on the right represents the general solution and the second the particular solution.

The constant of integration, A, differs for the outgoing and ingoing beams. Denote the former by I^+ and the latter by I^-. At some very deep level, $\tau = \tau_1$, let $I = I_1^+$. Then

$$A^+ = \left[I^+ - \frac{1}{1 - \mu D} B \right]_{\tau=\tau_1} e^{-\tau_1/\mu}\,. \tag{6}$$

Similarly, for the ingoing beam, $I \equiv 0$ for $\tau = 0$, or

$$A^- = -\left[\frac{1}{1 - \mu D} B \right]_{\tau=0}. \tag{7}$$

Now, unless I^+ or B increases exponentially with τ, a condition that is unacceptable, we must have $A^+ \to 0$ as $\tau_1 \to \infty$, for a slab of infinite thickness. Thus we get for our two equations:

$$\begin{aligned} 0 \le \mu \le 1\,, \qquad & I^+ = \frac{1}{1 - \mu D} B\,, \\ -1 \le \mu \le 0\,, \qquad & I^- = \frac{1}{1 - \mu D} B - e^{\tau/\mu} \left[\frac{1}{1 - \mu D} B \right]_{\tau=0}. \end{aligned} \tag{8}$$

Substitute these equations in equation (2). Then:

$$\int_0^1 I^+ d\mu + \int_{-1}^0 I^- d\mu = \int_{-1}^1 B\, d\mu = 2 \int_0^1 B\, d\mu\,. \tag{9}$$

In the second integral on the left-hand side let us replace μ by $-\mu$. Then we obtain

$$\int_0^1 \left[2 - \frac{1}{1 - \mu D} - \frac{1}{1 + \mu D} \right] B\, d\mu = -\int_0^1 e^{-\tau/\mu} \left[\frac{1}{1 + \mu D} B \right]_{\tau=0} d\mu \tag{10}$$

or

$$\int_0^1 \frac{\mu^2 D^2}{1 - \mu^2 D^2} B\, d\mu = \frac{1}{2} \int_0^1 e^{-\tau/\mu} \left[\frac{1}{1 + \mu D} B \right]_{\tau=0} d\mu\,, \tag{11}$$

a symbolic integrodifferential equation for B. The quantity in brackets is a function of μ alone. The definite integral on the right is, therefore, a function only of τ, which we in-

dicate as $f(\tau)$. The operator integral on the left is a function only of D. Hence equation (11) is really in the familiar symbolic form:

$$F(D)B = f(\tau)\,. \tag{12}$$

We obtain our general solution by setting $f(\tau) = 0$ and trying

$$B = e^{m\tau}\,. \tag{13}$$

Since

$$F(D) = e^{m\tau} = e^{m\tau}F(m)\,, \tag{14}$$

$$F(m) = \int_0^1 \frac{\mu^2 m^2}{1-\mu^2 m^2}\,d\mu = -1 + \frac{1}{2m}\,ln\left|\frac{1+m}{1-m}\right| = -1 + \frac{1}{m}\tanh^{-1} m = 0\,. \tag{15}$$

The equation,

$$\tanh m = m\,, \tag{16}$$

has only two roots that will satisfy condition (15). There is an infinite number of conjugate imaginary roots, but these would correspond to values of θ greater than π and hence can be disregarded.

The two significant roots are coincident at $m = 0$. Hence the linear solution:

$$B = a + b\tau\,, \tag{17}$$

to which we must add the particular solution,

$$T = \frac{1}{F(D)}\,f(\tau) = \frac{1}{F(D)}\,\frac{1}{2}\int_0^1 e^{-\tau/y}\left[\frac{1}{1+yD}\,B\right]_{\tau=0} dy\,. \tag{18}$$

We have changed the variable of integration from μ to y, in order to avoid confusion. The bracketed factor is a function of y, which we may call $\psi(y)$. Hence $F(D)$ operates only on the exponential. Thus, setting $m = -1/y$, in equation (15), we have

$$T = \frac{1}{2}\int_0^1 e^{-\tau/y}\,\frac{\psi(y)}{-1 + \frac{y}{2}\,ln\left|\frac{y+1}{y-1}\right|}\,dy\,. \tag{19}$$

In the present paper we shall not make any special use of the form of the denominator. After all, $\psi(y)$ depends in a peculiar way upon B, whose value we still do not know. The important conclusion is that we may write T in the form

$$T = \int_0^1 e^{-\tau/y}\phi(y)\,dy\,, \tag{20}$$

and let the undetermined function, ϕ, carry the burden. Set

$$B = a + b\tau + \int_0^1 e^{-\tau/y}\phi(y)\,dy \tag{21}$$

back in equation (10). Then

$$\int_0^1\int_0^1\left[-2 + \frac{y}{y+\mu} + \frac{y}{y-\mu}\right] e^{-\tau/y}\phi(y)\,dy\,d\mu - \int_0^1\int_0^1 \frac{y}{y-\mu}\,e^{-\tau/\mu}\phi(y)\,dy\,d\mu$$
$$-\int_0^1 e^{-\tau/\mu}(a - b\mu)\,d\mu = Q(0) = 0\,. \tag{22}$$

The left-hand side of this equation must vanish for all values of τ.

Before we attempt solution of these equations, let us set equation (21) back in our symbolic equations (8) for I. Then

$$I^{+} = a + b\tau + b\mu + \int_0^1 \frac{y}{y+\mu}\, e^{-\tau/y}\phi(y)\, dy\,, \tag{23}$$

$$\begin{aligned} I^{-} = a + b\tau - b\mu + \int_0^1 \frac{y}{y-\mu}\, e^{-\tau/y}\phi(y)\, dy \\ - e^{-\tau/\mu}\left[a - b\mu + \int_0^1 \frac{y}{y-\mu}\,\phi(y)\, dy\right]. \end{aligned} \tag{24}$$

In equation (24) we have changed μ to $-\mu$, so that $0 \le \mu \le 1$ for both equations. Now calculate the integral:

$$L(n) = \int_0^1 I^{+}\mu^n d\mu + \int_{-1}^0 I^{-}\mu^n d\mu\,, \tag{25}$$

or

$$L(n) = \int_0^1 [I^{+} + (-1)^n I^{-}]\,\mu^n d\mu\,. \tag{26}$$

The factor $(-1)^n$ enters because we changed the sign of μ for the negative beam. The result is

$$\begin{aligned} L(n) = \frac{a+b\tau}{n+1}[1+(-1)^n] + \frac{b}{n+2}[1+(-1)^{n+1}] \\ + \int_0^1\int_0^1\left[\frac{y}{y+\mu} + (-1)^n\frac{y}{y-\mu}\right] e^{-\tau/y}\mu^n\phi(y)\, dy\, d\mu \\ + (-1)^{n+1}\int_0^1 e^{-\tau/\mu}\left[a - b\mu + \int_0^1 \frac{y}{y-\mu}\,\phi(y)\, dy\right]\mu^n d\mu\,. \end{aligned} \tag{27}$$

By definition,

$$\begin{aligned} L(0) &= 2J = 2B\,, \\ L(1) &= \frac{\mathfrak{F}}{2} = \text{Constant}\,, \\ L(2) &= 2K\,, \end{aligned} \tag{28}$$

where J and K are the conventional parameters and $\pi\mathfrak{F}$ is the flux.

Break the first integral on the right-hand side into partial fractions, dividing the terms in μ^n by the respective denominators. The result is

$$\begin{aligned} L(n) = \frac{a+b\tau}{n+1}[1+(-1)^n] + \frac{b}{n+2}[1+(-1)^{n+1}] \\ + \int_0^1\int_0^1\Bigg[\sum_{l=1}^{n}\mu^{n-l}y^l(-1)^{l-1} \\ + (-1)^{n-1}\sum_1^n \mu^{n-l}y^l + 2y^n(-1)^n\Bigg] e^{-\tau/y}\phi(y)\, dy\, d\mu + Q(n)\,, \end{aligned} \tag{29}$$

where

$$\begin{aligned} Q(n) = (-1)^n\Bigg\{\int_0^1\int_0^1\left[-2 + \frac{y}{y+\mu} + \frac{y}{y-\mu}\right] y^n e^{-\tau/y}\phi(y)\, dy\, d\mu \\ - \int_0^1\int_0^1 \frac{y}{y-\mu}\,\mu^n e^{-\tau/\mu}\phi(y)\, dy\, d\mu - \int_0^1 (a - b\mu)\, e^{-\tau/\mu}\mu^n d\mu\Bigg\}. \end{aligned} \tag{30}$$

With $n = 0$, this expression agrees with $Q(0)$, previously defined in equation (22). Because of the exponential term, $Q(n) \to 0$ as $\tau \to \infty$. Further, we can write

$$Q(n) = \frac{1}{(D)^n} Q(0)\,, \tag{31}$$

where D is the operator of equation (3). Thus

$$Q(1) = \int^{\tau} Q(0)\, d\tau = \text{Constant}\,. \tag{32}$$

But $Q(1)$ can vanish at infinity only if the constant itself is zero. Thus, proceeding step by step, we find, in general, that

$$Q(n) = 0\,. \tag{33}$$

For $L(1)$, the other integral vanishes identically, and we find that

$$b = \tfrac{3}{4} \mathfrak{F}\,, \tag{34}$$

which defines b in terms of $\mathfrak{F}$. We are to define a and $\phi(y)$ in terms of b, so as to satisfy for all τ and n. The exponential factor in equation (30) is troublesome, but we can avoid the difficulty by adopting a set of weighted mean values through the layers. Multiply equation (30) by $\tau^k d\tau$ and integrate from 0 to ∞. The resulting equations agree with that obtained from equation (30) when we set $\tau = 0$ and replace n by $n + k + 1$.

Thus, if we can determine $\phi(y)$ to satisfy the equation

$$\int_0^1 \int_0^1 \left\{\left[-2 + \frac{y}{y+\mu} + \frac{y}{y-\mu}\right] y^n - \left[\frac{y}{y-\mu}\right]\mu^n\right\} \phi(y)\, dy\, d\mu - \int_0^1 (a - b\mu)\,\mu^n d\mu = 0 \tag{35}$$

for all n, we shall have the correct solution.

Let us write equation (21) in the form

$$B = \tfrac{3}{4} \mathfrak{F}\, [\tau + q(\tau)]\,, \tag{36}$$

and redefine a and $\phi(y)$ with respect to a multiplicative constant, so that

$$q(\tau) = a + \int_0^1 e^{-\tau/y} \phi(y)\, dy\,. \tag{37}$$

As Hopf[1] has shown, $q(\tau)$ is a slowly varying function of τ.

$$q(\infty) = 0.71044609 = a\,, \tag{38}$$

$$q(0) = \frac{1}{\sqrt{3}} = 0.577350269\,. \tag{39}$$

These results will provide a check on our later solutions.

In accord with the convention of equation (37), we shall set $b = 1$ in equation (35) and carry out the integration with respect to μ. In the second bracket we divide μ^n by $(\mu - y)$. The fractional remainder just cancels the similar term in the first bracket, so that the apparent singularity at $y = \mu$ disappears completely. Thus:

$$\int_0^1 \left(-2y^n + y^{n+1} ln\, \frac{1+y}{y} + \sum_{k=1}^{n} \frac{y^{n-k+1}}{k}\right) \phi(y)\, dy - \frac{a}{n+1} + \frac{1}{n+2} = 0\,. \tag{40}$$

[1] *Mathematical Problems of Radiative Equilibrium* ("Cambridge Tracts in Mathematics and Mathematical Physics," No. 31 [Cambridge: At the University Press, 1934]).

This is as far as we can carry the analysis without some explicit assumption about the function $\phi(y)$. In the absence of other information, let us assume that $\phi(y)$, whatever its explicit form may be, can be expanded in the series:

$$\phi(y) = \sum_{0}^{\infty} A_j y^j . \tag{41}$$

Negative values of j are clearly excluded because they would cause equation (40) to be infinite, when $n = 0$. When we set this equation in equation (40), the various terms of the coefficient of A_j become:

$$-2\int_0^1 y^{n+j} dy = -\frac{2}{n+j+1} . \tag{42}$$

$$\int_0^1 y^{n+j+1} ln\,(1+y)\,dy$$

$$= \begin{cases} \dfrac{2ln2}{n+j+2} - \dfrac{1}{n+j+2}\displaystyle\sum_{1}^{n+j+2}\dfrac{(-1)^{k-1}}{k} & (n+j \text{ odd}) \\[2ex] \dfrac{1}{n+j+2}\displaystyle\sum_{1}^{n+j+2}\dfrac{(-1)^{k-1}}{k} & (n+j \text{ even}), \end{cases} \tag{43}$$

$$-\int_0^1 y^{n+j+1} ln\,y\,dy = \frac{1}{(n+j+2)^2}, \tag{44}$$

$$\sum_{k=1}^{n}\int_0^1 \frac{y^{n+j-k+1}}{k}\,dy = \sum_{1}^{n}\frac{1}{k\,(n+j-k+2)}$$

$$= \frac{1}{n+j+2}\sum_{1}^{n}\left[\frac{1}{k} + \frac{1}{n+j-k+2}\right] = \frac{1}{n+j+2}\sum_{1}^{n}\left[\frac{1}{k} + \frac{1}{j+1+k}\right] \tag{45}$$

$$= \frac{1}{n+j+2}\left[\sum_{1}^{n}\frac{1}{k} + \sum_{1}^{n+j+1}\frac{1}{k} - \sum_{1}^{j+1}\frac{1}{k}\right].$$

Write C_{nj} for the coefficient of A_j, so that

$$\sum_{j=0}^{\infty} C_{nj} A_j - \frac{a}{n+1} = -\frac{1}{n+2}. \tag{46}$$

Then

$$C_{nj} = \frac{2ln2 - \displaystyle\sum_{1}^{n+j+1}\frac{(-1)^{k-1}}{k} + \sum_{1}^{n+j+1}\frac{1}{k} - \sum_{1}^{j+1}\frac{1}{k} + \sum_{1}^{n}\frac{1}{k}}{n+j+2} - \frac{2}{n+j+1} \tag{47}$$

for $n+j$ odd, and

$$C_{nj} = \frac{\displaystyle\sum_{1}^{n+j+1}\frac{(-1)^{k-1}}{k} + \sum_{1}^{n}\frac{1}{k} + \sum_{1}^{n+j+1}\frac{1}{k} - \sum_{1}^{j+1}\frac{1}{k}}{n+j+2} - \frac{2}{n+j+1} \tag{48}$$

for $n+j$ even. Equations (46), one equation for each value of n, are linear in the A_j's. The C_{nj}'s are numerical quantities, simply calculated. Some of the values appear in Table 1.

As a first test of the efficacy of the procedure, the solution of four simultaneous equations with four unknowns gave the values of a, A_0, A_1, and A_2. This assumption amounts to breaking off the series after three terms. The last column of Table 1 was not used.

At this point, we introduce a slight change of notation. With $\phi(y)$ defined as in equation (41), we obtain

$$\begin{aligned} \int_0^1 e^{-\tau/y}\phi(y)\,dy &= \sum_0^\infty A_j \int_1^\infty \frac{e^{-z\tau}}{z^{j+2}}\,dz \\ &= \sum_0^\infty A_j K_{j+2}(\tau)\,. \end{aligned} \tag{49}$$

The quantity $K_n(\tau)$ is the exponential integral of the nth order, defined by

$$K_n(\tau) = \int_1^\infty \frac{e^{-x\tau}}{x^n}\,dx\,. \tag{50}$$

TABLE 1

VALUES OF C_{nj}

n	j			
	0	1	2	3
0	−1.500000000	−0.704568546	−0.458333333	−0.339407795
1	−0.204568546	− .125000000	− .089407794	− .069444444
2	+0.125000000	+ .077258872	+ .055555555	+ .043280149
3	+0.243925539	+0.166666667	+0.126613482	+0.102083333

The *Mathematical Tables* project, under the supervision of G. Placzek,[2] has prepared extensive tables of the functions $K_n(\tau)$, for $n = 0$ to $n = 20$, and for $\tau = 0$ to $\tau = 10$. Satisfactory asymptotic expansions exist for other ranges.

In the present study we break the series after a finite number of terms. Because of the fact that the behavior of $K_n(\tau)$ resembles that of $K_{n+1}(\tau)$, the last term of the series effectively represents the functional character of the neglected terms.

Table 2 summarizes the results of several solutions, obtained according to various independent assumptions. The solutions are expressed in the following form:

$$B(\tau) = \tfrac{3}{4}\mathfrak{F}\,[\tau + q(\tau)] = \tfrac{3}{4}\mathfrak{F}\left[\tau + a + \sum_0^j A_j K_{j+2}(\tau)\right]. \tag{51}$$

Although we made no attempt to fit the constants of Solution I, our series has reproduced the theoretical values $q(\infty)$ and $q(0)$, of equations (38) and (39), with an accuracy better than one part in 10^5. If, in Solution II, we adopt the exact value for $q(\infty)$, we get $q(0)$ accurate to one part in 10^6. The remaining solutions, with one more term, are accurate to about two parts in a million.

[2] *The Functions* $En(x) = \int_1^\infty e^{-xu}u^{-n}du$ (Doc. No. MT-1) (Chalk River, Ontario: National Research Council of Canada, Division of Atomic Energy, [1946]).

There is an interesting and somewhat obscure point in the solution of the equations. The determinants resulting from the formal solution of the simultaneous equations (46) have a tendency to vanish. Formally, the tendency indicates an incipient indeterminacy. A linear dependence must exist either between the equations or between various parameters A_j. One consequence of this peculiar condition is the fact that the A_j's are not necessarily unique. Various linear combinations may give the same functional results to a high degree of accuracy.

A shift of only one unit in the fifth decimal place of a produces a change of three units in the second decimal place of A_2, in Solution II. Solutions III and V were obtained by identical procedures. Both satisfy the initial conditions to nine decimal places. The difference is that Solution V was carried out to twenty places of decimals, to remove the indeterminacy as far as possible. In Solution VI, the constant A_3 was arbitrarily adjusted to give an exact fit for $q(0)$. The shift amounted to only one part in a million.

Computations made from Solution IV with calculated values from Eddington,[3] Chandrasekhar,[4] Placzek,[5] and LeCaine[6] appear in Table 3. Mark's[7] exact values, computed by machine methods, are given for comparison.

TABLE 2

CONSTANTS

Solution No.	$a=q(\infty)$	A_0	A_1	A_2	A_3	$q(0)$
I	0.7104513	−0.2666602	0.3468140	−0.1196287	....	0.5773446
II	.71044609*	− .27086231	.3764936	− .1514577	....	.5773447
III	.71044609*	− .28070408	.54030420	− .63919530	0.36208123	.57734932
IV	.71044936	− .27186451	.41860309	− .31239946	.13433965	.56773815
V	.71044609*	− .28069496	.54016112	− .63878155	.36177922	.57734932
VI	0.71044609*	−0.28069496	0.54016112	−0.63878155	0.36178017	0.57735027*

* Exact value assumed.

From equations (8), (36), and (49) we easily derive the following formula for the emergent intensity:

$$I^+(0,\mu)=\left(a+A_0+\frac{A_1}{2}+\frac{A_2}{3}+\frac{A_3}{4}\right)+\left(1-A_1-\frac{A_2}{2}-\frac{A_3}{3}\right)\mu$$
$$+\left(A_2+\frac{A_3}{2}\right)\mu^2-A_3\mu^3-(A_0\mu-A_1\mu^2+A_2\mu^3-A_3\mu^4)\log\frac{\mu+1}{\mu}. \qquad (52)^{8}$$

In the computation we shall adopt the coefficients as given by Solution IV.

[3] *The Internal Constitution of the Stars* (Cambridge: At the University Press, 1930), p. 333, eq. (231.2); see also S. Chandrasekhar, *Ap. J.*, **99**, 189, Table 1, 1944.

[4] *Ap. J.*, **100**, 82, Table 1, 1944.

[5] *The Neutron Density near a Plane Surface* (Doc. No. MT-16) (Chalk River, Ontario: National Research Council of Canada, Division of Atomic Energy [1947]).

[6] *Phys. Rev.*, **72**, 566, 1947.

[7] *Phys. Rev.*, **72**, 563, 1947.

[8] We have obtained two separate formulas for I^+ and I^-, where Chandrasekhar attempts to use one formula for the complete range of μ (*Ap. J.*, **100**, 81, 1944). For example, he gets, in the second approximation:

$$I(0,\mu)=\tfrac{3}{4}\mathfrak{F}\left(\mu+0.694025-\frac{0.116675}{1+1.97203\mu}\right).$$

Note that Chandrasekhar's expression for $I(0,\mu)$ has an infinite discontinuity at $\mu=-1/1.9723$ and therefore does not satisfy the boundary condition (vanishing of the inward intensity) at this point. The

Table 4 gives in successive columns the values of $I^{+}(0, \mu)$ as computed from equation (52), the exact values[9] (Hopf), Chandrasekhar's fourth approximation,[10] and the values as deduced from the $H(\mu)$ function in Ambarzumian's functional equation. Chandrasekhar[11] has computed $H(\mu)$ by iteration from Ambarzumian's functional equation

$$H(\mu) = 1 + \tfrac{1}{2}\mu H(\mu) \int_0^1 \frac{H(\mu^1)\, d\mu^1}{\mu + \mu^1}; \tag{53}$$

TABLE 3

τ	$q(\tau)$					
	Computed (IV)	Correct Mark	Eddington (2d Approx.)	Placzek	Chandrasekhar (4th Approx.)	LeCaine
0.00	0.5773382	0.57735031	0.583	0.577	0.5774	0.5790
0.05	.6105623	.6107	.620	.610	.5974	.6108
0.10	.6278099	.6279	.635	.626	.6139	.6278
0.15	.6400963		.645	.638	.6274	
0.20	.6495643	.6495	.653	.648	.6386	.6495
0.25	.6571679		.660		.6479	
0.30	.6634362	.6634	.665	.662	.6557	.6635
0.35	.6686998		.670		.6621	
0.40	.6731871	.6731	.673	.672	.6676	.6735
0.50	.6803844	.6803	.679	.680	.6761	.6806
0.60	.6858845	.6858	.683	.686	.6823	.6861
0.70	.6901802	.6901	.686	.691	.6870	.6904
0.80	.6935930	.6935	.689	.695	.6905	.6939
0.90	.6963401	.6963	.692	.698	.6933	.6966
1.0	.6985750	.6985	.694	.700	.6954	.6988
1.2	.7019260	.7019	.697		.6987	.7022
1.4	.7042435		.699		.7008	
1.6	.7058797		.701		.7024	
1.8	.7070535		.702		.7035	.7080
2.0	.7079064	.7079	.703	.7096	.7044	
2.2	.7085327		.704		.7050	
2.4	.7088462		.704		.7055	
2.6	.7093432		.705		.7058	
2.8	.7096034		.705		.7064	
3.0	.7097999	.7098	.706	0.711	.7065	.70985
∞	0.7104494	0.7104461	0.710	Correct value assumed	0.7069	0.7104457

and we have computed $I(0, \mu)$ from the relation:

$$I(0, \mu) = \frac{\sqrt{3}}{4} \mathfrak{F} H(\mu). \tag{54}$$

third approximation for $I(0, \mu)$ has two such infinities. Further, these points of infinite discontinuity multiply without limit in the process of infinite approximation. In view of the existence of these infinities, the limiting function for $I(0, \mu)$ obtained by Chandrasekhar's method is not the *exact* Hopf function but differs from it at an enumerably infinite set of points (of measure zero). In other words, the two functions are *equal almost everywhere.* It is precisely because of this property that the differences between the two functions, though real and not to be ignored from a purely mathematical viewpoint, are nevertheless physically insignificant.

[9] S. Chandrasekhar, *Ap. J.*, **99**, 189, Table 2, 1944.

[10] *Ibid.*, **100**, 82, Table 2, 1944.

[11] *Ibid.*, **106**, 143, Table 1, 1947.

Mark[12] has obtained an asymptotic expansion near the boundary, from which he has constructed Table 5 for $q(\tau)$.

The high accuracy of the approximations and the general simplicity of the results obtained by the present method are gratifying. The foregoing procedure, developed for

TABLE 4

μ	$I(0, \mu)/\mathfrak{F}$			
	Computed IV	Exact (Hopf)	Chandrasekhar (4th Approx.)	Ambarzumian's Functional Equation
0.0......	0.4330036	0.43301	0.4330	0.43301
0.1......	0.5400318	0.54011	0.5319	0.54014
0.2......	0.6279790	0.62802	0.6205	0.62799
0.3......	0.7112144	0.71123	0.7046	0.71122
0.4......	0.7920933	0.79210	0.7861	0.79211
0.5......	0.8715594	0.87156	0.8660	0.87156
0.6......	0.9500923	0.95009	0.9449	0.95007
0.7......	1.0279502	1.02796	1.0231	1.02797
0.8......	1.1053614	1.10536	1.1007	1.10534
0.9......	1.1823876	1.18238	1.1779	1.18238
1.0......	1.2591280	1.25912	1.2548	1.25911

TABLE 5

τ	$q(\tau)$		
	Mark's Asymptotic Expansion	Correct	Solution IV
0................	0.5773	0.5773	0.5773
0.01............	.5882	.5882	....
0.02............	.5954	.5954	....
0.03............	.6013	.6012	....
0.05............	.6109	.6107	.6106
0.1..............	.6287	.6279	.6278
0.2..............	0.6522	0.6495	0.6496

strict radiative equilibrium, can be extended to the case of nongray atmospheres. We have to replace equation (15) by a more general equation, wherein m is the root of the expression:

$$-\beta+\frac{1}{m}\tanh^{-1}m=0\,.$$

We shall return to these more general problems in a later paper, if further study indicates that the method is useful.

[12] *Op. cit.*, p. 562.

In a recent paper, Kourganoff[13] has used the expansion (51) of our paper and determined the constants from the conservation of the net flux. He has fitted his solution for sixteen values of the optical depth τ by the method of least squares. Kourganoff has indicated in a very recent letter that he has reached an accuracy of about two parts in a million in a six-term expansion.

We would like to thank Mr. David Murcray, Mr. Willard Shrode, and Mr. John G. Wolbach for having helped us with the extensive numerical work in this paper.

[13] *CR*, November 15, 1948, p. 1020; *Contr. I.A.P.*, Ser. A, No. 34.

SUPERTHERMIC PHENOMENA IN STELLAR ATMOSPHERES

V. ON EMISSION LINES AT HIGH KINETIC TEMPERATURE

RICHARD N. THOMAS*
Institute for Advanced Study
Received March 17, 1949

ABSTRACT

The treatment of the radiation field of a high-kinetic-temperature chromosphere is continued. The conditions for emission lines to be formed and for an effective photosphere to be found in the chromosphere are investigated from a purely formal standpoint. For a quantitative investigation of the behavior of the Balmer series, particularly with regard to the transient appearance of emission lines, a detailed investigation of inelastic collision cross-sections seems required.

If one admits the quite general existence of an outer stellar atmosphere that takes the form of an extended high-kinetic-temperature chromosphere-corona, it appears possible to resolve several of the difficulties connected with the anomalous presence of emission lines; for the existence of such a high kinetic temperature implies a source of energy other than the photospheric radiation field. Hence we find the possibility that, in the chromosphere, energy from this other source eventually becomes radiation in a limited spectral region. In short, the atmosphere departs from the condition of radiative equilibrium.

The principal problem may be stated as follows: What is the contribution of the chromosphere to the general radiation field that the customary methods applied to the classical atmosphere predict? The question may be broken into two parts: (1) Does the chromosphere add to, or subtract from, the intensity calculated at the photospheric region? (2) When does the effective photosphere move into the chromosphere?

The terms "photosphere," etc., lose much of their meaning in the above context; so hereafter we refer to those regions of the atmosphere where $\partial T_e/\partial r < 0$ as the lower atmosphere or classical photosphere, and the regions where $\partial T_e/\partial r > 0$ as the chromosphere. With the term "effective photosphere" we shall attempt to retain the customary connotation of the term "photosphere," viz., the region of optical depth 1. Thus, when the effective photosphere in any spectral region lies in the chromosphere, we conclude that the classical-atmosphere description breaks down completely. For the majority of the stars, however, it appears that the energy distribution in at least the visible region of the continuum refers to the classical photosphere. The phenomena then investigated are the spectral lines and perhaps the far ultraviolet region of the spectrum.

In this preliminary discussion we consider purely formal answers to questions 1 and 2. That is, the chromosphere as defined above is completely characterized only when the population of each spectroscopic state is explicitly given; for the situation is, in general, far removed from thermodynamic equilibrium. We assume this description to be given by the b_n (introduced in Paper II)[1] and express the formal solutions to questions 1 and 2 in terms of these b_n. We do not, however, attempt to calculate the b_n but assume that their values are given. Solutions[1] for the solar chromospheric b_n will be used for numerical examples only.

* Frank B. Jewett Fellow for 1948–49.

[1] Paper II, *Ap. J.*, **108**, 142, 1948; Paper III, *Ap. J.*, **109**, 480, 1949.

I. THE DIFFERENTIAL CHROMOSPHERIC CONTRIBUTION AND QUESTION 1

Elsewhere it has been shown[2] to be extremely likely that the b_n exceed unity, in this case of high kinetic temperature. We have the defining equation for b_n:

$$N_n = b_n \left(\frac{h^2}{2\pi m k T_e}\right)^{3/2} \frac{\varpi_n}{\varpi_i \varpi_e} e^{\chi_n/kT_e} N_i N_e \,, \tag{1}$$

where N_n is the population of level n and the other symbols are conventional, and χ_n is measured relative to the ground state of the ion whose density is N_i. With the exception of metastable levels, we expect $b_{n'} > b_n$ for $n > n'$.[3]

Menzel has earlier remarked[4] on the condition for appearance of emission or absorption lines when $b_n \neq 1$. He states the condition as emission or absorption according as b_n exceeds or is less than $b_{n'}$. Fortunately for the hope that the high T_e will help clear up the emission-line problems, Menzel's criterion is not generally valid. We may reach more complete criteria by considering the expression for the difference between emission and absorption in a line. By writing down the Einstein transition conditions and using equation (1), we obtain, for the net emission,

$$\Delta E = \text{Const.} \left[1 - S \frac{\dfrac{b_{n'}}{b_n} e^{h\nu/kT_e} - 1}{e^{h\nu/kT_r} - 1} \right], \tag{2}$$

where we write: $S \equiv$ ratio of intensity at $\nu_{n'n}$ to that of a black body at T_r, and T_e and T_r are the kinetic and radiation temperatures, respectively. Thus we obtain the conditions:

$$\Delta E \lessgtr 0 \text{ according as } b_n \lessgtr b_{n'} \frac{e^{h\nu/kT_e}}{e^{h\nu/kT_r} - 1 + S} . \tag{3}$$

Thus the modification of Menzel's conditions is quite large when T_e differs much from T_r even if we were to consider ΔE alone as determining the emission or absorption. Equation (3), however, only provides an answer to question 1 above, relating to the positive or negative value of ΔE. We note that $\Delta E < 0$ is both a necessary and a sufficient condition for an absorption line to become still deeper in the chromosphere. Thus, even though $T_e \gg T_r$, a high enough value of $b_{n'}$ will provide blacker lines than the classical theory would predict. The result has a clear connotation for those arguments which explain the absorption by contrasting the optical depth within and slightly adjacent to the line. For large enough $b_{n'}$, the optical depth at the line center would correspond to a temperature far greater than that of the continuum, and we should then expect emission by the usual arguments. This point is a useful one to illustrate the effect which departures from thermodynamic equilibrium can have on equilibrium arguments.

II. THE INTEGRATED CHROMOSPHERIC EMISSION AND QUESTION 2

We see that $\Delta E > 0$ is a necessary, but not sufficient, condition for the formation of an emission line. For an emission line, the integrated net emission must fill up the original absorption line. Following Milne,[5] we may write down the equation of transfer in terms

[2] *Ap. J.*, **109**, 500, 1949.

[3] We adopt the convention $n'' > n > n'$.

[4] *Pop. Astr.*, **47**, 17, 1939.

[5] *Handbuch der Astrophysik* (Berlin: Julius Springer, 1930), chap. ii.

of the detailed processes.[6] We introduce the b_n, however, from equation (1), and obtain

$$\frac{dI_\nu}{d\tau} = -I_\nu + \frac{2h\nu^3}{c^2}\left[\frac{b_{n'}}{b_n}\, e^{h\nu/kT_e} - 1\right]^{-1}, \tag{4}$$

where

$$d\tau = a_\nu n_{n'}\left[1 - \frac{b_n}{b_{n'}}\, e^{-h\nu/kT_e}\right] ds\,. \tag{5}$$

Taking ds as measured positively outward, $\tau = 0$ at the bottom of the chromosphere, and τ_0 as the optical thickness of the top of the atmosphere along the direction s, there results:

$$I_\nu(\tau_0) = I_\nu(0)\, e^{-\tau_0} + \frac{2h\nu^3}{c^2}\, e^{-\tau_0}\int_0^{\tau_0} e^{\tau}\left[\frac{b_{n'}}{b_n}\, e^{h\nu/kT_e} - 1\right]^{-1} d\tau\,. \tag{6}$$

Any significant value for τ_0 will indicate that the chromosphere contributes to the structure of the absorption line. The perturbation by the chromosphere may be stated as the following: Suppose we are given some height in the classical photosphere above which lie N_H atoms of hydrogen. For rather low photospheric temperatures T_r, we will have essentially (n_{H_r} is the density of atoms in the ground state):

$$N_{n'r} = n_{H_r}\varpi_{n'}\, e^{-y_{1n'}}\beta_r^{-1}\,, \tag{7}$$

for the number of atoms in state n' above the photosphere, and β_r is the isothermal logarithmic density gradient at T_r. On the other hand, the existence of a chromosphere at high kinetic temperature beginning at the same level will give, essentially (n_{H_e} is the density of ionized hydrogen),

$$N_{n'e} = b_{n'}\left(\frac{h^2}{2\pi mkT_e}\right)^{3/2}\frac{\varpi_{n'}}{2}\, e^{x_{n'}}\, n_{H_e}^2\beta_e^{-1}, \tag{8}$$

since effectively all the hydrogen will be ionized. Using the condition

$$n_{H_e}\beta_e^{-1} \approx N_H \approx n_{H_r}\beta_r^{-1}, \tag{9}$$

we have

$$\frac{N_{n'e}}{N_{n'r}} = 0.2\cdot 10^{-15}\,\frac{n_{He}}{T_e^{3/2}}\, b_{n'}\, e^{y_{1n'}+x_{n'}}\,. \tag{10}$$

Thus for high enough $b_{n'}$ a very small τ_0 computed on a classical basis may become a τ_0 greater than unity on the high-temperature-chromosphere basis. For example, substituting the solar chromospheric values $T_e = 3.5\cdot 10^4$ and $N_e = 2\cdot 10^{11}$, we obtain

$$\frac{n_{2e}}{n_{2r}} = 0.5\cdot 10^{-2}\, b_2\,. \tag{10a}$$

When we solve for the solar chromosphere,[1] neglecting collisional excitation from level 2, we obtain b_2 as some 10^4. Thus the optical depth at the line center has increased by a factor of 50. For the solar case it appears that the centers of the early Balmer lines are formed rather high in the chromosphere.

[6] We note, by contrast with Milne's further development of this equation, that we are very much concerned with cyclic processes and therefore cannot solve for the ratio $b_n/b_{n'}$ independently of the values of the other b_n. In the following, we imply always the possibility of solution for the b_n by a development similar to that carried out for the hydrogen atmosphere of Papers II–III.

Returning to equation (6), we may further illustrate the situation by considering an isothermal atmosphere with constant b_n. We obtain

$$I_\nu(\tau_0) = I_\nu(0) + \left[\frac{2h\nu^3}{c^2}\left(\frac{b_{n'}}{b_n}\, e^{h\nu/kT_e} - 1\right)^{-1} - I_\nu(0)\right][1 - e^{-\tau_0}]\,. \tag{11}$$

For large τ_0, the condition for a chromospheric contribution sufficient to make $I_\nu(\tau_0) \geqslant I_\nu(0)$ is

$$\left(\frac{b_{n'}}{b_n}\, e^{h\nu/kT_e} - 1\right)^{-1} \geqslant (e^{h\nu/kT_r} - 1)^{-1} S(0)\,. \tag{12}$$

Condition (12) is just that given by equation (3). Thus, under this restricted situation equation (3) becomes necessary for emission and sufficient for nondepletion of the classical photospheric field by the chromosphere. For emission, we require $I_\nu(\tau_0) > I_\nu(T_r)$. The condition here is simply (12) with $S(0) = 1$, if $\tau_0 \gg 1$.

For the nonisothermal case, the same conclusions hold if the integrand of equation (6) is, apart from the e^τ factor, a sufficiently slowly varying function of τ, or in any event if it is an increasing function of τ.

Finally, we note that it has been shown in an earlier paper[1] that the condition

$$a_\nu n_{n'}\left[\frac{d\ln N_e}{ds}\right]^{-1} \gg 1 \tag{13}$$

leads for the ratio of chromospheric field to classical photospheric field:

$$\text{Ratio} = \frac{b_n}{b_{n'}}\,\frac{e^{y_{n'n}}}{e^{x_{n'n}}} = S_{n'n}(0)\,, \tag{14}$$

when we neglect the induced emission. The condition $S_{n'n} \geqslant 1$ insures that, somewhere in the chromosphere, absorption lines have disappeared.

The same sort of criterion may be applied to the continuum, where we now replace b_n by unity when we consider the free-bound continuum. Condition (14) follows directly from equation (6) if we lay down the condition equivalent to (13), namely, that in an optical thickness defined by the value $(d\ln N_e/ds)^{-1}$ for ds, the integrand of equation (6) does not materially change, apart from the e^τ factor.

Again by way of illustration we may quote the results[1] for the solar chromosphere. The essential region of interest is in the Lyman lines; for the results are not so sensitive to the neglect of collisional excitation from level $n = 2$. We obtain a very large τ_0 when we choose as the base of the chromosphere that region for which Wildt obtains[7] $N_e = 2\cdot 10^{11}$ and $T_e = 3.5\cdot 10^4$. We obtain a value $S_{1n} \gg 1$ in equation (14). Thus we conclude that the Lyman region in the sun has an energy output far exceeding that of a black body at 6000°. The exact numerical value of S_{1n} depends on the b_2 value, if b_2 is sufficiently large. In any event, however, the Lyman contribution will not be less than $20Cb_2$ for S_{12}, at the chromospheric level in question.

III. THE MARGINAL APPEARANCE OF EMISSION LINES

The considerations on the Balmer lines are of somewhat greater interest than those on the Lyman lines because of their more accessible location in the spectrum. In particular, when one considers emission lines, those occurrences[8] where the early members of the

[7] *Ap. J.*, **105**, 36, 1947.

[8] Struve, *A.J.*, **53**, 108, 1948.

series are in emission and the later ones in absorption become of interest. The necessary conditions for such a situation are, from equation (3) [neglecting S and 1]:

$$b_3 > b_2\, e^{h\nu/kT_e}\, e^{-h\nu/kT_r} \qquad 1 < b_2\, e^{h\nu/kT_e}\, e^{-h\nu/kT_r} \tag{15}$$
$$\nu \backsim H_\alpha\,, \qquad \nu \backsim \text{Balmer limit}\,.$$

Thus the essential question—for given T_e and T_r—is the b_2/b_n ratio.

From the work on the solar chromosphere, where collisional excitation from level 2 has been neglected, one finds for the above relation on H_α:

$$\frac{b_2\, e^{h\nu/kT_e}}{b_3\, e^{h\nu/kT_r} - 1} \approx \bar{S}_2^{-1} \left[\frac{1}{(1+\epsilon)(1+\eta)} + p \right], \tag{16}$$

where

$$0 < \eta\,, \qquad p < 1$$

and ϵ is of the form:

$$\epsilon = \frac{\epsilon_1}{\bar{S}_2} \qquad 0 < \epsilon_1 < 1\,,$$

and $\bar{S}_2$ is S evaluated at H_α and averaged over all directions. Thus $\bar{S}_2$ is somewhat less than the observed residual intensity of H_α. We see that in this case we expect no emission in the Balmer series as a consequence of the presence of a high-kinetic-temperature chromosphere.

If, however, we add to the equations of condition on b_n a term involving collisional excitation from level 2, we must divide the expression (16) by a term of the form

$$1 + (C N_e T_e^{1/2})\, \bar{S}_2^{-1}\,, \tag{17}$$

where C is some constant depending on the cross-section for collisional excitation from level 2. For sufficiently great N_e and T_e, we then see the chance of bringing the earlier chromospheric lines into emission.

Such a situation as pictured may well provide the possibility of treatment of the appearance of emission lines in RR Lyrae; for, at the stage of the velocity-curve where the emission lines occur, whether one speaks of shock waves or waves of finite amplitude, one must admit the presence of a T_e an order of magnitude or more greater than the usually accepted T_r. Also, N_e must rise. One then has the requisite conditions for the appearance of emission lines. A quantitative treatment of the situation should provide the series member where the emission changes to absorption, if one is given T_e and N_e. Or, not knowing these parameters, one might investigate the possibility of inferring them from the observations on series members where emission changes to absorption. As a preliminary step, however, one requires the evaluation of collisional cross-sections in the Balmer lines.

In summary, we find, upon inquiry into the purely formal expression for the condition that emission lines appear in a star possessing a high-kinetic-temperature atmosphere, that a knowledge of the inelastic collision cross-section is essential. So far as we can go in purely formal development, the solutions indicate that a typical case of the appearance of emission lines—RR Lyrae—is compatible with the formal relations. It would then appear that the calculation of thermal collision cross-sections for H is the next step in this study.

I am greatly indebted to Dr. Lyman Spitzer, Jr., for reading and discussing the paper during its preparation.

SELF-CONSISTENT FIELD WITH EXCHANGE FOR *Ca* XIII*

W. H. Davis†

Brown University, Providence, R.I.

Received March 14, 1949

ABSTRACT

Since *Ca* XIII appears to be responsible for one of the coronal lines, it seemed desirable to find the Fock wave functions for the 3P ground state of this ion. These wave functions are tabulated. Two rough checks have been made with experiment. One check is the comparison of the Hartree energy parameters with observed energy difference, and the other is the comparison of the calculated and observed energy differences corresponding to the $3P_1-3P_2$ transition responsible for the coronal line.

INTRODUCTION

In 1945 Edlén[1] identified certain spectral lines in the sun's corona with transitions in highly ionized atoms. One of these lines was attributed by him to the transition $3P_1-3P_2$ in the configuration $(1s)^2(2s)^2(2P)^4$ of *Ca* XIII (a calcium atom ionized twelve times). This line is forbidden by the ordinary selection rules and, according to Edlén, occurs only in sources of very low density. It was decided to make a theoretical investigation, using the Fock method, of the 3P ground state of *Ca* XIII, and to compare theoretical and experimental energy differences.

METHOD OF SOLUTION

The Fock method was chosen for the investigation of *Ca* XIII, since it provides the most accurate wave functions for ions or atoms with as many electrons as *Ca* XIII. However, before using the Fock method proper, it is necessary to find the wave functions by the Hartree method, since these provide a good first approximation to the Fock solutions. The fundamental difference between the Hartree and Fock methods is that the former uses a resultant wave function which is a determinant of the 1-electron wave functions. The resultant Fock wave function, therefore, satisfies the Pauli exclusion principle, but the resultant Hartree wave function does not.

The Fock and Hartree methods have been applied to many atoms. The details of the method can therefore be found in many places.[2] Hence we shall content ourselves with a few general statements. We assume that the 1-electron wave functions are products of two functions. The first gives the dependence on the angular position found in the hydrogen atoms, and the second gives the as yet unknown dependence $P_{nl}(r)$ on the distance from the nucleus. The differential equations which the $P_{nl}(r)$ functions must satisfy are then determined from the variation principle of quantum mechanics. For the special case of the 3P ground state of *Ca* XIII we get the following Fock equations:

$$P''_{nl}(r)+\left[2V_{nl}(r)-\frac{l(l+1)}{r^2}-\epsilon_{nl}\right]P_{nl}(r)+T_{nl}(r)=0,$$

* Part of a dissertation presented to the Graduate School of Brown University in partial fulfilment of the requirements for the degree of Doctor of Philosophy.

† Now at the University of Buffalo, Buffalo, New York.

[1] *M.N.*, **105**, 323, 1945.

[2] D. R. Hartree, *Proc. Cambridge Phil. Soc.*, **24**, 89, 1926.

where

$$2V_{1s}(r) = \frac{2z}{r} - [W_0(1s, 1s) + 2W_0(2s, 2s) + 4W_0(2p, 2p),$$

$$T_{1s}(r) = [W_0(1s, 2s) - \epsilon_{1s,2s}]P_{2s}(r) + [2rW_1(1s, 2p)]P_{2p}(r),$$

$$2V_{2s}(r) = \frac{2z}{r} - [2W_0(1s, 1s) + W_0(2s, 2s) + 4W_0(2p, 2p)],$$

$$T_{2s}(r) = [W_0(1s, 2s) - \epsilon_{1s,2s}]P_{1s}(r) + [2rW_1(2s, 2p)]P_{2p}(r),$$

$$2V_{2p}(r) = \frac{2z}{r} - [2W_0(1s, 1s) + 2W_0(2s, 2s) + 3W_0(2p, 2p) - \tfrac{3}{2}r^2W_2(2p, 2p)],$$

$$T_{2p}(r) = rW_1(1s, 2p)P_{1s}(r) + rW_1(2s, 2p)P_{2s}(r),$$

$$W_K(nl, n'l') = 2\int_0^\infty \left[\int_0^\rho P_{nl}(\rho_1)P_{nl}(\rho_1)\,\rho_1^K d\rho_1\right]\rho^{-2K+2}d\rho.$$

The Hartree equations for the ground state of *Ca* XIII differ from the above Fock equations only by the omission of the $T_{nl}(r)$ and the $W_2(2p, 2p)$ terms.

For the actual integration of the Fock and Hartree equations, analytical methods are impracticable. Experience of others has suggested that the Milne method of numerical integration is the most useful when an electrical calculator is available.

The general technique of solving the Fock and Hartree equations is one of successive approximations. We make successive estimates of the $V_{nl}(r)$ and $\epsilon_{nl,\,n'l'}$ until the wave functions satisfy the boundary conditions as well as the differential equations. The $T_{nl}(r)$ terms in the Fock equations make normalization by a constant multiplier impossible. This necessitates the adjustment of one additional constant and thus renders the solutions of the Fock equations even more lengthy than the solutions of the Hartree equation.

RESULTS

The Hartree wave functions have been obtained for the $(1s)^2(2s)^2(2p)^4$ and the $(1s)^2(2s)(2p)^5$ states of *Ca* XIII. The Fock wave functions have been obtained for the 3P ground state of *Ca* XIII. The Fock wave functions and the corresponding ϵ energy parameters are listed in Table 1. (The ϵ's are not the true energies but only approximations to the true energies.) The solutions are accurate to about four decimal places or better for small r and about three decimal places for large r. The ϵ parameters are accurate to two or three decimal places. The ratios a^F_{nl}/a^H_{nl} below have the following significance. The a^H_{nl} are the quantities $\lim_{r\to 0} P_{nl}/r^{l+1}$ for the Hartree case, and the a^F_{nl} are the corresponding quantities for the Fock case. The ratios of these quantities may be useful in solving the Fock equations for other highly ionized atoms:

$$\frac{a^F_{1s}}{a^H_{1s}} = 0.9996\,, \qquad \frac{a^F_{2s}}{a^H_{2s}} = 1.0123\,, \qquad \frac{a^F_{2p}}{a^H_{2p}} = 1.0250\,.$$

We know that an excited state should have less energy than the ground state. This condition is satisfied by the ϵ parameters. The greater energy would also correspond to a greater concentration of charge. This condition is predicted by the wave function also, since the ground-state wave functions are shifted toward the origin as compared to the excited state of wave functions.

The difference between the Fock solution and the Hartree ground-state solution is rather small, but not negligible, for this tightly bound ion. As usual, the Fock solution predicts a more compact atom and, as a result, also gives larger ϵ parameters. This is a step in the right direction, since it is well known that the Hartree solutions in general give an atom which is not compact enough.

TABLE 1

FOCK WAVE FUNCTIONS FOR 3P STATE OF *Ca* XIII

r	$P_{1s}(r)$	$P_{2s}(r)$	$P_{2p}(r)$	r	$P_{1s}(r)$	$P_{2s}(r)$	$P_{2p}(r)$
0	0	0	0	0.38	0.046	−1.6061	1.3950
0.005	0.7920	+0.2399	0.0064	0.40	0.034	−1.5299	1.3151
0.010	1.4336	+0.4328	0.0243	0.42	0.025	−1.4481	1.2344
0.015	1.9465	+0.5840	0.0521	0.44	0.018	−1.3630	1.1542
0.020	2.3496	+0.6984	0.0881	0.46	0.013	−1.2766	1.0754
0.025	2.6594	+0.7806	0.1312	0.48	0.010	−1.1904	0.9987
0.030	2.8901	+0.8344	0.1799	0.50	0.007	−1.1055	0.9247
0.035	3.0540	+0.8635	0.2334	0.52	0.005	−1.0230	0.8538
0.040	3.1618	+0.8713	0.2906				
0.045	3.2228	+0.8599	0.3506	0.56	0.003	−0.8675	0.7226
0.050	3.2448	+0.8328	0.4128	0.60	0.002	−0.7275	0.6063
0.055	3.2348	+0.7919	0.4765	0.64	0.001	−0.6044	0.505
0.060	3.1986	+0.7394	0.5410	0.68	0.001	−0.498	0.418
0.065	3.1412	+0.6770	0.6059	0.72	...	−0.407	0.343
0.070	3.0670	+0.6066	0.6708	0.76	...	−0.331	0.281
0.075	2.9796	+0.5295	0.7351	0.80	...	−0.268	0.229
0.080	2.8821	+0.4471	0.7987	0.84	...	−0.215	0.185
				0.88	...	−0.172	0.150
0.09	2.6672	+0.2708	0.9223	0.92	...	−0.137	0.120
0.10	2.4329	+0.0858	1.0396	0.96	...	−0.109	0.097
0.11	2.2087	−0.1020	1.1492	1.00	...	−0.086	0.077
0.12	1.9845	−0.2875	1.2502	1.04	...	−0.068	0.061
0.13	1.7713	−0.4672	1.3421	1.05	...	−0.053	0.049
0.14	1.5722	−0.6384	1.4244	1.12	...	−0.042	0.039
0.15	1.3889	−0.7992	1.4972	1.16	...	−0.033	0.031
0.16	1.2220	−0.9483	1.5605	1.20	...	−0.025	0.024
0.17	1.0713	−1.0848	1.6145	1.24	...	−0.019	0.019
0.18	0.9363	−1.2083	1.6596	1.28	...	−0.015	0.015
0.19	0.8160	−1.3187	1.6961	1.32	...	−0.011	0.011
0.20	0.7095	−1.4163	1.7245	1.36	...	−0.008	0.009
				1.40	...	−0.005	0.007
0.22	0.533	−1.5736	1.7588		...	−0.003	0.005
0.24	0.398	−1.6845	1.7669		...	−0.002	0.003
0.26	0.295	−1.7541	1.7527		...	−0.001	0.002
0.28	0.218	−1.7880	1.7201		...	−0.001	0.001
0.30	0.161	−1.7918	1.6727		...	...	0.001
0.32	0.118	−1.7708	1.6138				
0.34	0.086	−1.7301	1.5463		$\epsilon_{1s}=329.7$	$\epsilon_{2s}=58.91$	$\epsilon_{2p}=54.24$
0.36	0.063	−1.6739	1.4727				

COMPARISON WITH EXPERIMENT

We have two rather rough checks with experiment. The first check is a comparison of the energy of transition from the excited $(1s)^2(2s)(2p)^5$ state to the ground state, $(1s)^2(2s)^2(2p)^4$, as deduced from the Hartree ϵ parameters, with that deduced from the corresponding spectral lines (this is *not* the coronal line) (Table 2). The agreement is only within 20 per cent. This large discrepancy is not surprising, since, according to the Hartree theory, the ϵ parameters give only approximate values for the energies. To get a more accurate test, we should have to evaluate the energy integrals.[3]

[3] D. R. Hartree and M. M. Black, *Proc. R. Soc., London, A*, **139**, 311, 1933.

We can make a second check by comparing the energy difference corresponding to the $3P_1-3P_2$ transition in the ground state of *Ca* XIII as calculated by the perturbation theory[4] with that determined from the observed coronal line. In the theoretical calculations we consider the spin-orbit interaction (Russel Saunders coupling) as the perturbing term. When we perform this perturbation, making use of the properties of the operators involved, we get the following relation:

$$\Delta E_{^3P_1-^3P_2} = 2\frac{h^2}{16m^2c^2}\int_0^\infty P_{2p}^2(r)\left[\frac{1}{r}\left(\frac{\partial V_{2p}}{\partial r}\right)\right]dr\,,$$

where $V_{2p}(r)$ is the potential in which the 2p electron is assumed to move and $\Delta E_{3p_1-3p_2}$ is the energy difference desired. When we make use of the Fock P_{nl} functions to evaluate the above equation, we get 22,240 cm^{-1}. The experimental value computed from the coronal line is 24,464 cm^{-1}. The discrepancy of about 10 per cent is not surprising, considering the assumptions that we have used. Probably the greatest part of this error lies in the neglect of the magnetic interaction of different electrons. However, this comparison does give a rough check on the wave functions.

TABLE 2

Experiment*		From ϵ Parameters	
Identification	Experimental Value (Cm^{-1})	Identification	Value (Cm^{-1})
$(2s)^2(2p)^4\,{}^3P_2\rightarrow(2s)(2p)^5\,{}^3P_2$	618,246	$(2s)^2(2p)^4\leftrightarrow(2s)(2p)^5$	501,000
$(2s)^2(2p)^4\,{}^3P_1\rightarrow(2s)(2p)^5\,{}^3P_2$	593,782		

* B. Edlén, *M.N.*, **105**, 323, 1945.

CONCLUSION

The Fock wave functions have been found for the 3P ground state of *Ca* XIII.[5] Two rather rough checks have been made with experiment, which show that the wave functions are at least reasonably close to the true ones. These Fock wave functions could be used to evaluate other quantities of astrophysical interest. For example, the author intends to calculate the transition probability for the "forbidden" coronal line attributed to *Ca* XIII. In addition, the Fock wave functions could be useful in making good initial approximations to the solutions for other highly stripped atoms responsible for coronal lines. It is intended at Brown University to carry through the Fock solution for *Ca* XII.

The author wishes to express his sincere thanks to Professor A. O. Williams, Jr., who suggested the subject of this thesis and who supervised the general development, as well as to Professor R. T. Beyer, who made the initial estimates for the potential field of *Ca* XIII.

[4] E. U. Condon and G. H. Shortley, *The Theory of Atomic Spectra* (Cambridge: At the University Press, 1935).

[5] On request the author will be pleased to send tables of potential functions or any other data required.

THE MILKY WAY AT THE JUNCTION OF GEMINI, MONOCEROS, AND ORION

Bart J. Bok, Margaret Olmsted, and Betty D. Boutelle
Harvard College Observatory
Received April 15, 1949

ABSTRACT

The present study is based largely on photographically determined color indices and magnitudes of stars in the *Henry Draper Extension* for the section between galactic longitudes 160° and 173°, latitudes −3° and +9°.

The structural features of the region are surveyed, and an attempt is made to determine what is the greatest well-determined distance for an object in this section of the Milky Way. The conclusion is reached that no known clusters or nebulae, O stars, c stars, or B stars are found at distances greater than 3000 parsecs and that the only known objects that are possibly at greater distances from the sun are three cepheid variables, one of which may be as distant as 5000 parsecs. It seems unlikely that, in the anticenter direction, the Milky Way system stretches more than 4000–5000 parsecs beyond our sun.

The space reddening is highly variable over the section. For Field 1, at $l = 171°$, $b = 0°$, we find relative freedom from overlying obscuration, with a value of $A_{pg} \leqq 0.5$ mag/kpc to a limit of 3000 parsecs indicated.

For Field 2, at $l = 166°$, $b = 0°$, we find, however, $A_{pg} = 1.2$–1.5 mag/kpc to a limit of 1500 parsecs, in agreement with an independent spectrum-color survey (*Ap. J.*, **109**, 139, 1949) by McCuskey. Fields 3 and 4, at galactic latitudes +3° and −2°, adjacent to Field 2, yield space reddening comparable to that found for Field 2. Fields 5, 6, and 7, with $l = 164°$–$170°$ and $b = +7°$, are all relatively free from obscuration, with $A_{pg} = 0.5$ mag/kpc to a limit of 2000 parsecs representing a fair average result.

Incomplete color data for three fields with galactic latitudes −3° to −7° give evidence for the presence of strong near-by overlying absorption, presumably caused by extensions of the Taurus-Orion complex of dark nebulae. One field, No. 11, is reserved for subsequent and more detailed study; it is located near $l = 171°$, $b = +3°$, and falls in the region of clusters and bright nebulosity south of Wolf's great dark nebula. The space reddening appears to be quite irregular.

In the preliminary analysis of the star densities, considerable stress is laid upon a comparison with the results obtained previously for a region at $l = 185°$, $b = 0°$. Negative density gradients, with an average density 0.5 ⊙ at a distance of 1000 parsecs, are found for the B8–A0 stars; the A1–A7 and F0–F8 stars yield average densities equal to 0.5 ⊙ at distances of 500 parsecs or less. For the late-type giants the average space densities are fairly constant over the first 500 parsecs from the sun.

In 1945 Bok and Mrs. Rendall-Arons[1] published the results of an investigation on the stellar distribution for a section of the Milky Way in Monoceros. The section under investigation was between galactic longitudes 176° and 186°. The present investigation deals with the section between galactic longitudes 160° and 173°, directly north of the one previously investigated. The basic materials for this new study are spectral types from the *Henry Draper Extension*[2] and blue-red color indices determined from plates taken with various cameras at the Oak Ridge station.

The Milky Way at the junction of the three constellations, Gemini, Monoceros, and Orion, has the distinctive smooth appearance of the anticenter regions. The section under investigation lies between $\alpha = 6$–7 hours; $\delta = +5°$ to $+20°$; it is shown nicely on Chart 35 of the Ross-Calvert *Atlas of the Milky Way*. The southern boundary of the section is roughly the line between Betelgeuse and Procyon, whereas γ Geminorum is the northern apex. To the west of the section, beginning at galactic latitude −3°, are the complex obscured regions associated with the Orion and Taurus nebulosities. Since we are —in accordance with the plan outlined in the earlier paper—primarily interested in regions free from obvious obscuration, we have omitted regions south of galactic latitude

[1] *Ap. J.*, **101**, 280, 1945; *Harvard Reprints*, No. 273.

[2] *Harvard Ann.*, Vol. **100**, No. 5, 1931.

$b = -3°$, whereas to the north of the galactic circle we have gone to $b = +9°$. We had originally intended to study colors and spectra for eleven centers, but a preliminary investigation led to the elimination of four centers affected by rather irregular local obscuration. The seven remaining centers border the conspicuous obscuration to the north of S Monocerotis, which has been studied in a classical paper by Wolf.[3] The obscured region has also been studied by Andrews,[4] who finds that the dark nebula at a distance of about 800 parsecs produces a total absorption of 1.5–2.0 mag. Before we proceed to describe the results of our own analysis, we shall describe briefly what, on the basis of the available published material, may be learned about the galactic structure for this section of the Milky Way.

I. STRUCTURAL FEATURES

The distribution of the dark nebulosity over the region has been described very well in Wolf's paper. The three principal centers of bright nebulosity are near 12 Mon (a cluster, NGC 2244 and bright nebulosity, NGC 2237), near S Mon (= 15 Mon; NGC 2264), near R Mon, and near BD+10°1159 (NGC 2245 and 2247). Struve and Elvey[5] and Struve, Elvey, and Linke[6] list, altogether, nine patches of nebulosity in this section of the Milky Way. The emission nebulosity near S Mon (Sp. O7s) has been found by Struve and Elvey and by Greenstein and Henyey[7] to have strong [*O* II] 3727 and relatively weak $H\alpha$; several near-by patches have the same characteristics. NGC 2237 near 12 Mon shows strong $H\alpha$, $H\beta$, $H\gamma$, $H\delta$, $N_1 + N_2$, and [*O* II] 3727. Finally, NGC 2245, with an associated star of spectral class B8, shows an absorption spectrum.

The T Tauri variable, R Mon, and the associated variable nebula discovered by Hubble have recently been studied by Greenstein,[8] who has also given references to earlier studies of the star and nebula. Greenstein places the star and nebula at a distance of 400–500 parsecs, at about the distance of the near-by star S Mon and its associated bright and dark nebulosity.

The region near 12 Mon is especially interesting. Five of the eleven *Henry Draper* O stars between $\alpha = 5^h40^m–7^h00^m$ and $\delta = +3°$ to $+20°$ belong to NGC 2244, and three of the remaining six O stars are within 2° of the cluster. The distance and total absorption of NGC 2244 can be reliably estimated from Zug's[9] spectra and colors and from the Stebbins, Huffer, and Whitford colors.[10] The distance to NGC 2244 is of the order of 1300–1400 parsecs, and the total absorption between our sun and the cluster is 1.3 mag. This leads to a value for the photographic absorption per kiloparsec of

$$A_{pg} = 1.0 \text{ mag/kpc} .$$

The color excesses of three O stars directly north of NGC 2244 indicate an average photographic absorption of the order of

$$A_{pg} = 0.5 \text{ mag/kpc} .$$

These absorptions are confirmed by the colors of B stars. Since NGC 2244 lies at the northern border of a region of obscuration, it is not surprising that the value of A_{pg} for centers a few degrees to the north of the cluster is smaller than that for the cluster itself.

[3] *Festchrift für Hugo v. Seeliger* (Berlin: Julius Springer, 1924), p. 313.

[4] Harvard dissertation, unpublished; for summary see *Pub. A.A.S.*, **7**, 211, 1933.

[5] *Ap. J.*, **89**, 522, 1939.

[6] *Ap. J.*, **90**, 301, 1939.

[7] *Ap. J.*, **87**, 80, 1938.

[8] *Centennial Symposia* ("Harvard Observatory Monographs," No. 7 [Cambridge, Mass.: The Observatory, 1948]), p. 25; and *Ap. J.*, **107**, 377, 1948.

[9] *Lick Obs. Bull.*, No. 454, 1935.

[10] *Ap. J.*, **91**, 20, 1940; *Mt. W. Contr.*, No. 621.

A small value of A_{pg} ($\leqq 0.5$ mag/kpc) is also found for the cluster NGC 2264. Trumpler[11] places this cluster at a distance of 450 parsecs. A slightly larger value might be preferable, but the cluster is not likely to be at a distance in excess of 600 parsecs. To this distance the reddening is slight and the absorption small though patchy.

Trumpler[11] lists twelve galactic clusters in the region under investigation. With the exception of three, he places these clusters at distances under 3000 parsecs. The most remote cluster, NGC 2141, has an estimated distance of 4860 parsecs. We doubt that this distance can be accepted without reservation. The cluster lies within the limits of one of the four centers which were eliminated from our investigation because of excessive overlying obscuration. Color-index measurements by Miss Olmsted indicate that this overlying absorption amounts to 2 mag. at 1000 parsecs and that Trumpler's distance must be reduced considerably. Trumpler describes the cluster as a "well resolved thin but rich cluster of exclusively faint stars (15–18 mag)."

The other two distant clusters in Trumpler's list are NGC 2259 and NGC 2269, both with estimated diameters of 3′–4′ and distances of 3900 parsecs. The first of these is in a clear patch bordered by heavy obscuration north and west of S Mon, whereas the second is near obscuration directly east of 12 Mon. Again the distance estimates by Trumpler are most likely to be too large. Cuffey[12] has shown this to be the case for several small clusters for which Trumpler and others had estimated the distance from angular diameter and appearance alone. A case in point is NGC 2194, for which Cuffey[13] finds a distance of 1200 parsecs from the color-magnitude array, whereas Trumpler's estimate was 2520 parsecs. Cuffey finds, incidentally, for NGC 2194 a space reddening equivalent to a total photographic absorption of 2.7 mag. at the distance of the cluster.

It is interesting to note that no cluster in the section is known with certainty to be at a distance from our sun in excess of 3000 parsecs. Since the section of the Milky Way under investigation (l = 160°–173°) is one of the least obscured in the general direction of the anticenter, considerable interest attaches to the greatest distance to which galactic objects can definitely be traced in this section. Among the known objects that are presumably most remote and for which fair distance estimates can be made are the O stars, the B stars, the c stars, and the cepheid variables.

We have already commented on the distribution of the eleven known O stars in this section of the Milky Way. Nine of these O stars are in or near 12 Mon, and, with the possible exception of HD 45166, these are certainly not farther than 1800 parsecs from the sun. S Mon is another O star, well within 1000 parsecs, and the single remaining O star (m = 7.1) is also relatively near by (650 parsecs).

The B stars are also scarce among the fainter stars in the section l = 160°–173°. The *Henry Draper Extension* for an area of 340 square degrees yields only nine new B0 stars and a single Oe5 star. Bok and Miss Wright[14] have already drawn attention to the paucity of faint early B stars for a field in Monoceros (l = 180°). In Table 1 we have listed side by side the distribution of the B0–B2 and B3–B5 stars for an area of 67 square degrees in Monoceros (l = 180°, b = 0°), for an area of 65 square degrees at l = 165°, b = 0°, and for an area of 60 square degrees at l = 165°, b = +5°. It was noted by Bok and Miss Wright that the numbers for the Monoceros field represented a rapid thinning-out of the B stars with increasing distance from the sun. This is even more marked at b = +5°.

The total number of known c stars is eight, whereas one might have expected as many as twenty on the basis of averages for the entire galactic belt. The three most remote c stars are at l = 166°, b = +7°, all with apparent magnitudes between 8.0 and 8.5 and

[11] *Lick Obs. Bull.*, No. 420, 1930.

[12] *Harvard Ann.*, Vol. **106**, No. 2, 1938.

[13] *Ap. J.*, **97**, 93, 1943.

[14] *Ap. J.*, **101**, 309, 1945; *Harvard Reprints*, No. 274.

spectral types B9 and A0p. Allowing for a possible absorption of 0.5 mag/kpc (see below), we place them at a distance of about 2600 parsecs from the sun; there are no known c stars beyond the 3000-parsec limit.

Data for faint cepheid variables are very incomplete for this part of the sky. Dr. Payne-Gaposchkin has kindly permitted us the use of a manuscript catalogue of known galactic cepheids. For the interval $l = 160°–180°$, $b = -10°$ to $+10°$, she lists twenty-one long-period cepheids and three cluster-type variables. Her derived distances, corrected for an absorption of 0.7 mag/kpc, place all but eight of these at distances less than 3000 parsecs from the sun. Five of these eight stars are south of the galactic circle in Orion, where the average photographic absorption is in excess of the average value assumed by Dr. Payne-Gaposchkin. The remaining three stars are VW, VZ, and WW Mon, discovered by Hoffmeister, with estimated distances of 3500, 5500, and 3700 parsecs. These three stars, all near $l = 169°$, $b = +1°$, require further study and are the only known objects to lie beyond 3000 parsecs from the sun.

TABLE 1

DISTRIBUTION OF FAINT B STARS

m_{pg}	B0–B2			B3–B5		
	Mon $l = 180°$ $b = 0°$	Gem–Ori $l = 165°$ $b = 0°$	Gem–Ori $l = 165°$ $b = +5°$	Mon $l = 180°$ $b = 0°$	Gem–Ori $l = 165°$ $b = 0°$	Gem–Ori $l = 165°$ $b = +5°$
8.0– 9.0......	1	4	0	5	11	2
9.0–10.0......	5	3	2	23	24	8
10.0–11.0......	2	3	3	33	40	8

It will be of considerable general interest to pursue further the problem of the extent of our galactic system in the direction of the anticenter. Spectral absolute-magnitude surveys to faint limits provide the most obvious means for extending the search; infrared surveys, like those now under way at the Warner and Swasey Observatory, should be especially valuable. None of the known novae in our section of the Milky Way are beyond the 3000-parsec limit, but a systematic search for faint novae in some of the more transparent low-latitude fields might be profitable. But, obviously, the greatest interest would attach to a search for faint cepheids, preferably to be combined with a study of the color excesses of the variables of known period. Star-count surveys to the faintest attainable magnitude limits will be helpful in the analysis for the distance to which our Milky Way system stretches beyond our sun.

To complete the general picture of what we may learn about galactic structure solely on the basis of published material, we should turn now to an over-all description of the absorption characteristics of the section on the basis of the color excesses by Stebbins, Huffer, and Whitford.[10] It will, however, be more profitable to discuss this material in conjunction with our own color data.

II. SPECTRAL TYPES AND COLOR INDICES

The spectral types for the stars for which the color indices have been measured are the published ones from the *Henry Draper Extension*.[2] The color indices for the several fields were determined mostly from plates taken with the 8-inch Ross (IR) camera of the Oak Ridge station. The blue series were made on Cramer Hi-Speed plates without a filter; the red series on Eastman 103*a*-E plates with a ciné-red filter. The principal observer with the IR camera was Guillermo Haro, now of the Tacubaya Observatory, Mexico.

As noted below, a group of special check plates was taken with the 24–33-inch Jewett-Schmidt telescope (observer: Bok) and another with the 16-inch Metcalf telescope (observer: Henry A. Sawyer).

The procedure of measurement and reduction follows closely that described in the paper by Bok and Mrs. Rendall-Arons.[1] The principal difference is that practically all the photometry is based on direct polar comparisons and that hardly any use was made of comparisons with the C regions. This proved to be a fortunate circumstance, since it was shown in a study by Bok and Miss Sawyer[15] that the present standard red magnitudes of the C regions are in error by perhaps as much as 0.3 mag. The standards used in the present study are again those of *Trans. I.A.U.*, **1**, 71, 1922, for the photographic magnitudes and those of the *Harvard Ann.*, Vol. **89**, No. 5, 1935, for the photored magnitudes. The recent checking of the basic red magnitudes by Nassau and Burger[16] supports the standards used in the present research.

Corrections for differential extinction were generally quite small; they were applied as in the earlier investigation.

Special care was taken to avoid the introduction of errors arising from color equation. As a standard precaution, all normal polar-sequence stars are plotted as black dots in our graphs, whereas the "r" stars are shown by red dots. This precaution was applied equally to photographic and photored polar reduction curves.

As before, the principal interest attaches to the color excesses of the stars of spectral types B and A. In agreement with the earlier investigation, we have assumed normal color indices as follows:

B0–B5	−0.35 mag.
B8–A0	− .15
A1–A7	+0.05

Inside the circle on each plate free from distance correction, we have measured, in addition to all B and A stars, a number of stars of later spectral types. It was hoped that these stars would provide an additional check on possible zero-point errors in our color indices; such errors could be produced by photometric nonuniformity of the sky during exposures and similar effects. While the observed average color indices of these stars are listed in the tables for each field, they are, unfortunately, of little value until reliable normal color indices for unreddened late-type stars become available. For a rough check on possible systematic errors affecting the color indices of all stars in a field, we have used the following normal blue-red color indices:

F0–F8	+0.58	K0–K2	+1.38
G0–G5	+0.92	K5–M	+1.84

These are more positive than the means for the Harvard Standard Regions, as given by Mrs. Gaposchkin[17] by about the amount of the correction suggested by Bok and Miss Sawyer.[15] In deciding on these average values, we have, furthermore, attempted to take into account the difference in color between late-type giants and dwarfs. Because of the obvious uncertainties in the normal colors, the observed colors for the F–M stars have been used only in a general rough check of the zero-point of the colors. The *difference* in observed color index between the B and A and the F stars is always, however, a dependable indicator for space reddening.

[15] *Harvard Bull.*, No. 918, 1946.

[16] *Ap. J.*, **103**, 25, 1946.

[17] *Harvard Ann.*, **89**, 113, 1935.

FIELD 1

Center (1900): $\alpha = 6^h24^m$; $\delta = +7°40'$; $l = 171°$; $b = 0°$

Field 1 is in a smooth and regular part of the Milky Way. Directly south of it lies the complex cluster NGC 2244 and the associated emission nebulosity NGC 2237 (12 Mon belongs to this group), for which we have already found an indicated absorption of the order of 1 mag/kpc to a distance of 1300 parsecs. We mentioned further that the absorption amounts to only 0.5 mag/kpc in the clear part north of NGC 2244.

Since Field 1 occupies a key position (low latitude, no obvious overlying obscuration) in this section of the Milky Way, we have thought it worth while to check the color indices for the HDE stars from independent series of polar comparison plates taken with the 8-inch Ross (IR), the 16-inch Metcalf (MC), and the 24–33-inch Jewett-Schmidt (J) telescopes at the Oak Ridge station.

The number of comparisons, the probable error of a magnitude determination from a single plate, and the corresponding error for the mean of the plates of a given series are shown in Table 2. In the last line of this table we have listed the systematic differences from the mean for the plates of each series. Several interesting conclusions may be derived from Table 2. It is to be noted that the Jewett-Schmidt telescope gives the poorest results, as far as accidental errors are concerned. The reason is probably that very short exposure times, 1 minute and less, had to be used to obtain images of the field stars that were not too dense for measurement. Polar comparisons of 3–10 minutes and longer yield considerably smaller accidental errors than those of Table 2.

The smallness of the accidental errors for the MC telescope should not be taken at its

Fig. 1.—This chart represents the section of the Milky Way at the junction of Gemini, Monoceros, and Orion. The epoch of the chart is 1900; the centennial precession for the center of the chart is: +5.5 min. in right ascension; −3′ in declination. The positions of *all HD stars to photographic magnitude 7.5* are shown as black disks. *The O and B stars with known color excesses by Stebbins, Huffer, and Whitford* (*Mt. W. Contr.*, No. 621, 1940) are indicated by black disks surrounded by a circle for the stars of magnitude 7.5 and brighter and by open circles for the fainter stars. *The cepheids VW Mon*, mag. 13.2–14.2, Per. 1.53 day; *VZ Mon*, mag. 14.3–15.2, Per. 5.08 days; *WW Mon*, mag. 12.6–14.1, Per. 4.66 days and the *nebular variable R Mon* are shown. The *stars γ Gem, ξ Gem, α Ori, μ Ori, ξ Ori, ν Ori, ε Mon, S (=15) Mon and 12 Mon* are marked on the chart. The large numbers 1–7 mark the *centers of the areas used in the study of spectra and color indices*. LF8 is the *center for which spectra and color indices have been determined at the Warner and Swasey Observatory* (*Ap. J.*, **109**, 139, 1949). *Galactic clusters* are indicated by broken circles with diameters equal to the diameter of each cluster according to Trumpler (*Lick Obs. Bull.*, No. 420, 1930); they are identified by small letters *a* to *p*, as listed below. *Diffuse nebulosities*, according to Cederblad (*Lund Medd.*, Ser. II, No. 119, 1946), are presented as small squares for diameters less than 6′ and squares of the dimensions given by Cederblad for the larger ones; they are identified by small letters *q* to *z*, as listed below, with *C* indicating continuous nebular spectra and *E* emission spectra. The more conspicuous patches of *dark nebulosity* are shown by full-drawn lines of irregular shape.

Galactic Clusters		Diffuse Nebulosities	
a	NGC 2141	q	NGC 2238 .. and NGC 2237
b	2169	r	IC 446 C
c	2186	s	2169 C
d	2194	t	NGC 2244 E
e	2236	u	IC 448 C
f	2244	v	NGC 2245 C
g	2251	w	2247 C
h	2254	x	2261 C+E
k	An 5	y	2264 E
m	NGC 2259	z	IC 454 ..
n	2264		
p	2269		

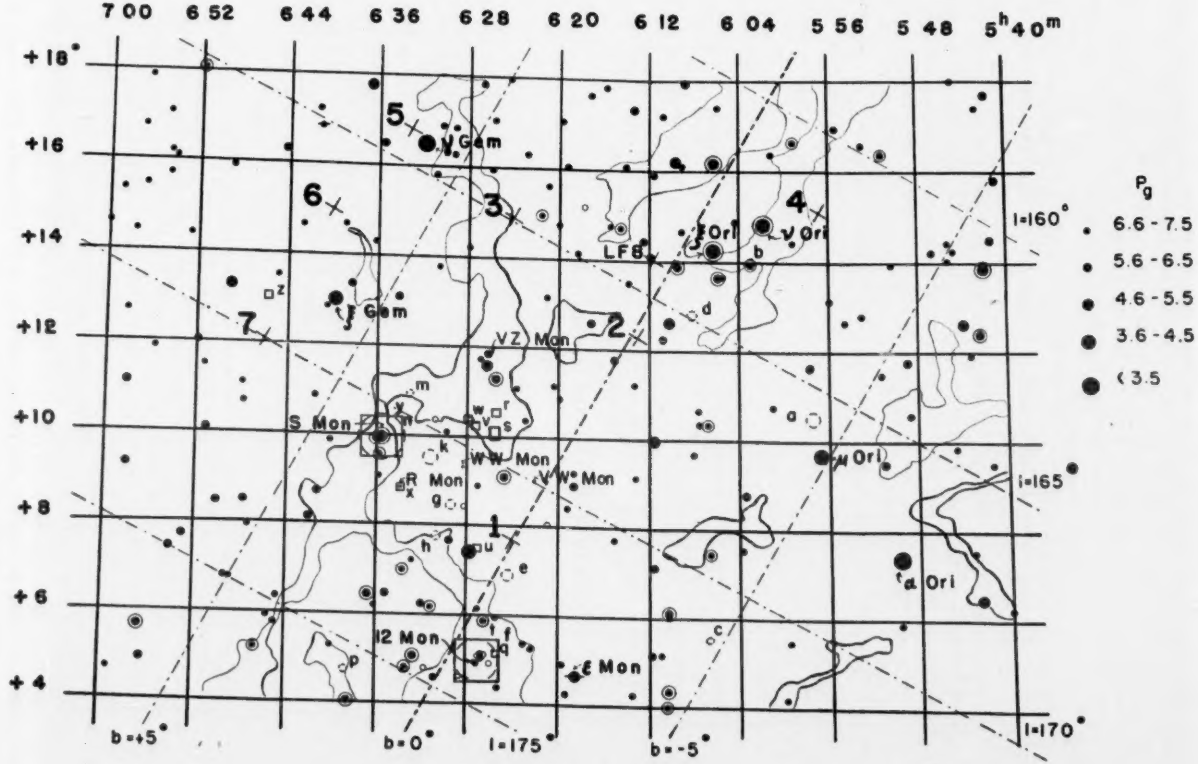

FIG. 1.—Legend on facing page

face value. The few MC plates were taken within a very short time of one another, and the listed error is a measure principally for the internal agreement of the measures—which is excellent. Only the very best nights were used for the MC observations, whereas for the IR and J we had to be satisfied with a mixture of good and excellent nights. We conclude that our Schmidt-type telescope had better *not* be used in the future for polar comparisons of very short exposure times.

The measured area had a radius of about 2°. No differential systematic errors were found depending on a star's position in the field, and almost complete freedom from "distance correction" seems indicated.

The data shown in Table 2 depend on thirty-four stars measured in common on all IR, MC, and J plates. Many more stars were measured on the IR plates, two hundred and forty-eight of them in all. The resulting mean color indices are given in Table 3.

TABLE 2

	Blue			Red		
	IR	MC	J	IR	MC	J
No. of plates	5	4	10	5	4	5
Av. p.e. per measure	±0.12	±0.08	±0.16	±0.10	±0.05	±0.17
Av. p.e. per star	±0.05	±0.04	±0.05	±0.05	±0.02	±0.07
Syst. diff. from mean	+0.07	−0.07	0.00	−0.01	−0.06	+0.08

TABLE 3

MEAN OBSERVED COLOR INDICES IN FIELD 1

m_{pg}	Spectral Type						
	B0–B5	B8–A0	A1–A7	F0–F8	G0–G5	K0–K2	K5–M
8.25	....	+0.02(1)	....	....	....	....	....
8.75	....	+ .19(4)	+0.30(2)	+0.59(1)	+1.13(3)	....	....
9.25	....	− .09(6)	....	+ .38(2)	+1.17(4)	....	....
9.75	+0.32(1)	− .19(2)	− .01(5)	+ .23(5)	+0.20(3)	+1.40(4)	+1.81(3)
10.25	− .14(1)	− .15(10)	− .06(9)	+ .20(2)	+0.52(2)	+1.27(3)	+1.58(2)
10.75	−0.06(1)	− .03(7)	+ .06(16)	+ .35(9)	+0.60(8)	+1.30(4)	+1.85(4)
11.25	....	+ .08(19)	+ .06(26)	+ .35(16)	+0.88(8)	+1.23(8)	+1.61(5)
11.75	....	+0.09(7)	+0.13(21)	+0.49(5)	+0.68(3)	....	+1.65(3)

An inspection of the mean color indices for stars of spectral types F–M would seem to indicate that the observed color indices in Field 1 are too small by at least 0.10 mag. This conclusion is, however, not confirmed by Table 2, where the IR color indices are, if anything, slightly more positive than the mean for the MC and J. We have, therefore, not applied any systematic correction to the average color indices of Table 3. We have already commented on the lack of reliable normal colors for the F–M stars and about the possible effects on the means of the unknown ratio of dwarfs to giants.

We conclude from Table 3 that the A1–A7 stars give no indication for the presence of space reddening, with the possible exception of the most distant group. This means, essentially, freedom from reddening effects to a distance of 1000 parsecs. The fainter B8–A0 stars show definite indications for space reddening, with a total absorption of 0.4 mag. at 1200 parsecs and 0.7 mag. at 1500 parsecs.

Fig. 2.—The galactic cluster NGC 2244 and associated diffuse nebulosities NGC 2237 and NGC 2238. A 3× enlargement of a 75-minute exposure on 103a-O backed plate taken with the 24–33-inch Jewett-Schmidt telescope of the Oak Ridge Station.

The results from the early B stars confirm, with two exceptions, the smallness of the interstellar absorption. The positive color index of a single B5 star ($m_{pg} = 9.77$) need hardly concern us, since it is offset by much smaller excesses for two fainter earlier B stars. Our own color excesses of early B stars suggest a total photographic absorption of 0.9 mag. at 3000 parsecs. The other exceptionally high absorption is found for two B stars observed by Stebbins, Huffer, and Whitford [10] which would indicate a total photographic absorption of 0.8 mag. at 900 parsecs. Since these two stars are not far from NGC 2244, the somewhat greater absorption is not surprising. The four remaining excesses by Stebbins, Huffer, and Whitford lead to the following absorptions:

Parsec	Mag.	Parsec	Mag.
1100	0.0	2600	0.5
1800	0.6	5200	0.6

We conclude, therefore, on the basis of all available evidence, that the total photographic absorption derived from space reddening for the direction of Field 1 is represented by

$$A_{pg} = 0.3 \text{ mag/kpc}$$

to a limiting distance of 3000 parsecs. Our own as well as other colors show that the absorption for this direction is not so high as

$$A_{pg} = 0.5 \text{ mag/kpc} ;$$

but, at the same time, the presence of some reddening seems definitely established.

FIELD 2

Center (1900): $\alpha = 6^h13^m$; $\delta = +12.^\circ3$; $l = 166^\circ$; $b = 0^\circ$

This field lies directly at the galactic circle. The field has some irregular absorption overlying it, but the irregularities are slight. Inside the limits covered by our color survey we find the galactic cluster NGC 2194, which, according to Cuffey[13] is highly reddened; Cuffey finds a reddening corresponding to a total absorption of 2.7 mag. at 1200 parsecs.

Our basic plate material for the color-index survey is considerable, comparable in extent to that for Center 1. It consists of polar comparison plates made with the 8-inch Ross (IR), 16-inch Metcalf (MC), and the 24–33-inch Jewett-Schmidt (J) telescopes at Oak Ridge. The number of comparisons, the probable error of a magnitude determination from a single plate, and the corresponding error for the mean of the plates of a given series are shown in Table 4. In the last line of this table we have listed the systematic differences from the mean for the plates of each series. There is no marked variation with magnitude in the systematic differences, and we conclude that the color indices on the IR, MC, and J system yield essentially similar results; we note again that none of the systematic differences is as high as 0.10 mag.

We also note here the smallness of the size of the derived accidental errors of the magnitudes derived from the MC plates and the relatively large probable errors for the Jewett plates. This confirms our conclusions that polar comparisons depending on very short exposures with the Schmidt camera produce rather large accidental errors. The IR magnitudes have probable errors intermediate between those from the MC and J plates.

The results of Table 4 depend on only 34 stars measured in common on all IR, MC, and J plates. Altogether, 185 stars were measured on the four blue and the five red IR plates. The resulting mean color indices are given in Table 5.

A comparison between the average normal color indices for the various spectral intervals and the observed means shows that the averages for the F, G, and K stars are

about as we expect them to be; this result confirms the absence of systematic errors in excess of 0.10 mag. in the color indices derived from the IR plates.

The color excesses derived from the IR polar comparisons show that considerable space reddening is present in Field 2. On the basis of the observed color excesses for the B0–B5, B8–A0, and A1–A7 stars, we find the total photographic absorption to vary as follows with distance:

Distance	500	1000	1500	(parsecs)
K_{pg}	0.6	1.5	2.1	(mag.)

This is somewhat smaller than the total absorption found by Cuffey for NGC 2194, but somewhat larger than the absorption indicated by the five B stars measured in this section by Stebbins, Huffer, and Whitford.[10]

TABLE 4

	Blue			Red		
	IR	MC	J	IR	MC	J
No. of plates	4	4	10	5	4	7
Av. p.e. per measure	±0.09	±0.04	±0.13	±0.12	±0.06	±0.16
Av. p.e. per star	±0.04	±0.02	±0.04	±0.05	±0.03	±0.07
Syst. diff. from mean	+0.06	−0.01	−0.05	+0.04	−0.06	+0.02

TABLE 5

MEAN OBSERVED COLOR INDICES IN FIELD 2

m_{pg}	Spectral Type						
	B0–B5	B8–A0	A1–A7	F0–F8	G0–G5	K0–K2	K5–M
8.25	....	+0.18(2)	+0.35(1)	+0.27(2)	+1.08(1)	....	....
8.75	+0.75(1)	+ .05(5)	+ .14(1)	....	....	....	....
9.25	+ .34(1)	+ .10(2)	+ .10(5)	....	+1.16(2)	+1.39(2)	....
9.75	+ .03(1)	− .04(3)	+ .10(3)	+ .46(2)	+1.25(1)	+1.32(4)	+2.21(1)
10.25	+ .41(3)	+ .18(4)	+ .19(5)	+ .52(6)	+0.67(3)	+1.28(2)	+1.82(3)
10.75	+0.36(3)	+ .29(6)	+ .33(11)	+ .42(6)	+0.71(4)	+1.30(6)	+1.83(2)
11.25	....	+ .34(3)	+ .50(15)	+ .63(13)	+0.99(14)	+1.27(2)	....
11.75	....	+0.41(1)	+0.35(8)	+0.57(8)	+0.64(6)	+0.84(5)	+1.63(2)

It is of interest to compare our results with those obtained recently by Dr. Sidney W. McCuskey for Field LF8 in the Warner and Swasey Observatory survey.[18] The total absorptions derived from the Warner and Swasey color excesses for LF8 ($\alpha = 6^h14^m$; $\delta = +14\overset{\circ}{.}0$), which were communicated to us in advance of publication by Dr. McCuskey, are:

Distance	500	1000	1500	2000	2500	(parsecs)
K_{pg}	0.3	1.0	2.0	2.4	2.4	(mag.)

The agreement between these two wholly separate determinations (different spectral classifications; different telescopes used for determination of magnitudes and color indices; wholly independent reduction of results) is quite satisfactory.

[18] Cf. McCuskey and Seyfert, *Ap. J.*, **106**, 1, 1947.

We conclude that, according to the various lines of evidence, the total photographic absorption in this field can be represented by

$$A_{pg} = 1.2\text{–}1.5 \text{ mag/kpc}$$

to a limiting distance of 1500 parsecs, with McCuskey's results indicating a total absorption of 2.4 mag. at 2500 parsecs.

It is necessary to comment on the dissimilarity of space reddening for two fields so relatively close to each other as Fields 1 and 2. They are only a little more than 5° apart in galactic longitude and both are directly on the galactic equator; but, in spite of this, Field 1 shows only a total absorption of less than 1 mag. at 2500 parsecs, whereas for Field 2 the corresponding absorption is more nearly of the order of 3 mag. Since this rather surprising result is given by color excesses derived with a variety of techniques and telescopes, there can be little doubt about its reality. Apparently, Field 1 happens to be in a direction not affected by the Taurus and Orion complexes of dark nebulosity, whereas Field 2 is under the influence of extensions of these large clouds of galactic obscuration.

FIELD 3

Center (1900): $\alpha = 6^h24^m$; $\delta = +14^\circ\!.9$; $l = 165°$; $b = +3°$

FIELD 4

Center (1900): $\alpha = 5^h57^m$; $\delta = +15^\circ\!.1$; $l = 162°$; $b = -2°$

These two fields are a little distance north and south of the galactic circle, at very nearly the same galactic longitude as Field 2.

Field 3 lies in a rich and fairly uniform part of the Milky Way, bordered by regions with irregular obscuration. It is marked by an almost complete absence of early B stars and a scarcity of B8–A0 stars, but the number of A1–A7 stars is fairly large.

The color indices of 196 stars in Field 3 were determined from five blue and five red polar comparison plates made with the 8-inch Ross (IR) camera. With one exception, the systematic differences, individual plate minus mean of five, were small; one blue plate yields magnitudes that are systematically too large by 0.33 mag. as compared to the mean of the five blue plates. We have used in our analysis the uncorrected color indices, and our derived color excesses could be too high by 0.10–0.15 mag. The observed mean color indices are shown in Table 6. The color indices for the late-type stars are close to normal, and we have no reason for the application of a systematic correction to the observed average color indices of the early-type stars. The derived color excesses indicate a total absorption slightly in excess of 1 mag. at 1000 parsecs. This is confirmed by two near-by reddened stars (650 parsecs) for which Stebbins, Huffer, and Whitford[10] have measured excesses, but it is to be noted that, at a somewhat greater distance from the center of Field 3, the same authors have an unreddened star at very nearly the same distance. Our single early B star yields an absorption of 0.8 mag. at 1500 parsecs. We conclude that the color excesses for Field 3 indicate a slightly smaller absorption than for Field 2, with

$$A_{pg} = 1.0 \text{ mag/kpc}$$

being a fair average.

Field 4 at $b = -2°$ lies in a rich field, again bordered by obscuration. A long-exposure Schmidt plate shows that there is some irregularity in the surface distribution of the faint stars, with the largest surface densities for the eastern half of the region.

The color indices of one hundred and eighty-eight stars in Field 4 were determined from four blue and four red polar comparisons with the 8-inch Ross (IR) camera. The plates showed good agreement. The mean observed color indices are shown in Table 7.

The color indices of the late-type stars again do not suggest the need for systematic corrections. The data for Field 4 seem to be quite consistent. The three faint early B's in the field are all quite reddened, with an absorption of at least 2 mag. indicated at 1500 parsecs. This result is confirmed by the value of 1.4 mag. at 1000 parsecs derived from the B8–A0 and A1–A7 stars. The Stebbins, Huffer, and Whitford[10] color excesses for this section are generally small, but the stars are bright and near by. We shall accept the value of A_{pg} derived from our own color excesses:

$$A_{pg} = 1.4 \text{ mag/kpc}$$

to a limiting distance of 1500 parsecs.

TABLE 6

MEAN OBSERVED COLOR INDICES IN FIELD 3

m_{pg}	Spectral Type						
	B0–B5	B8–A0	A1–A7	F0–F8	G0–G5	K0–K2	K5–M
8.25	....	−0.06(2)	+0.16(3)	+0.45(1)	....	....	....
8.75	....	− .16(4)	− .16(2)	+ .21(1)	+0.77(1)	....	....
9.25	−0.07(1)	....	+ .12(4)	+ .45(3)	....	+1.32(1)	....
9.75	....	+ .20(1)	+ .29(7)	+ .66(1)	+1.31(1)	+1.31(2)	....
10.25	....	+ .10(4)	+ .20(9)	+ .53(6)	+0.70(3)	+1.38(2)	+2.00(3)
10.75	....	− .17(1)	+ .33(19)	+ .57(14)	+1.01(6)	+1.31(7)	+2.08(8)
11.25	....	+0.42(2)	+ .37(26)	+ .55(19)	+0.89(11)	+1.07(6)	+1.66(4)
11.75	....	....	+0.40(3)	+0.69(1)	+0.67(2)	....	+1.61(1)

TABLE 7

MEAN OBSERVED COLOR INDICES IN FIELD 4

m_{pg}	Spectral Type						
	B0–B5	B8–A0	A1–A7	F0–F8	G0–G5	K0–K2	K5–M
8.25	....	+0.02(2)	....	+0.81(1)	+0.95(2)	....	....
8.75	....	.00(1)	+0.40(2)	+ .72(1)	+0.96(2)	+1.93(1)	....
9.25	....	+ .02(3)	+ .14(7)	+ .52(3)	+0.63(1)	....	....
9.75	....	+ .17(6)	+ .28(4)	+ .39(4)	....	+1.35(4)	+1.31(1)
10.25	....	+ .13(6)	+ .21(4)	+ .73(8)	+1.01(3)	+1.55(3)	+1.90(2)
10.75	+0.46(2)	+ .23(14)	+ .42(13)	+ .57(9)	+0.98(7)	+1.59(4)	+2.08(1)
11.25	+0.73(1)	+ .26(4)	+ .41(23)	+ .47(3)	+0.87(9)	+1.47(3)	+2.12(6)
11.75	....	+0.39(3)	+0.43(13)	+0.46(2)	+1.17(3)	+1.32(1)	+1.42(1)

FIELD 5

Center (1900): $\alpha = 6^h33^m$; $\delta = +16\overset{\circ}{.}8$; $l = 164°$; $b = +6°$

FIELD 6

Center (1900): $\alpha = 6^h40^m$; $\delta = +15\overset{\circ}{.}0$; $l = 167°$; $b = +7°$

FIELD 7

Center (1900): $\alpha = 6^h46^m$; $\delta = +12\overset{\circ}{.}1$; $l = 170°$; $b = +7°$

These three fields are in the zone of galactic latitude +5° to +10° and are free from strong obvious overlying obscuration. Field 5 is probably affected by some irregular

overlying absorption, which, however, seems limited to a considerable number of very small areas. There is some suggestion of star deficiency in the northernmost parts of the field. Fields 6 and 7 are both quite uniform, and the stellar distribution on long-exposure Schmidt plates gives no indication of overlying irregular obscuration.

TABLE 8

MEAN OBSERVED COLOR INDICES

m_{pg}	Spectral Type					
	B8–A0	A1–A7	F0–F8	G0–G5	K0–K2	K5–M
	Field 5					
8.25	+0.08(1)	+0.23(2)	+0.63(1)	+1.48(1)	+1.08(1)	....
8.75	− .12(2)	....	....	+0.92(2)	....	....
9.25	....	+ .14(3)	+0.26(4)	+1.04(2)	+0.90(1)	....
9.75	− .08(3)	− .02(3)	+0.25(4)	+1.21(2)	+1.35(5)	+1.56(1)
10.25	+ .10(2)	+ .06(13)	+0.32(1)	+0.88(4)	+1.06(2)	+1.79(1)
10.75	+ .11(4)	+ .18(15)	+0.51(12)	+0.85(3)	+1.28(2)	+2.20(2)
11.25	+0.27(4)	+ .33(19)	+0.75(9)	+0.64(13)	+1.42(1)	+2.01(5)
11.75	....	+0.45(7)	+1.25(1)	+0.55(3)	....	....
	Field 6					
8.25	+0.05(5)	....	+0.38(1)	....	....	....
8.75	− .22(2)	+0.01(5)	....	....	....	....
9.25	− .21(2)	+ .12(4)	+ .87(1)	....	....	....
9.75	− .10(7)	+ .16(2)	+ .78(4)	+0.81(3)	+1.59(3)	+1.69(1)
10.25	− .10(9)	− .04(12)	+ .36(9)	+ .61(2)	+1.27(5)	+1.69(4)
10.75	− .08(7)	+ .03(18)	+ .28(11)	+ .91(6)	+1.28(5)	+1.42(3)
11.25	− .01(4)	+ .06(19)	+ .28(20)	+ .50(4)	+1.18(2)	....
11.75	+0.16(1)	+0.29(2)	+0.30(1)	+0.44(11)	....	....
	Field 7					
8.25	−0.07(1)	+0.32(1)	+0.69(1)	+0.62(2)	+1.33(2)	....
8.75	....	.00(1)	+0.45(5)	+ .99(4)	+1.83(1)	....
9.25	− .03(3)	+ .04(4)	+0.39(1)	+ .80(2)	+1.24(4)	....
9.75	− .04(3)	+ .08(11)	+0.39(4)	+ .98(6)	+1.43(3)	+1.42(3)
10.25	− .02(6)	+ .25(8)	+0.39(18)	+ .57(2)	+1.07(10)	+1.62(4)
10.75	+ .29(9)	+ .25(14)	+0.63(11)	+ .64(5)	+1.50(2)	+1.44(8)
11.25	+0.27(5)	+0.42(10)	+0.60(13)	+ .93(7)	....	+1.75(7)
11.75	....	....	+1.10(3)	+0.80(1)	....	+1.60(1)

The color indices of Table 8 are all determined from blue and red polar comparisons taken with the 8-inch Ross (IR) camera. In the case of one or more large residuals, special check plates were taken on which remeasures were made of a selected sequence of about thirty stars. The final derived color indices are shown in Table 8. About two hundred stars were measured in each field.

The color excesses appear to be relatively small in all three fields. There are no indications that the extended Taurus-Orion obscurations reach to as far as galactic latitude +7°; they are apparently confined to latitudes south of +3°. The average color indices

of the F–M stars vary irregularly; but, keeping in mind the small numbers of stars in each average and the uncertainties in the spectral classification and in the admixture of giants and dwarfs, we conclude that in only one case is there a justification for the application of an over-all systematic correction; for Field 6 we have applied a systematic correction of +0.10 mag. to all excesses derived from Table 8.

In Field 5 the A1–A7 stars show no effect of reddening to $m = 11.0$. The B8–A0 stars begin to show evidence for reddening at $m = 10.0$, with a maximum indicated value of

$$A_{pg} = 0.8 \text{ mag/kpc}$$

to a distance of 1000 parsecs. There is only a single early B star in the field; the indicated total absorption at 2100 parsecs is 0.6 mag. This would support a considerably smaller value of A_{pg} than the one given above.

The observed excesses in Field 6 are quite small. The brightest B8–A0 and A1–A7 stars indicate some near-by reddening, but this is not confirmed by the more distant stars. There are no data from clusters or early B stars. A value of

$$A_{pg} = 0.5 \text{ mag/kpc}$$

to a limiting distance of 1000 parsecs is a good compromise. There are no data for greater distances.

In Field 7 we again have definite evidence for slight reddening. The B8–A0 and A1–A7 stars indicate the presence of an absorption of about 0.8 mag. at 1000 parsecs. There are, surprisingly, six early B stars in this field with estimated distances of 1200–1900 parsecs. The color indices of none of these stars had previously been measured, but from our results we derive a value of

$$A_{pg} = 0.5 \text{ mag/kpc}$$

to a limiting distance of 2000 parsecs.

There appears to be no reason for separate analysis of these three fields. In what follows, we shall assume that

$$A_{pg} = 0.5 \text{ mag/kpc}$$

to a limiting distance of 2000 parsecs describes average conditions for the section at $l = 163°–173°$; $b = +5°–+9°$.

We may add here that Hubble's counts of faint galaxies[19] indicate a total photographic absorption of 2.4 mag. at $b = +5°$ and of 1.5 mag. at $b = +10°$.

FIELDS 8–11

The original program for the section under investigation included four more fields. Every one of these fields was found to be affected by irregular absorption, and no attempt was made to complete the analysis for these fields. A brief summary of the preliminary results follows.

Field 8 ($\alpha = 5^h52^m$; $\delta = +8°$; $l = 167°$; $b = -7°$).—Long-exposure plates made with the Jewett telescope show this field to be affected by considerable overlying absorption. The "wishbone" dark nebula, shown nicely on Chart 33 of the Ross-Calvert *Atlas of the Milky Way*, in part overlies this field. The dark nebulosity is apparently an extension of the Taurus complex and is presumably relatively near the sun.

The color excesses for this field indicate the presence of considerable reddening. At 300 parsecs the total photographic absorption derived from the color excesses already amounts to 0.7 mag.; the total absorption at 1000 parsecs is of the order of 2 mag.

Field 9 ($\alpha = 6^h02^m$; $\delta = +10.°5$; $l = 166°$; $b = -3°$).—This field shows a fairly uniform surface distribution of the stars, but it is clearly located on the edge of a region of

[19] *Ap. J.*, 79, 8, 1934; *Mt. W. Contr.*, No. 485.

considerable obscuration. The measured color indices give evidence for considerable reddening. At 400 parsecs from the sun the indicated photographic absorption is already equal to 1 mag., whereas the total photographic absorption at 1000 parsecs is about 2 mag. With such a high absorption, the field is not a suitable one for detailed study of the density distribution.

We have already noted above that the cluster NGC 2141, estimated by Trumpler to be at a distance of 4860 parsecs, falls within the limits of this field. If our estimated photographic absorption is correct, this distance should be reduced to about half this value.

Field 10 ($\alpha = 6^h10^m$; $\delta = +2\overset{\circ}{.}5$; $l = 174°$; $b = -5°$).— The measured color indices for this field indicate considerable reddening near by, with 1 mag. of photographic absorption at 550 parsecs. The available evidence does not indicate much of an increase of absorption with distance beyond 550 parsecs.

Long-exposure photographs give evidence for irregular near-by obscuration overlying most of the field. There are some stars with photoelectric colors by Stebbins, Huffer, and Whitford[10] bordering on this field. These give evidence of little reddening, but the long-exposure photographs show them to be in regions free from obvious overlying obscuration. The selection of the center for color studies was not a happy one, and we shall therefore not include this field in our density analysis.

Field 11 ($\alpha = 6^h35^m$; $\delta = +9°$; $l = 171°$; $b = +3°$).—This field is probably the most interesting one of the whole group, but it happens to border on the great dark nebula and is a region of highly irregular obscuration. S Mon and the associated cluster and nebulosities are in this field, and the three remote cepheid variables VW, VZ, and WW Mon are near it.

The results from the available data on color excesses are inconclusive. Three of the stars with excesses measured by Stebbins, Huffer, and Whitford[10] are unreddened (limit 1000 parsecs), whereas a fourth star would indicate 2 mag. photographic absorption at 720 parsecs. Our own color indices indicate an average absorption of the order of 1 mag/kpc, but there are indications of considerable fluctuation over the field. This field should be studied as a part of a more detailed analysis of the distribution of spectra, colors, and related star counts for the regions bordering the dark nebula of Wolf.[3] We plan to undertake this study in the near future.

III. DENSITY FUNCTIONS

From the data on the excess reddening of the stars in the *Henry Draper Extension*, we have succeeded in deriving approximate values for the photographic absorption for seven fields in the section under investigation. It is now of interest to analyze the density distributions for the various spectral subdivisions in this same section of the Milky Way.

In 1945 Bok and Rendall-Arons[1] presented the results of a similar analysis for a field at $l = 185°$, not far from the area under investigation. A complete analysis of the present material will be postponed until the star counts for the section by Father James Connolly, S.J., become available, but it is of interest now to make a comparative study of the stellar distribution for three areas in the present section and for "Region D" of Bok and Rendall-Arons. For purposes of comparison, we reproduce here, as Table 9, Table 13 of the paper by Bok and Rendall-Arons.

Our measured color indices refer in each case to relatively small fields of fairly uniform surface distribution, which appear to be similar to their surroundings in structure and in freedom from overlying localized obscuration. The derived absorptions may therefore be considered as applying to areas larger than those actually covered by the color survey. Furthermore, our color analysis has indicated the existence of fairly similar conditions in several neighboring fields covered by the color survey; we found in the preceding sections that the results are very similar for Fields 2, 3, and 4 and also for Fields 5, 6, and 7, but we found that Field 1 had to be treated separately.

The enlarged regions for which the counts with respect to spectral subdivisions were actually carried out and the assumed absorption characteristics are tabulated in Table 10. For comparison purposes we have also given the data of Bok and Rendall-Arons for

TABLE 9

SUMMARY OF STAR DENSITIES (NUMBER OF STARS PER 1000 CUBIC PARSECS) IN MONOCEROS REGION D

(Corrected for $A_{pg}=0.6$ Mag/Kpc)

d	Spectral Type				
	B8–A0	A1–A7	F0–F2	F5–F8	gG0–gM
50	0.12	0.43	1.3	3.3	0.27
100	.15	.34	0.93	1.9	.27
150	.16	.32	0.76	1.2	.28
200	.18	.27	0.55	0.8	.27
300	.18	.28	0.28	......	.25
400	.17	.27	......	......	.23
500	.15	0.23	......	......	0.19
600	.13	......	......	......	......
700	.13	......	......	......	......
800	.10	......	......	......	......
900	.08:	......	......	......	......
1000	0.06:	......	......	......	......

TABLE 10

THE ENLARGED REGIONS USED FOR THE DENSITY ANALYSES

	Region			
	A	B	C	Mon "D"
Assumed value of A_{pg}	0.3 mag/kpc	1.4 mag/kpc	0.5 mag/kpc	0.6 mag/kpc
Limit to which A_{pg} applies	3000 pcs	1500 pcs	2000 pcs	2000 pcs
Basic color data from fields	1	2-3-4	5-6-7	......
Limits of α and δ	6^h08^m–6^h19^m $+7°$–$+10°$ and 6^h20^m–6^h32^m $+4°$–$+10°$ and 6^h32^m–6^h40^m $+4°$–$+8°$	6^h04^m–6^h24^m $+10°$–$+16°$	6^h37^m–6^h57^m $+5°$–$+17°$ and 6^h20^m–6^h37^m $+13°$–$+18°$	6^h25^m–7^h05^m $-7°$–$+3°$
Average gal. long. and lat.	$l=171°$; $b=0°$	$l=165°$; $b=0°$	$l=186°$; $b=+7°$	$l=182°$; $b=0°$
Total area (sq. deg.)	35	29	84	100

"Region D." It will be noted that Regions A, B, and D are all centered upon the galactic equator, whereas C lies 7° to the north of it.

Counts were made in the *Henry Draper Catalogue* and *Extension* between the limits of α and δ indicated in Table 10. To supplement the data for the brighter stars and to provide the much-needed link between the average distribution for the immediate vicinity of the sun and the stellar distribution at greater distances, we have again used

the counts from a paper by Seydl[20] for the stars brighter than $m = 7.0$ in the zone of galactic latitude 0° to ±10°. All counted numbers were reduced to a unit half-magnitude interval and to a total area of the sky of 100 square degrees. The derived values of log $A'(m)$ were plotted and smooth curves drawn to represent the combined results from Seydl's counts and our own HD and HDE counts. The results are shown in Tables 11–16; the magnitudes used are photographic.

TABLE 11

DERIVED VALUES OF LOG $A'(m)$ FOR THE B8–A0 STARS

REGION	MAGNITUDE														
	4.0	4.5	5.0	5.5	6.0	6.5	7.0	7.5	8.0	8.5	9.0	9.5	10.0	10.5	11.0
A......	9.11	9.50	9.86	0.20	0.50	0.78	1.06	1.29	1.50	1.72	1.91	2.09	2.24	2.38	2.51
B......	9.11	9.50	9.86	0.20	0.50	0.78	1.14	1.43	1.66	1.84	1.98	2.11	2.20	2.19	2.00
C......	9.10	9.49	9.86	0.22	0.51	0.77	0.98	1.20	1.40	1.58	1.75	1.92	2.06	2.15	2.19
D......	9.11	9.49	9.86	0.21	0.54	0.80	1.02	1.30	1.56	1.80	2.03	2.22	2.39	2.58	2.75

TABLE 12

DERIVED VALUES OF LOG $A'(m)$ FOR THE A1–A7 STARS

REGION	MAGNITUDE														
	4.0	4.5	5.0	5.5	6.0	6.5	7.0	7.5	8.0	8.5	9.0	9.5	10.0	10.5	11.0
A....	9.32	9.49	9.70	9.90	0.10	0.32	0.59	+0.89	1.19	1.46	1.70	1.95	2.16	2.36	2.53
B....	9.30	9.48	0.65	9.86	.10	.31	.57	− .82	1.08	1.37	1.70	1.98	2.27	2.52	2.56
C....	9.30	9.47	9.63	9.82	.08	.30	.53	+ .78	1.10	1.39	1.70	2.00	2.25	2.43	2.55
D....	9.33	9.47	9.66	9.87	0.10	0.34	0.58	+0.82	1.04	1.28	1.56	1.87	2.18	2.44	2.63

TABLE 13

DERIVED VALUES OF LOG $A'(m)$ FOR THE F0–F8 STARS

REGION	MAGNITUDE													
	4.5	5.0	5.5	6.0	6.5	7.0	7.5	8.0	8.5	9.0	9.5	10.0	10.5	11.5
A............	9.19	9.44	9.69	9.92	0.18	0.44	0.68	0.92	1.18	1.48	1.78	2.08	2.30	2.42
B............	9.19	9.44	9.70	9.94	.22	.54	.87	1.17	1.48	1.74	1.94	2.08	2.18	2.20
C............	9.19	9.45	9.69	9.94	.18	.48	.75	1.04	1.30	1.59	1.91	2.14	2.31	2.43
D............	9.19	9.44	9.69	9.93	0.18	0.42	0.67	0.91	1.16	1.40	1.66	1.89	2.11	2.27

B8–A0 Stars.—Table 11 shows that for a distance of 1000 parsecs from the sun the densities in D are considerably in excess of those in A, B, and C. We note, for example, that, in spite of a larger value of A_{pg} in D as compared to A, the value of log $A'(m)$ at $m = 11.0$ is greater for D than for A. Whereas in D we previously found average densities 0.6 ⊙ at 1000 parsecs, we have in A an average density of only 0.4 ⊙ at 1000 parsecs. The computed space densities in B agree well with those for A. The effect of the differ-

[20] *Pub. Nat. Obs. Prague*, No. 6, 1929.

ence in absorption for A and B is shown nicely in the small value of log $A'(m)$ for $m = 11.0$. The effect of galactic latitude is noticeable in C. The average density at 1000 parsecs equals 0.3 ⊙ or less, with a continued rapid falling-off indicated. The presence of steep negative density gradients for the B8–A0 stars at $l = 160°–175°$ is established.

TABLE 14

DERIVED VALUES OF LOG $A'(m)$ FOR THE G0–G5 STARS

REGION	MAGNITUDE														
	4.5	5.0	5.5	6.0	6.5	7.0	7.5	8.0	8.5	9.0	9.5	10.0	10.5	11.0	11.5
A......	8.70	8.99	9.28	9.54	9.85	0.16	0.49	0.83	1.15	1.46	1.72	1.96	2.17	2.34	2.51
B......	8.83	9.08	9.33	9.61	9.88	.18	.52	.83	1.14	1.46	1.70	1.91	2.11	2.28	.....
C......	8.84	9.06	9.28	9.51	9.77	.05	.32	.59	0.91	1.23	1.57	1.91	2.18	2.41	.....
D......	8.83	9.10	9.32	9.54	9.78	0.04	0.32	0.60	0.91	1.20	1.50	1.79	2.04	2.21	.....

TABLE 15

DERIVED VALUES OF LOG $A'(m)$ FOR THE K0–K2 STARS

REGION	MAGNITUDE												
	5.0	5.5	6.0	6.5	7.0	7.5	8.0	8.5	9.0	9.5	10.0	10.5	11.0
A.....	9.22	9.56	9.81	0.06	0.32	0.55	0.80	1.03	1.27	1.51	1.75	1.98	2.23
B.....	9.25	9.54	9.83	.11	.36	.64	.88	1.14	1.36	1.55	1.76	1.92	2.07
C.....	9.31	9.55	9.82	.09	.38	.66	.94	1.22	1.48	1.73	1.92	2.09	2.20
D.....	9.34	9.56	9.78	0.05	0.35	0.63	0.89	1.18	1.46	1.75	1.98	2.09	2.16

TABLE 16

DERIVED VALUES OF LOG $A'(m)$ FOR THE K5–M STARS

REGION	MAGNITUDE											
	5.5	6.0	6.5	7.0	7.5	8.0	8.5	9.0	9.5	10.0	10.5	11.0
A...........	8.90	9.13	9.42	9.69	9.97	0.25	0.53	0.85	1.12	1.40	1.67	1.97
B...........	8.85	9.10	9.36	9.59	9.84	.08	.32	.56	0.81	1.06	1.30	1.54
C...........	8.85	9.09	9.36	9.67	0.01	.31	.60	.90	1.17	1.47	1.70	1.95
D...........	8.93	9.16	9.40	9.64	9.92	0.22	0.53	0.86	1.18	1.52	1.76	1.93

A1–A7 Stars.—The values of log $A'(m)$ in all four fields show a striking similarity. A density analysis with the aid of an (m, log π) table, corrected for absorption effects (which have only relatively little influence because of the small distances involved) gives densities of the order of 0.5 ⊙ at a distance of 500 parsecs.

F0–F8 Stars.—The numbers of counted stars were so small that we have considered it advisable to combine the results for the F0–F2 and F5–F8 stars. There is still considerable local variation in the star numbers, with a maximum range of a factor of 2 in the counted numbers.

A density analysis shows that the density gradients in A, B, and C do not have quite so large negative values as the gradient previously derived for D. The average space density of the F0–F8 stars for our section at 400 parsecs from our sun is, however, still less than 0.5 ⊙, thus confirming the existence of steep negative gradients found from the earlier investigations.

G–M Stars.—Because of the uncertainties in the percentages of dwarfs at successive apparent magnitudes, we shall not give here a detailed analysis for space densities. Sections 4 and 5 of the paper by Bok and Rendall-Arons show the kinds of results that may be obtained, if one makes certain assumptions about the percentages of dwarfs; the analysis refers there to "Region D." The most striking difference between D and the new regions, A, B, and C, is that the new regions show a marked excess of G0–G5 stars over D.

For the K0–K2 and K5–M stars, the numbers in A and D are remarkably similar. Region B is poorest in faint K–M stars, with the deficiency becoming especially great for the K5–M stars with m = 9–11.

Preliminary density analyses confirm the results obtained previously for D, viz., that the average space densities are fairly constant over the first 500 parsecs from the sun.

A STUDY OF THE GALACTIC STRUCTURE IN A CLEAR REGION IN CYGNUS

J. J. NASSAU AND DONALD A. MACRAE
Warner and Swasey Observatory, Case Institute of Technology
Received April 2, 1949

ABSTRACT

This paper, like previous ones of the series, is primarily concerned with the study of the fluctuation of the stellar luminosity function. The field under investigation has an area of 11 square degrees with a center at R.A. = $20^{h}00^{m}$, Dec. = $+38.^{\circ}0$ (1950). It is relatively free from space absorption, with the exception of about 1 square degree at its southern boundary.

The photographic and photored magnitudes and the spectral types of 1230 stars were obtained. Stars of spectral type F0 and later, with a few exceptions, were classified either as giants or as dwarfs down to the limiting photographic magnitude of 12.2. For nearly all stars brighter than 11.0 mag., four luminosity classes were used.

The linear absorption coefficient in the clear region (areas A, B, and C) was derived from 683 stars and found to be 0.53 mag. per kiloparsec.

The division of the stars into giants and dwarfs in each spectral group indicates that there is a rapid decrease in the ratio of dwarfs to giants between the F0–F5 group and the G8–K3 group. In the former we have about 83 per cent dwarfs and in the latter about 7 per cent.

Space densities, corrected for absorption, were computed for each spectral group in areas A, B, and C (Table 10 and Fig. 5). The densities were used to compute luminosity functions at distances of 100, 200, 400, and 600 parsecs. These show very little variation with distance. Likewise, no significant differences exist when our results are compared with the standard van Rhijn luminosity function, with the exception of the range of absolute magnitude between -1.5 and $+1.0$. Here the maximum excess in our case in $\log \phi(M)$ is 0.3.

The color excesses of the stars in the obscured region (area D) indicate that an interstellar cloud sets in at about 900 parsecs with a maximum absorption of about 0.9 mag. over and above the general absorption of the other three areas. A comparison between the general star counts to the seventeenth photographic magnitude in area D and in the other areas yields nearly the same value for the total absorption.

An analysis of the space density of the stars in area D indicates that the density for the early-type stars is between two and three times greater than the corresponding density in the other areas.

I. INTRODUCTION

The present investigation is a part of a general program of this observatory dealing in a broad sense with the study of the fluctuations of the stellar luminosity function in fields near the galactic plane. The field under discussion (LF3b) has for its center the point whose 1948 co-ordinates are $\alpha = 20^{h}00^{m}$, $\delta = 38.^{\circ}0$ ($l = 41.^{\circ}8$, $b = +3.^{\circ}2$). It is circular in shape with a diameter of $3.^{\circ}7$ and an area of 10.9 square degrees. The "Great Rift" is 4° east of its center. A portion of a parabola-shaped obscuration is included near its southern boundary; otherwise the area appears to be free of pronounced dark nebulae. Two other regions (LF3 and LF3a), which are part of the same general program, partially overlap LF3b (Fig. 1).

This field was chosen not only on account of our desire to extend and strengthen our data on this interesting part of the Milky Way but also for its relatively high transparency. A group of remote cepheid variables discovered by Baade[1] are in this region.[2] An extensive survey of faint M stars in the same region is now in progress at this observatory. A portion of the survey has been completed.[3]

[1] *Ap. J.*, **79**, 475, 1934.

[2] Oort and Oosterhoff, *B.A.N.*, **9**, 325, 1942.

[3] Nassau and van Albada, *Ap. J.*, **109**, 391, 1949.

FIG. 1.—A reproduction of the Ross *Atlas*. The circles represent: LF3 (*upper left*), LF3a (*lower*), and LF3b (*upper right*). P Cygni is the central star in LF3.

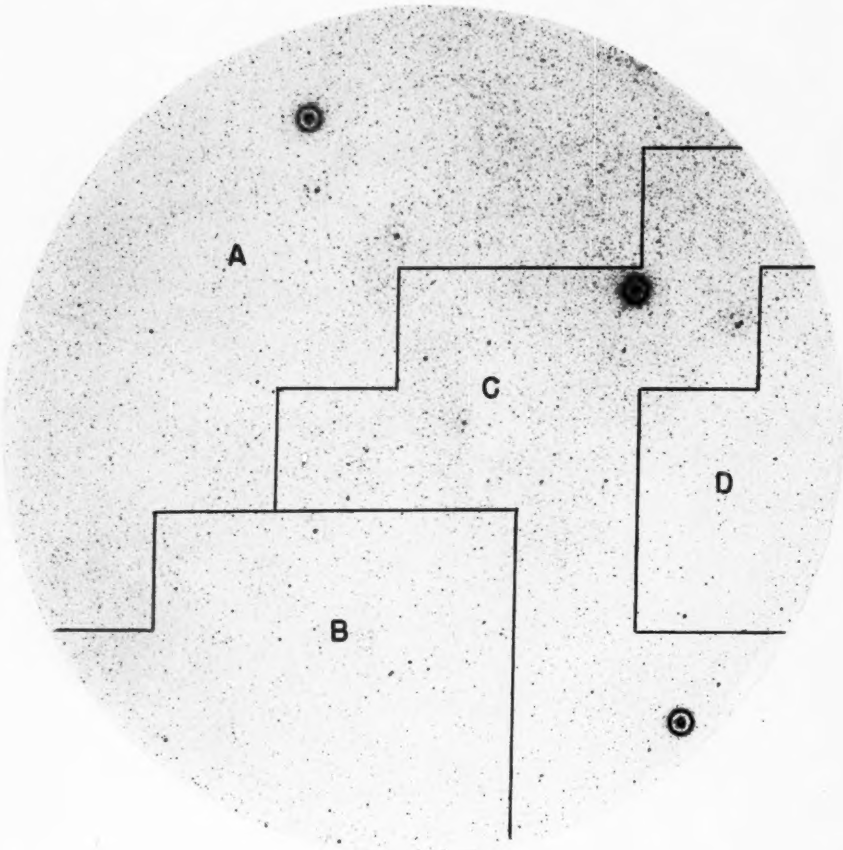

Fig. 2.—Division LF3b into four areas. In this reproduction north is to the left

II. OBSERVATIONAL DATA

MAGNITUDES

The photographic-magnitude sequence was determined by direct comparison with the North Polar Sequence on Eastman II*a*-O plates. Twelve plates yielded a mean error for the mean magnitude of each star of ± 0.07. (Mean errors are used throughout this paper.) The photored magnitudes of the same stars were obtained by direct comparison with a standard photored[4] sequence at the pole. Eastman 103*a*-E plates and a Wratten No. 22 filter were used. Ten independent determinations were made which yielded for the mean error of the mean magnitude of each star the value ± 0.06.

The magnitudes of the field stars were measured on three, and sometimes four, pairs of plates. In each pair, one plate was taken with the telescope east of the piers and the other with the telescope west. The average mean error of the adopted photographic magnitude of each field star was ± 0.10, and the corresponding photored value was ± 0.08. No serious systematic differences in the magnitudes in different parts of the field were observed. Nearly all the photometry was done with a graduated scale of stellar images. The photoelectric densitometer was used in determining the magnitudes of the brighter stars on plates of shorter exposure time.

Although we were able to classify stars fainter than photographic magnitude 12.15, the limit of completeness of our survey is taken as 12.0 mag. The total number of stars available for analysis is 1230.

SPECTRA

The criteria for classification have been described in previous papers.[5, 6] Three or more plates of good quality were examined independently by both of us. These plates (Eastman II*a*-O emulsion, exposure 30 minutes) were taken with the 4° objective-prism arrangement on the Burrell telescope. The width of the spectra was about 0.25 mm. Shorter-exposure plates were taken for study of the bright stars. In many cases we have examined as many as five plates, including some taken with the 2° prism, in order to clear up discrepancies in the classification or to overcome difficulties with overlapping spectra. The adopted spectral class for each star is therefore the average of several determinations.

All stars of spectral class F0 and later were classified either as giants[7] (III) or dwarfs (V), with some exceptions when the stars were too faint or their spectra badly overlapping. For stars of spectral classes F0 and later, with photographic magnitudes brighter than 11.0, four luminosity classes were used.

COMPARISON OF DATA WITH OTHER INVESTIGATIONS

Our magnitudes and spectral classes were compared with the corresponding data obtained from the two overlapping fields, LF3[8] and LF3a;[9] no significant differences were observed. In the case of LF3a, for example, we had in common 215 stars. The average systematic difference (LF3a *minus* LF3b) in m_{pg} for these stars was $+0.05 \pm 0.01$. The average color difference of the 115 stars between magnitudes 9 and 11 for which colors were available in both fields was less than 0.01 mag.

[4] Nassau and Burger, *Ap. J.*, **103**, 25, 1946.

[5] Nassau and Seyfert, *Ap. J.*, **103**, 117, 1946.

[6] Nassau and van Albada, *Ap. J.*, **106**, 20, 1947.

[7] The luminosity notation of Morgan, Keenan, and Kellman, *An Atlas of Stellar Spectra* (Chicago: University of Chicago Press, 1943), is used throughout this paper.

[8] Nassau and Harris, unpublished.

[9] Annear, unpublished.

Only 81 of our stars, mostly bright, are in Schalén's[10] field in Cygnus. A comparison between his photographic magnitudes and ours showed a difference (Uppsala *minus* Case) of 0.08 ± 0.02. Comparing the spectra, we found that stars which we had classified as A0–A5 were classified later by Schalén, in some cases, as late as F5. This might prove of considerable interest, since many of the stars in this region are metallic-line A stars. In the later classes, beginning with F8, there is good agreement between the two systems of classification. The agreement in the luminosity classification in the two systems is also satisfactory.

Comparing the 93 stars between magnitude 9 and 11 common to the *Henry Draper Extension*[11] and our own list, we found a systematic difference (HDE *minus* Case) of +0.04 ± 0.02 mag. As far as we were able to ascertain, there is no scale difference between the two magnitude systems in this region. We found no systematic difference between the two systems of classification, with the exception of the spectra for early-type stars. There is a tendency for our B5 stars to be classified as B8, B9, or even A0 in the HDE. From G8 to K5 we classified earlier by one subdivision. The agreement in the range A0–G5 and among the M-type stars is good.

Our field includes 50 stars in common with the *Henry Draper Catalogue*. With this very limited material it is difficult to draw significant conclusions, but it appears that the tendency observed in the HDE in the case of B5 stars is present in the HD as well.

III. INTRINSIC COLORS

EARLY-TYPE STARS

Our present knowledge of the intrinsic colors of early-type stars appears to be limited. For their determination we drew upon three sources.

Seares and Joyner[12] have obtained the intrinsic photovisual colors (C) of B3–M stars near the pole. The number of stars at the extremes of the range of spectral types is too small to give by themselves reliable mean intrinsic colors, but from A0 to K0 the number of stars in each spectral class is sufficient. Their work has established the intrinsic color index of an A5 star as zero, and we have adopted this result. Table 1, column 2, gives their values for the early-type stars, which must be strengthened, if possible, by data from additional sources.

From King's extra-focal photometry of 100 bright stars[13] we obtained a second estimate of the colors. His values, reduced to zero at A5, are shown in Table 1, column 3.

The photoelectric colors (C_1) of stars brighter than visual magnitude 6.0 and more than 15° from the galactic equator given by Stebbins and Huffer[14] were reduced to the international scale (C) by means of the ratio[12]

$$\frac{C}{C_1} = 1.90 . \tag{1}$$

The zero point was adjusted so that the intrinsic color of a B8 star is equal to -0.29 mag., the value obtained from the two previous determinations. It was felt that this procedure partially overcame the effect of the hydrogen absorption at A0. The results thus obtained are given in Table 1, column 4. Our adopted photovisual colors (col. 5) were obtained by a judicious averaging of the values given by these three determinations.

In order to reduce these color indices to our photored system, we utilized the data obtained for 23 stars between magnitude 6.5 and 10.9 (mostly bright stars of spectral classes

[10] *Uppsala Medd.*, No. 55, 1931.

[11] *Harvard Ann.*, Vol. **100**, No. 1, 1925.

[12] *Ap. J.*, **98**, 261, 1943.

[13] *Harvard Ann.*, Vol. **85**, No. 3, 1923.

[14] *Pub. Washburn Obs.*, Vol. **15**, Part 5, 1934.

between A0 and A5 at the pole) for which photovisual and photored magnitudes were available.[4] The ratio of the photored color index (*RI*) to the photovisual color (*C*) is

$$\frac{RI}{C} = 1.33\,. \tag{2}$$

The intrinsic red indices derived by the use of this ratio are given in Table 1, column 6. The same values are repeated for the sake of completeness in Table 3, second column.

LATER SPECTRAL TYPES

Intrinsic colors for the rest of the main-sequence stars as well as for the giants were obtained as follows. The red magnitudes of 202 stars within about 2° of the North Pole have been determined (unpublished). The photographic magnitudes of these stars and their color indices on the international scale have been given by Seares, Ross, and Joyner.[15] For the spectra we used the classifications given by Nassau and Seyfert.[5] The mean ratio of *RI* to *C* for all these stars was found to be 1.33. The ratio was also calculated for all spectral groups having 10 or more stars each, and no systematic variation with spectral class was found. Since the coefficient of interstellar absorption in the direction of the North Pole has been determined,[5, 12] it was possible to confirm the validity of the ratio 1.33 in the case of intrinsic colors. With this ratio and the color indices obtained by Nassau and Seyfert,[5] the intrinsic red color indices of all stars B8 and later were computed. The resulting intrinsic red indices (RI_i) are given in Table 3, beginning with spectral class A2. The colors of G0 III and G2 III stars were taken from the values of the corresponding dwarfs by adding 0.13 mag.

TABLE 1

INTRINSIC COLOR INDICES

Spectrum	(2)	(3)	(4)	(5)	(6)	Spectrum	(2)	(3)	(4)	(5)	(6)
B0	......	−0.44	−0.47	−0.47	−0.62	B8	−0.29	−0.29	−0.29	−0.30	−0.40
B2	......	− .47	− .43	− .45	− .60	B9	− .23	−0.23	− .24	− .25	− .33
B3	−0.44	− .41	− .40	− .43	− .57	A0	−0.15	......	−0.19	−0.15	−0.20
B5	−0.39	−0.31	−0.36	−0.38	−0.50						

IV. PHOTOGRAPHIC ABSORPTION FROM RED EXCESS

The regions LF3, LF3a, and LF3b contain 31 stars (mostly B0) for which Stebbins, Huffer, and Whitford[16] have determined photoelectric colors. In the same paper Stebbins and his associates give normal colors for stars between B0 and A0. Thus an estimate of the ratio of photored excess (E_r) to the corresponding excess on the photoelectric scale (E_1) could be made. It was found to be 3.12. We are indebted to Mr. Harris[8] and Mr. Annear[9] for the colors of the majority of the stars used in the determination.

The ratio E_r/E_1 was also obtained independently from the data of the six-color photometry of Stebbins and Whitford[17] as follows. From their paper we have $E_1 = 0.130$,

[15] *Pub. Carnegie Inst. Washington*, No. 532, 1941.

[16] *Ap. J.*, **91**, 20, 1940.

[17] *Ap. J.*, **98**, 20, 1943.

$A_{pg} - A_1 = 0.813$, and $A_r - A_1 = 0.411$. (The effective wave length of our red magnitudes is 6200 A.) Therefore,

$$E_r = A_{pg} - A_r = 0.402\ ,$$

$$\frac{E_r}{E_1} = 3.10\ . \tag{3}$$

To obtain the ratio of the total photographic absorption (A_{pg}) to the red excess, we have adopted the mean value $A_{pg}/E_1 = 8.2$ given by van Rhijn,[18] which was the result of an exhaustive discussion of the observational material of many investigators. Combining this with equation (3), we have

$$\frac{A_{pg}}{E_r} = 2.6\ . \tag{4}$$

Stebbins and Whitford[17] showed that the range of A_{pg}/E_1 is from 7.1 to 10.9. Therefore, the range of A_{pg}/E_r is from 2.3 to 3.5. In many of the regions of relatively high obscuration in which investigations have been carried out at this observatory, values of this ratio higher than that adopted yield unreasonable values of the absorption.

V. ABSOLUTE MAGNITUDES

EARLY-TYPE STARS

The problem of assigning absolute magnitudes to early-type stars presents many well-known difficulties. From relatively recent determinations we have chosen three which are semi-independent in observational material and method of treatment. Nordström[19] has collected and discussed the observational material up to 1936. His assigned values are given in the second column of Table 2.

The absolute magnitudes given by Stebbins, Huffer, and Whitford[16] are the values obtained by Plaskett and Pearce and by Strömberg, derived from proper motions of the *General Catalogue* corrected for absorption. In addition to these, they included new values derived from radial velocities and from close pairs of B stars having the same color excess. Their results are given in the third column. Wilson,[20] basing his determinations on the radial velocities of 987 stars and on the proper motions of 1496 stars, obtained absolute magnitudes of early-type stars which are given in the fourth column. The data of Table 2 were plotted, and a smooth curve was drawn. From the curve we read the adopted photovisual absolute magnitudes which are presented in the last column. The corresponding photographic magnitudes, given in the third column of Table 3, were obtained by applying the color indices given in Table 1, column 5.

STARS OF SPECTRAL CLASSES A2–K5

Our source for the absolute magnitudes of stars later than A0 was the work of Russell and Moore.[21] Their values were reduced to photographic magnitudes by making use of the color indices given by Nassau and Seyfert.[5] The resulting absolute magnitudes are collected in the third column of Table 3.

ABSOLUTE PHOTOGRAPHIC MAGNITUDES PER UNIT VOLUME OF SPACE

Table 4 indicates the spectral groups into which the stars were combined for statistical consideration. The dispersion in absolute magnitude for each individual spectral class

[18] *Groningen Pub.*, No. 51, 1946.

[19] *Medd. från Lunds Astr. Obs.*, Ser. II, No. 79, 1936.

[20] *Ap. J.*, **94**, 12, 1941.

[21] *Ap. J.*, **87**, 389, 1938.

was taken as ±0.7 mag. in nearly all cases. This is in line with the values given by Russell and Moore[22] but is somewhat greater than the values given by Wernberg.[23] For the broader spectral groups proper adjustment of the dispersion was made. These values of σ are given in Table 4, third column for dwarfs and fifth column for giants.

TABLE 2

PHOTOVISUAL ABSOLUTE MAGNITUDES OF EARLY-TYPE STARS

Spectrum	Nord-ström	Stebbins	Wilson	Adopted	Spectrum	Nord-ström	Stebbins	Wilson	Adopted
B0	−2.7*	−3.9	−3.1	−3.5	B8	+0.3	−0.8	....	−0.1
B2	−2.0	−3.0	−2.3	−2.3	B9	+ .5	−0.4	....	+ .2
B3	−1.0	−2.2	−1.7	−1.8	A0	+0.3	....	....	+0.5
B5	−0.3	−1.6	−0.8	−1.0					

* Average for B0 and B1.

TABLE 3

INTRINSIC RED INDICES AND PHOTOGRAPHIC ABSOLUTE MAGNITUDES

SPECTRUM	MAIN SEQUENCE		SPECTRUM	MAIN SEQUENCE		GIANTS	
	RI_i	M		RI_i	M	RI_i	M
B0	−0.62	−4.0	G0	+0.46	+4.3	+0.59	+1.1
B2	− .61	−2.8	G2	+0.60	+4.6	+0.73	+1.1
B3	− .57	−2.2	G5	+0.84	+5.2	+0.97	+1.4
B5	− .50	−1.4	G8	+1.04	+5.9	+1.16	+1.5
B8	− .40	−0.4	K0	+1.13	+6.4	+1.32	+1.5
B9	− .33	0.0	K2	+1.21	+6.8	+1.60	+1.6
A0	− .20	+0.4	K3	+1.26	+7.2	+1.73	+1.6
A2	− .08	+1.0	K5	+1.37	+7.7	+1.86	+1.5
A3	− .05	+1.2					
A5	+ .00	+1.7					
F0	+ .15	+2.6					
F2	+ .23	+3.0					
F5	+ .28	+3.4					
F8	+0.40	+3.9					

TABLE 4

ABSOLUTE PHOTOGRAPHIC MAGNITUDES PER UNIT VOLUME OF SPACE

SPECTRUM	MAIN SEQUENCE		GIANTS		SPECTRUM	MAIN SEQUENCE		GIANTS	
	M_0	σ_0	M_0	σ_0		M_0	σ_0	M_0	σ_0
B0	−3.5	0.8	....	....	F0–F5	+3.5	0.8	+2.0	0.8
B2–B3	−2.0	.9	....	....	F8–G2	+4.5	.8	+2.0	.8
B5	−1.0	.7	....	....	G5	+6.0	.7	+2.0	.8
B8–A0	+0.5	.8	....	....	G8–K3	+7.5	0.9	+2.0	0.8
A2–A5	+2.0	0.8	....	....					

[22] *Ap. J.*, **92**, 354, 1940. [23] *Ann. Uppsala Obs.*, Vol. 1, No. 4, 1941.

To reduce the absolute magnitudes of Table 3 to values appropriate to a unit volume of space (M_0), we have applied the Malmquist[24] corrections. The necessary values of $d \log A(m)/dm$ were obtained from Seydl's[25] data. The values of M_0, rounded off to the nearest 0.5 mag., are shown in the second and fourth columns of Table 4.

VI. INTERSTELLAR ABSORPTION IN THE REGION

Guided by the general appearance of our direct photographs of the region and by the prints of the Ross *Atlas*, we divided our field into four areas within each of which the obscuration appeared relatively uniform. These areas are shown in Figure 2. The well-known parabolic obscuration is within the boundaries of area D. In this area the color excesses show a marked difference from those of the remaining areas. It is excluded for the present and will be discussed separately. The other three areas were treated together because no significant differences in the average color excesses were apparent.

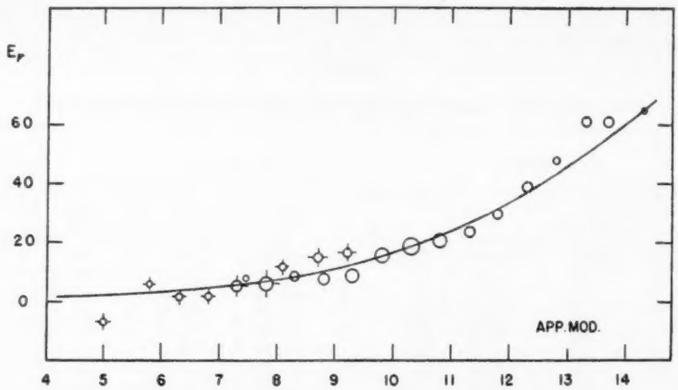

FIG. 3.—Relation between observed color excesses and apparent modulus

Figure 3 shows the relation between the observed color excess and the apparent modulus derived from 683 main-sequence stars (B2–K0) in the three areas. The color excesses for stars from B2 to A5 are represented by open circles, while those for the stars from F0 to K5 are indicated by circles and bars. The radius of the circle in each case is proportional to the square root of the number of stars employed in forming the mean E_r. The grouping of stars was made in half-magnitude intervals in apparent modulus.

A curve drawn through the points in Figure 3 leads directly to the change of absorption with distance. However, small irregularities in such a curve may produce spurious irregularities or clouds in the absorption. It is therefore appropriate to inquire how closely a linear relation between color excess and distance would fit the observed data.

From equation (4) we have

$$A_{pg} = K\,r = 2.6E_r\,,$$

where K is the absorption coefficient in magnitudes per parsec and r the distance in parsecs. From

$$M = m - 2.6E_r + 5 - 5 \log r$$

and

$$\log K = \log (2.6E_r) - \log r\,,$$

[24] *Lund Medd.*, Ser. II, No. 22, 1920.

[25] *Pub. Prague*, No. 6, 1929.

we obtain

$$\log K = -\frac{2.92 + B}{5}, \tag{5}$$

where

$$B = u - v, \tag{6}$$

$$u = m - M, \tag{7}$$

$$v = 5 \log E_r + 2.6 E_r. \tag{8}$$

Each point in Figure 3 leads to a pair of values of u and v and hence to a determination of B. The average value of B yields a final mean value of the absorption coefficient K.

In forming the mean value of B, attention must be paid to the weights to be assigned to each individual value corresponding to each point in Figure 3. The weight should be proportional to the number of stars, n; but, in addition, it must provide for the fact that the same error in E_r produces widely different errors in B at different parts of the curve.

TABLE 5

CALCULATION OF THE LINEAR ABSORPTION COEFFICIENT

u	E_r	v	B	n	w_B	u	E_r	v	B	n	w_B
7.5	0.08	−5.1	12.6	10	1	11.3	0.24	−2.5	13.8	34	13
8.3	.09	−5.0	13.3	23	3	11.8	.30	−1.8	13.6	31	12
8.8	.08	−5.3	14.1	33	6	12.3	.39	−1.0	13.3	34	13
9.3	.09	−5.0	14.3	52	12	12.8	.48	−0.4	13.2	20	8
9.8	.16	−3.6	13.4	65	20	13.3	.61	+0.5	12.8	26	11
10.3	.19	−3.1	13.4	83	30	13.7	.61	+0.5	13.2	23	10
10.8	0.21	−2.8	13.6	55	20	14.4	0.65	+0.8	13.6	4	2

Table 5 shows the color-excess data for the B2–A5 stars and the calculated values of B along with the corresponding weights (w_B). In calculating w_B we have used equations (6), (7), and (8), assuming that the mean errors of E_r and u for a single star were 0.1 and 1.0 mag., respectively. The weighted mean value of B is 13.50. The corresponding value for the F0–K5 dwarfs is 13.31, but the weight of this determination is low on account of the nearness of these stars to the sun. The adopted value of B based on all 683 stars is 13.47 ± 0.11, which leads to an absorption coefficient of 0.53 mag. per kiloparsec. The accidental error of the linear absorption coefficient is only a few hundredths of a magnitude.

The curve in Figure 3, as well as the straight line in Figure 4, was drawn on the basis of this value of the linear coefficient. The fit appears to be satisfactory.

The giant stars from F0 to K3 were not included in the above discussion. Instead, their intrinsic colors were obtained from their observed colors and the adopted interstellar absorption in the region. The mean difference between these and the corresponding intrinsic colors of the dwarfs is +0.05 ± 0.02 mag., a value less than expected (Table 3); but, considering the limited material available (76 stars), we may conclude that the adopted absorption is not seriously in error.

VII. SPECTRAL DATA

The spectrum and magnitude data for the stars in the regions A, B, and C, which comprise 9.9 square degrees, are shown in Tables 6*a* and 6*b*. The tabulation of photographic magnitudes is in intervals of half a magnitude. For stars brighter than 11.0 mag. we recognize three luminosity classes, namely, III, IV, and V. The region had practically

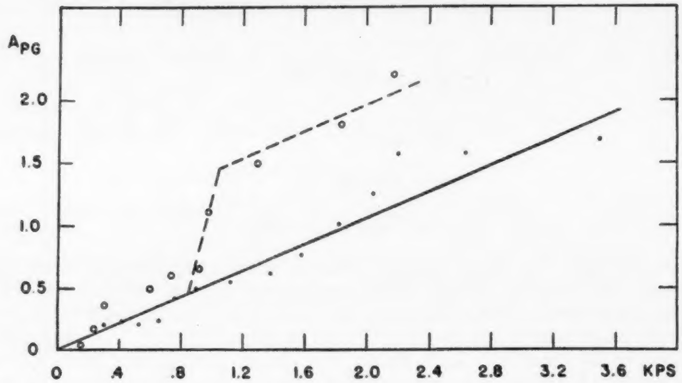

FIG. 4.—Total photographic absorption in regions A, B, and C. The dashed lines show the absorption in region D.

TABLE 6a

REGIONS A, B, AND C

m_{pg}	B0	B2	B5	B8	B9	A0	A2	A3	A5	F0				F2				F5				F8				G0			
										V	IV	III	Un	V	IV	III	Un	V	IV	III	Un	V	IV	III	Un	V	IV	III	Un
≤6.0		2	1																										
6.25			1																										
6.75			1			1	1																						
7.25								1	1	1																			
7.75			2	2	1	1													1										
8.25		4	1	2		3	1																						
8.75		3	1		4	5	1	1	2									1											
9.25		3	3	7	3	3	1	1								1		2								1			
9.75		4	7	2	8	10	6	8	3	2	2			1		1		3				1				3	1		
10.25		4	6	3	8	8	13	4	7	7	1	2						3	2	1			2	1		2		1	
10.75	1	6	13	3	9	17	13	9	16	6	2			6		2		6		2		8		2		6	1	2	2
11.25		10	11	13	9	18	16	17	8	10		2	1	7		3	5	14		2	7	17		4	5	8			1
11.75	1	3	20	14	3	20	13	18	19	9			10	9		3	12	10		1	20	18		2	14	10		3	11
12.1		1	13	5	3	7	10	9	5	2			6	2		3	3	3		1	9				10	5			12
Total	2	40	80	51	48	93	75	68	61	37	5	4	17	25	0	13	20	42	3	7	36	44	2	9	29	35	2	6	26

TABLE 6b

REGIONS A, B, AND C

m_{pg}	G2				G5				G8				K0				K2–K3				K5				M	
	V	IV	III	Un	V	IV	III	Un	V	IV	III	Un	V	IV	III	Un	V	IV	III	Un	V	IV	III	Un	V	III
≤6.0																										
6.25																										
6.75																										
7.25					1										1				1							
7.75					2										1				1							
8.25							1								1											
8.75							1										1									2
9.25						1	1			1					2				1							1
9.75										1	3		1		5											
10.25		1			1		2		1	1	4				2				2							
10.75		1			4	1	4	1		5	12		2	4	11				5			1	2			5
11.25	3	3		1	4		3	1	1		13	1	1		7	2			8	2			2			
11.75	2	1		2	3		7	6			13	1			6	2			7				1			1
12.1	4			2															2	1					1	
Total	9	6	0	5	15	2	19	8	2	8	45	2	4	4	36	4	1	0	27	3	0	1	5	0	1	9

no supergiants. For stars fainter than 11.0 mag. we give two classes only; where we were able to designate stars as class IV we included them with the dwarfs for stars up to G2 and with the giants for stars of class G5 and later. We were unable to assign luminosity classes to a number of stars, primarily because of overlapping spectra. Such stars are included in the column marked "Un."

For region D, which comprises 0.96 square degrees, the corresponding data are given in Table 7. F0–G2 stars classed as IV were grouped with the dwarfs, while for G5 IV and later this class was grouped with the giants.

VIII. PERCENTAGES OF DWARFS

The percentage of dwarfs for various spectral and apparent magnitude groups as obtained from the observational data of LF3b are listed in the left-hand part of Table 8. These data refer primarily to the faint stars and are subject to accidental fluctuations,

TABLE 7

REGION D

m_{pg}	B0–B2	B5	B8–A0	A2–A5	F0–F5			F8–G2			G5 III	G8–K3		TOTAL
					V	III	Un	V	III	Un		III	Un	
7.75	1													1
8.25	1													1
8.75				1								1		2
9.25	1			1	1									3
9.75	1	3	1	4	1			1				1		12
10.25	2	1	5	3	1						1	1		14
10.75		2	7	3	5			2				3		22
11.25	3	3	8	7	5	1	2	3	1	2	1	3		39
11.75		3	7	2	4		2	5		1	3	5	1	33
12.1		1	1	3	1			3		2				11
Total	9	13	29	24	18	1	4	14	1	5	5	14	1	138

especially in the G8–K3 group, where the number of stars is small. Some procedure must be found for smoothing the figures and, more important, for extrapolating to the brighter stars for which little data are available.

It is clear that the decrease in percentage of dwarfs with advancing spectral type for a single magnitude interval depends primarily on the mean absolute magnitudes of the various spectral groups and to some extent on the relative numbers of giants and dwarfs per unit volume of space. The second effect will be negligible if the absolute ratio of giants to dwarfs is constant for all spectral classes, but this cannot be assumed, and hence it is impossible to predict the change of percentage of dwarfs with spectral group. Our density analysis suggests, however, that the ratio is indeed nearly constant.

It is also apparent that the increase in percentage of dwarfs with increasing apparent magnitude within a spectral group is partly due to the effect of whatever absorption is present. The more distant giants will be obscured, while the fainter dwarfs will be unaffected, and their numbers will increase with apparent magnitude more rapidly than will the giants. In addition, variation of the space density of the giants or dwarfs with distance will affect the percentages of dwarfs for various apparent magnitudes.

It has been clearly brought out by Bok and Rendall-Arons,[26] however, that, if the numbers of dwarfs are well determined at the tenth to eleventh magnitude, it is possible

[26] *Ap. J.*, **101**, 280, 1945.

to predict the percentages of dwarfs among the brighter stars on a very plausible assumption. The F8–G2 dwarfs brighter than $m_{pg} = 11.5$ will be closer than 200 parsecs, and the later-type dwarfs brighter than the same limit will be still closer. It is reasonable, therefore, to assume in the present state of our knowledge that the density of these dwarfs is constant down to these magnitudes. In our case the number of dwarfs of 10–11 mag. is well determined; hence the number of dwarfs in the brighter magnitude intervals for each spectral group can be calculated. Thus we were able to predict the percentages of giants and dwarfs and to carry out the density analysis for the giants. It was assumed that the density for the dwarf F8–G2, G5, and G8–K3 stars was uniform over the first 200 parsecs. The resulting percentages of dwarfs in the three spectral groups for the brighter stars and the smooth values for the fainter stars as given in the right-hand side of Table 8 were calculated on this basis. The F0–F5 dwarfs extend over too great a distance to make the same assumption valid; the percentages of dwarfs for this group were assumed to remain constant at 83, as observed in the 10–12-mag. range.

TABLE 8

PERCENTAGE OF DWARFS

Spectra	m_{pg}					
	Observed Data		Smoothed Values			
	10.5	11.5	6–8	8–10	10–11	11–12
F0–F5	85	85	....	83	83	83
F8–G2	80	85	72	75	77	82
G5	45	40	23	23	31	42
G8–K3	7	4:	5.5	6.5	8.5	10

When the density analysis for the giants was carried out, after applying the percentages of the right-hand side of Table 8, it was found that the counts could be satisfied by a constant density. It is worth emphasizing that this constant density for the giants is not in itself an assumption. The density for the giants at 700 parsecs is quite independent of any assumption about the density of the dwarfs. The rapid decrease with advancing spectral type in the ratio of the number of dwarf to giant stars shown by the data in Table 8 has been noted in previous investigations. In the case of the stars near the North Pole the values obtained by Nassau and Seyfert[5] show this decrease, but it is a somewhat more gradual one, as would be expected from the fact that this region has a galactic latitude of 28°.

IX. ADOPTED VALUES OF LOG $A'(m)$

In order to obtain the value of log $A'(m)$[27] for the bright stars, we have used the data of Seydl[25] and the results of a separate analysis from the data of the *Henry Draper Catalogue*. In the latter case the spectrum data for an area of 100 square degrees was used in the region of our field. The magnitudes used in the Seydl counts were reduced to photographic. The separation into giants and dwarfs within each spectral group was made by means of the data of Table 8.

The data for the fainter stars were taken directly from Tables 6*a* and 6*b*. The unclassified stars given in these tables were divided into giants and dwarfs in accordance

[27] $A'(m)$ is the number of stars per 100 square degrees of the sky between $m - \frac{1}{4}$ and $m + \frac{1}{4}$, where m is the apparent photographic magnitude.

with Table 8. The values of log $A'(m)$ thus obtained were plotted against magnitude, and smooth curves were drawn through the points. Except for the B2 and B5 groups, no marked discontinuities were observed where the data of the various sources overlapped. Table 9 presents the smoothed values of log $A'(m)$ which were used in the succeeding analysis.

X. CALCULATION OF DENSITIES

The calculation of the space densities from the observed numbers of stars is a classical problem, and many procedures are available. We have used one described recently by Malmquist[28] in which the numbers of stars in the various distance shells are read directly from the log $A'(m)$-curve. The effect of the small dispersion in absolute magnitude for stars of a given spectral group is allowed for in this method by entering the log $A'(m)$-

TABLE 9

ADOPTED LOG $A'(m)$ IN LF3b

m_{pg}	B0–B2	B5	B8–A0	A2–A5	F0–F5		F8–G2		G5		G8–K3	
					g	d	g	d	g	d	g	d
4.0	9.37	.....	9.17	9.22	.....	.....	.....	.....	.....	.....	.....	.....
4.5	9.63	.....	9.54	9.47	.....	.....	.....	.....	.....	.....	.....	.....
5.0	9.91	.....	9.89	9.72	.....	.....	.....	.....	.....	.....	.....	.....
5.5	0.14	.....	0.22	9.98	.....	.....	.....	.....	.....	.....	.....	.....
6.0	0.38	0.47	0.55	0.23	.....	9.82	9.00	9.32	9.01	8.47	9.72	8.45
6.5	0.60	0.63	0.84	0.48	.....	0.12	9.28	9.64	9.32	8.78	0.00	8.75
7.0	0.80	0.79	1.11	0.73	.....	0.42	9.55	9.96	9.61	9.08	0.28	9.05
7.5	0.98	0.95	1.37	0.98	.....	0.70	9.86	0.26	9.96	9.38	0.57	9.35
8.0	1.14	1.11	1.60	1.23	.....	0.97	0.14	0.56	0.25	9.69	0.85	9.65
8.5	1.30	1.28	1.83	1.48	0.49	1.22	0.42	0.85	0.53	0.00	1.11	9.95
9.0	1.42	1.44	2.03	1.73	0.75	1.47	0.67	1.15	0.81	0.29	1.42	0.25
9.5	1.53	1.60	2.18	1.98	1.01	1.72	0.95	1.43	1.08	0.59	1.68	0.55
10.0	1.62	1.76	2.31	2.24	1.27	1.97	1.22	1.72	1.31	0.88	1.93	0.85
10.5	1.70	1.92	2.40	2.46	1.52	2.22	1.47	2.02	1.52	1.17	2.18	1.15
11.0	1.77	2.09	2.49	2.61	1.78	2.47	1.72	2.31	1.70	1.45	2.42	1.45
11.5	1.81	2.25	2.56	2.71	2.04	2.72	1.95	2.60	1.88	1.75	2.68	1.75
12.0	1.84	2.41	2.62	2.75	2.30	2.97	2.15	2.88	2.05	2.03	2.92	2.05

curve with an adjusted value of m. The effect of the absorption was determined by the method of Seeliger.[29]

If the variable m_0 is defined by the equation

$$m_0 = M_0 - 5 + 5 \log r_0 ,$$

where M_0 is the mean absolute magnitude of the stars considered, per unit volume of space, Malmquist has shown that the number of stars at the distance r_0 corresponding to m_0 is given by

$$n(m_0) = \frac{\sigma_0}{\sigma_m} A'(m) . \tag{9}$$

In this formula

$$m = m_0 + \frac{\sigma_0 \epsilon_m}{\sigma_0 + \sigma_m} .$$

[28] *Uppsala Medd.*, No. 84, 1942.

[29] See Bok, *The Distribution of the Stars in Space* (Chicago: University of Chicago Press, 1937), p. 14.

The quantity ϵ_m is the familiar Malmquist correction[24] to change M_0 into M_m, and σ_m is the corresponding corrected value of σ_0, the dispersion per unit volume of space, viz.,

$$\epsilon_m = M_m - M_0 = -\sigma_0^2 \frac{d \ln A'(m)}{dm},$$

$$\sigma_m^2 = \sigma_0^2 \left[1 + \sigma_0^2 \frac{d^2 \ln A'(m)}{dm^2}\right].$$

The assumptions under which equation (9) is valid are that the frequency function of the absolute magnitudes in an element of space is of the Gaussian form and independent of the distances of the stars and, further, that the log $A'(m)$-curve can be represented by an expression of the first or second degree in m. We have found that the second assumption does not impose a serious restriction on the analysis in this field.

Malmquist's formula has been modified slightly for greater convenience in the analysis. When the second derivative of the log $A'(m)$-curve is small, terms in μ^2 can be neglected, and equation (9) takes the form

$$\log n(m_0) = -\text{Mod.}\cdot\mu + \log A'\left(m_0 + \frac{\epsilon_m}{2+\mu}\right), \tag{10}$$

where

$$\mu = +\frac{\sigma_0^2}{2\,\text{Mod.}} \cdot \frac{d^2 \log A'(m)}{dm^2} = \frac{\sigma_m}{\sigma_0} - 1$$

and

$$\epsilon_m = -\frac{\sigma_0^2}{\text{Mod.}} \cdot \frac{d \log A'(m)}{dm}.$$

If the log $A'(m)$-curve is a straight line, $\mu = 0$, and the formula is further simplified.

The quantities μ and ϵ_m are to be evaluated at the point

$$m = m_0 + \frac{\epsilon_m}{2+\mu}.$$

They are most conveniently determined by numerical differentiation of the values read from the smoothed log $A'(m)$-curve. Next a graph relating m to m_0 is constructed, and the right-hand side of equation (10) is computed for values of m_0 differing by five-tenths over the range of the counts. The effect of the increasing volume of the successive shells is allowed for, and the resultant densities are ready to be corrected for the effect of absorption.

As a test of the method, an independent analysis of the B8–A0 stars was carried out by means of an $(m, \log \pi)$ table. No significant differences could be found in the two analyses. The Malmquist method has much to recommend it in its directness and its definitiveness. The $(m, \log \pi)$ table retains the advantage of showing clearly at all times how the stars of each magnitude group are distributed in space.

XI. RESULTS OF DENSITY ANALYSIS

The results of the density analysis are given in Table 10 and Figure 5. In the latter the ordinates represent the logarithms of the number of stars per 1000 cubic parsecs; the abscissae are distances in parsecs. The dotted portions of the curves and the figures in parentheses in the table represent the less certain determinations.

The densities for the early-type stars all show a decrease with distance from the sun. It is most marked in the case of the B8–A0 stars. The log $A'(m)$-curves for the B2 and B5

TABLE 10

SUMMARY OF DENSITIES, STARS PER 1000 CUBIC PARSECS

r	B2	B5	B8–A0	A2–A5	Main Sequence F0–F5	Main Sequence F8–G2	Main Sequence G5	Main Sequence G8–K3	Giants F0–F5	Giants F8–G2	Giants G5	Giants G8–K3
20	......	......	......	......	(3.4)	2.4	2.8	15.2	......	......	......	......
60	......	......	......	(0.64)	2.0	2.4	2.8	15.2	......	......	......	......
100	......	......	(0.120)	.53	1.65	2.4	2.8	15.2	......	0.030	0.044	0.170
150	......	......	(.161)	.45	1.40	2.4	2.8	......	......	.030	.044	.170
200	0.0050	......	.174	.42	1.28	2.4	......	......	......	.030	.044	.170
300	.0053	(0.021)	.174	.37	1.15	2.4	......	......	0.038	.030	.044	.170
400	(.0050)	.015	.162	.37	1.08	......	......	......	.038	.030	.044	.170
500	(.0047)	.012	.144	.40	(1.05)	......	......	......	.038	.030	.044	.170
600	(.0044)	.010	.120	.37	......	......	......	......	.038	.030	.044	.170
800	(.0038)	.0075	.080	(0.22)	......	......	......	......	0.038	0.030	0.044	0.170
1000	.0031	.0062	.058	......	......	......	......	......	......	......	......	......
1200	.0028	.0055	.041	......	......	......	......	......	......	......	......	......
1500	.0021	.0048	(0.027)	......	......	......	......	......	......	......	......	......
2000	.0015	(.0043)	......	......	......	......	......	......	......	......	......	......
2500	.0009	(0.0041)	......	......	......	......	......	......	......	......	......	......
3000	0.0007	......	......	......	......	......	......	......	......	......	......	......

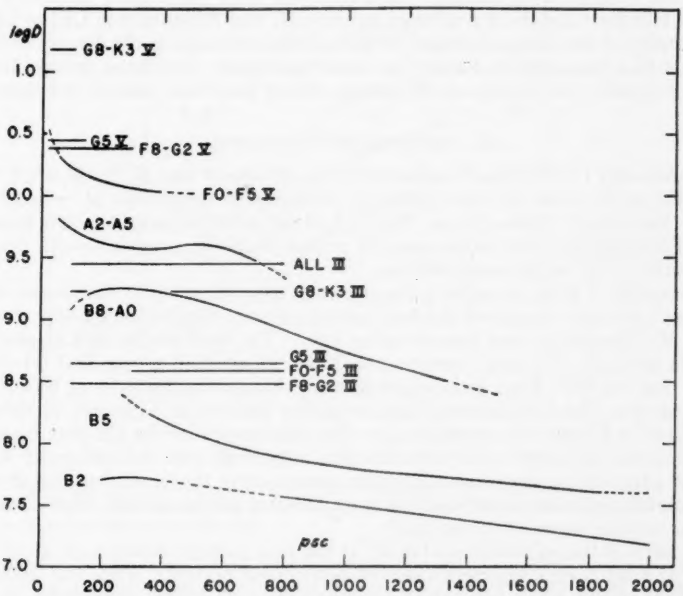

FIG. 5.—Logarithm of densities per 1000 cubic parsecs plotted as a function of the distance in parsecs.

stars were less satisfactory, but there is nevertheless no doubt of the reality of a negative density gradient for these stars. Some of this effect can be attributed to the variation of density with distance from the galactic plane, since our region is at galactic latitude $+3\overset{\circ}{.}2$.

It is appropriate to call attention to the uncertainties in the density analysis due to the lack of separation of B0, B2, and B5 stars at the faint limit of the *Henry Draper Catalogue*. Stars designated as "B" in this catalogue were arbitrarily divided equally between B2 and B5. Furthermore, the Seydl counts for B2 stars are averages for a zone 10° on either side of the galactic plane. Because these stars are so closely concentrated to this plane, the average number per square degree will not be representative except for the very brightest stars. This is also true for the counts obtained from the 100 square degrees around our field that were taken directly from the HD. The counts of B5 stars will be affected in the same way but to a lesser extent. Finally, there is a certain amount of arbitrariness in combining our counts of B stars with the counts for the brighter stars averaged over all longitudes in view of the well-known clustering of these stars.

The constant densities of the giant stars would have to be modified if different percentages of giants and dwarfs are found to exist among the apparently bright stars. The densities of the giants at 600–800 parsecs and the densities of the dwarfs at 100–200 parsecs are based on observed numbers of these stars. The absorption has virtually no effect on the derived densities of the dwarfs.

There is a gradual progression in the densities from one end of the spectral sequence to the other which will be recognized as reflecting the general character of the luminosity function for the stars at large. The least luminous stars outnumber the brightest by a factor of the order of 3000, although the latter seem to be particularly numerous in this field. In LF3b there are about five times as many B2 and B5 stars as in LF1 or LF2.[30]

The density of the giants of classes F0–K3 is about the same as the density of the A2–A5 stars, which have approximately the same luminosity. The latter group includes a number of metallic-line A stars which perhaps should have been treated as F stars in the analysis.

XII. THE LUMINOSITY FUNCTION

The luminosity function $\phi(M)$ is defined by the statement that $\phi(M)\Delta M$ is the number of stars per cubic parsec between absolute photographic magnitude $M - \frac{1}{2}\Delta M$ and $M + \frac{1}{2}\Delta M$. The data of Table 10 and Figure 5, along with the mean absolute magnitude (M_0) and dispersions of the various spectral groups (Table 4), provide us with the means of calculating $\phi(M)$ at various distances.

The numbers of stars per cubic parsec for each spectral group at the chosen distance were spread out over a range of absolute magnitude according to the appropriate values of σ and M_0. The giants were treated as one group. The numbers for each absolute magnitude in intervals of 1 mag. were summed over all spectral groups and tabulated as $\phi(M)$ at that distance. Four such functions were obtained at distances of 100, 200, 400, and 600 parsecs. The formulation of the luminosity function at a distance of 100 parsecs is illustrated in Figure 6, in order to show the roles played by the absolute magnitudes and dispersions. A change in the mean absolute magnitude for a spectral group will have a marked effect on the luminosity function because both the density of this group and the absolute-magnitude range to which it contributes will be altered. This effect is discussed in another paper of this series.[31]

The results of the calculations of $\phi(M)$ at the four chosen distances are given in Figure 7. The solid curves represent the well-determined portions, while the dashed portions refer to regions where less certain densities were used. These uncertainties are due to

[30] McCuskey and Seyfert, *Ap. J.*, **106**, 1, 1947.

[31] McCuskey, *Ap. J.*, **109**, 414, 1949.

the unknown numbers of dwarfs at distances of 400 and 600 parsecs and to the fact that the number of highly luminous stars at 100 and 200 parsecs is poorly determined. No serious extrapolation of the density-curves was made in any of the solutions for $\phi(M)$.

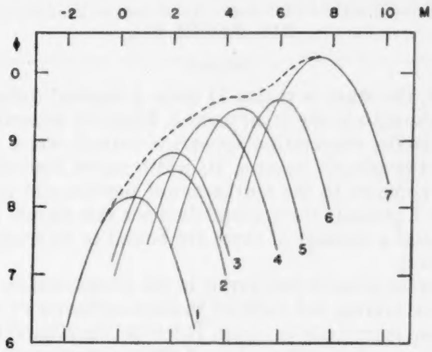

FIG. 6.—Formation of the luminosity function (at 100 parsecs). The abscissa gives the absolute magnitude, the ordinate the values of log $\frac{1}{4}$ ϕ (M). Curves: *1*, B8–A0 stars; *2*, all giants; *3*, A2–A5; *4*, F0–F5; *5*, F8–G2; *6*, G5; *7*, G8–K3. The luminosity function is shown by the dotted curve.

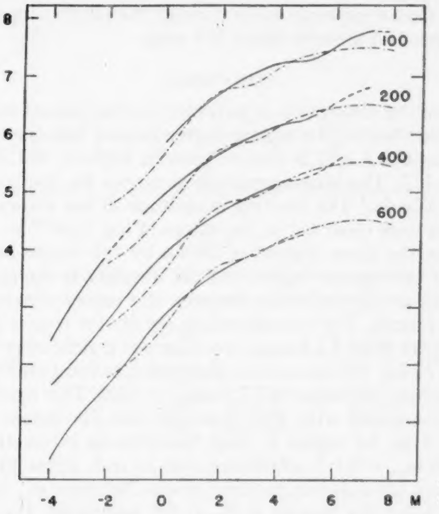

FIG. 7.—Luminosity functions at 100, 200, 400, and 600 parsecs. The ordinate log ϕ (M) for the curve at 100 parsecs is shown. The scales for the other distances are displaced downward by 1, 2, and 3 units. The abscissa gives the absolute magnitude.

A comparison of our results with van Rhijn's luminosity function[32] (dots and dashes, Fig. 7) shows a general agreement over nearly all the range of M. The two determinations differ in shape, but the curves crisscross one another in such a way as to leave the total number of stars per cubic parsec roughly the same. Between absolute magnitudes

[32] *Groningen Pub.*, No. 47, p. 17, 1936.

0 and -2 (B5 stars) we find an excess in our field at 200 and 400 parsecs amounting to three- or four-tenths in the logarithm; but this is reduced at 600 parsecs, where the decreasing density of the early-type stars comes into play.

XIII. REGION D

COLORS

As has been stated, the stars in region D show a marked difference in color excess when compared with the stars in the other regions. From the general appearance of direct photographs, an interstellar obscuration appears to extend over a number of degrees in a direction parallel to the galactic equator. Its width varies from about 1° to 4° or more. Our present study is confined to the northernmost portion and covers an area of 0.96 square degrees. Table 7 presents the spectral data for this region. In all, we are dealing with only 138 stars, and a number of these are bound to be foreground stars with respect to the obscuration.

In order to examine for possible field errors in the determination of the colors of these stars, we computed the average red index of 16 main-sequence F5 and F8 stars brighter than 11.0 photographic magnitude in region D and in the adjacent region C. The average was obtained by first reducing the colors of F8 stars to that of F5. The results were: *RI* (region D) = 0.30 mag., and *RI* (region C) = 0.25 mag. No serious field error in the colors is indicated because the intrinsic red index of an F5 star is 0.28 mag.

The open circles of Figure 4 show the results of the color-excess analysis in this region. The two broken lines drawn approximately through the points suggest that the cloud sets in at about 900 parsecs and absorbs about 0.9 mag.

STAR COUNTS

Another estimate of the absorption is provided by the general star counts. Four areas were chosen, each three-tenths of a square degree in area and one in each of the four regions. The areas in regions A and B were at galactic latitude $+3.^\circ0$, and the areas in regions C and D at $+1.^\circ7$. The blue-magnitude sequence for the counts was determined by Nassau and van Albada.[3] The limiting magnitude of the stars counted was 17.0. No significant differences were observed in the values of log $A(m)$[33] for regions A, B, and C; the average curve for the three regions is shown by full circles in Figure 8, where the ordinate is log $A(m)$ per square degree and the abscissa is the apparent photographic magnitude. We found no discontinuity between the values obtained from our spectral survey and the star counts. The corresponding results for region D are shown by open circles. For stars fainter than 12.5 mag. we observed a deficiency of stars in region D, obviously due to the cloud. The amount of absorption as compared with the other regions slowly increases, reaching the value of 0.7 at $m_{pg} = 16.0$. This result is of the right order of magnitude when compared with that obtained from the colors.

The curve of log $A(m)$ for region D (Fig. 8) shows an interesting excess of stars between $m_{pg} = 9.5$ and $m_{pg} = 11.5$, which seems to be real. Table 11 gives the numbers of stars per square degree for different spectral groups between $m_{pg} = 9.5$ and $m_{pg} = 11.5$. The second column is for the regions A, B, and C combined; the third column is for a region bordering region D; and the fourth column is for region D. The percentage excess of stars in region D when compared with the three regions combined is given in the last column. It appears that the early-type stars are those which contribute to the excess. In our studies of LF3 and LF3a, which are adjacent areas and at lower latitude, we found an excess of early-type stars over other areas in the Milky Way.

In spite of the limited material available, an analysis of the stellar density in this region was made, first, from our spectral data and, second, from the general star counts.

[33] $A(m)$ is the number of stars per 100 square degrees of the sky between $m-\frac{1}{2}$ and $m+\frac{1}{2}$.

ANALYSIS OF B5–A5 STARS IN REGION D

The analysis was carried out by means of an (m, log π) table. The sudden increase in the absorption and the fact that the distribution of M is not Gaussian make this method of analysis more suitable. The luminosity function of the B5–A5 stars at r = 400 parsecs was calculated from the results of our density analysis in the clear region. It has a maximum at $M_0 = +2$ and is asymmetric with a larger number of stars on the side of smaller M. With this luminosity function an (m, log π) table was constructed, and the general absorption of 0.53 mag. per kiloparsec was introduced. The analysis revealed the gradual decrease in density of the B5–A5 stars from 400 parsecs in agreement with what had been found before.

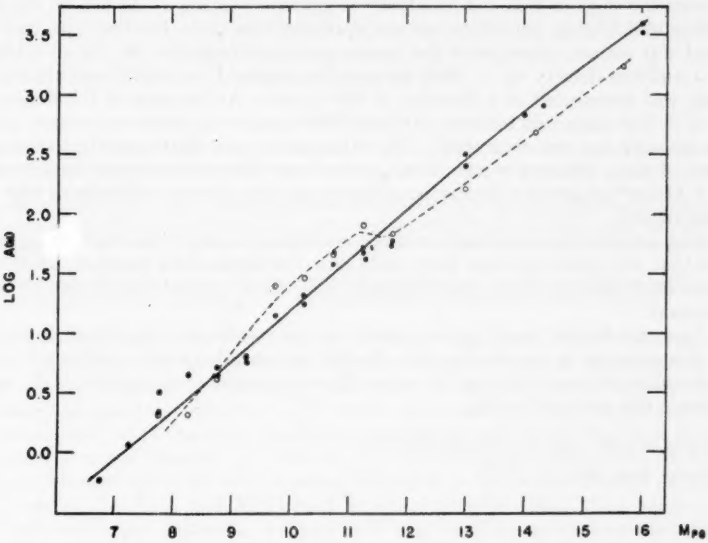

FIG. 8.—Star counts for regions A, B, and C are shown as full circles and for region D as open circles

TABLE 11

NUMBER OF STARS PER SQUARE DEGREE BETWEEN m_{pg}=9.5 AND m_{pg}=11.5

Spectrum	Regions A, B, C	Region near D	Region D	Excess (Per Cent)	Spectrum	Regions A, B, C	Region near D	Region D	Excess (Per Cent)
B0–B2....	2.5	9	6	140	F0–F5.....	10.0	12	15	50
B5........	3.7	5	9	143	F8–G2....	7.6	6	9	18
B8–A0....	10.7	12	21	96	G5........	2.1	5	2	....
A2–A5....	11.0	10	17	54	G8–K3....	9.4	15	8	....

A cloud of 0.9-mag. thickness was then introduced in front of the 1000-parsec shell, and the density was adjusted to fit the counts of the B5–A5 stars in region D. It was

found necessary to increase the density in the 630- and 1000-parsec shells to three times that previously obtained in order to provide a satisfactory representation.

ANALYSIS OF GENERAL STAR COUNTS IN REGION D

The basis of the analysis for the general star-count material was a luminosity function taken from the work of Bok and MacRae[34] at galactic latitude 2°. As before, the general absorption of 0.53 mag. per kiloparsec was applied to the table. For the three regions the observed star counts agreed with the counts predicted from the (m, log π) table, indicating a uniform density up to 2500 parsecs. For region D an additional absorption of 0.9 mag. was introduced at a distance of 900 parsecs. An increase in the density by a factor of 2–3 at distances between 600 and 1000 parsecs satisfied our counts and is in agreement with our previous result. The stars which contribute mostly to the greater numbers of stars between 9 and 12 mag. are those between absolute magnitudes -1 and $+3$. Miller[35] observed a similar excess in the number of stars in discussing star counts near our region.

We may add that an examination of the individual colors of the stars in region D indicated that the more luminous stars contribute the larger color excesses, while the less luminous stars seem to have nearly normal colors when the general absorption is taken into account.

We leave for future investigation, based on the combined data for all three LF regions, the question as to whether this density increase is closely associated with the parabolic obscuration which lies in region D or is a general characteristic of very low latitudes in this part of the sky.

[34] *Ann. New York Acad. Sci.*, **42**, 219, 1941.

[35] *Harvard Ann.*, **105**, 297, 1937.

THE SPECTRUM OF HD 187399

Paul W. Merrill
Mount Wilson and Palomar Observatories
Received February 24, 1949

ABSTRACT

Bright hydrogen lines were discovered at Mount Wilson in 1921. A few slit spectrograms at several observatories showed a considerable difference between the displacements of dark hydrogen lines and those of other elements.

The present study with higher dispersion shows that the star is a spectroscopic binary with a period of 28 days and a velocity range of 209 km/sec. There are two sets of dark hydrogen lines, both of variable intensity, one of which usually yields the same velocity as the lines of other elements, while the other has a nearly constant negative displacement.

The facts suggest that the binary orbit is enveloped by a cloud of incandescent hydrogen whose outer absorbing layers are rapidly expanding. The system resembles β Lyrae in certain respects.

Bright hydrogen lines were discovered in the spectrum of HD 187399[1] from an objective-prism photograph of the $H\alpha$ region[2] taken at Mount Wilson on September 6, 1921. The first slit spectrogram was probably that taken at Mount Wilson on April 9, 1924, with a one-prism spectrograph attached to the 60-inch telescope. On this plate, $H\beta$ had a bright component, while the other hydrogen lines were wholly dark. The dark hydrogen lines yielded a radial velocity of -66 km/sec, lines of other elements -13 km/sec. Swings and Struve[3] found an even greater difference in the displacements on spectrograms taken at the Lick and McDonald observatories in 1942. Their values were: H, -65 km/sec; other elements, $+62$ to $+18$ km/sec. The anomalous negative displacement of the hydrogen lines suggested an expanding shell, although other atoms seem not to take part in the expansion. Moreover, the lines of *Mg* II and *Si* II were stronger than in the typical shell spectrum. The star obviously deserved further observation.

The present account is based on grating spectrograms, dispersion 10 A/mm (20 A/mm in the red), taken with the 100-inch telescope on Mount Wilson during the years 1944–1948 (see Table 1). The emulsion of most of the plates was Eastman II*a*-O.

The measurable lines are due to H, *He* I, and ionized metals (*M* II), chiefly *Mg* II, *Si* II, *Ca* II, *Ti* II, and *Fe* II. The H lines exhibit great variations in intensity and structure. The other stellar lines, although rather weak, are fairly narrow and are measurable with reasonable accuracy; with the exception of *Ca* II lines, which are fairly strong on some plates and scarcely visible on others, they exhibit little variation in appearance. Their displacements, however, differ greatly from plate to plate. The *Ca* II lines appear considerably stronger at the extreme velocities, especially toward the minimum velocity, than at the intermediate velocities when they are superposed on the interstellar lines. A study of the plates and of several tracings yields the impression that the apparent change in intensity is too great to be due wholly to contrast or Eberhard effect. There may be a faint *Ca* II component having about the same displacement, -95 km/sec, as that of the anomalous, nearly fixed hydrogen component B (see section on "Hydrogen Lines"). This

[1] MWC 321; BD+29°3754; 1900 R.A. $19^h44^m.7$, Dec. +29°10′; mag. 7.7; spect. A0 (Harvard), B9eβ (Mt. Wilson).

[2] Merrill, Humason, and Burwell, *Mt. W. Contr.*, No. 294; *Ap. J.*, **61**, 389, 1925.

[3] *Ap. J.*, **97**, 194, 1943.

component may be responsible for some apparent enhancement of the shifting *Ca* II lines when they have large negative velocities. The interstellar *Ca* II lines are sharp; they appear somewhat stronger than normal when the stellar lines are superposed on them.

TABLE 1

RADIAL VELOCITIES

(Km/Sec)

Plate Ce	Date	JD 243	Velocity and Number of Lines			
			H	*He* I	*M* II	*Ca* II int.
3525	1944 Aug. 2	1305.75	(−101) 1, (+25)	....	+ 36 10	−11.9
3562	Sept. 6	1340.72	(−120) 1	− 36 1	− 43 5	....
3571	Sept. 8	1342.65	− 90 15	− 85 2	− 86 23	−10.4
4321	1946 July 13	2015.76	− 96 16	−132 3	−132 24	−11.4
4366	Aug. 15	2048.69	− 54 16	− 39 3	− 47 19	−10.2
4418	Sept. 14	2078.67	− 85 15, +12 8*	+ 24 2	+ 19 15	− 9.6
4732	1947 June 30	2367.84	(− 94) 6, +39 7	+ 39 2	+ 39 29	− 9.4
4777	Aug. 3	2401.68	−115 10, ?*	(− 6) 2	− 13 21	− 9.6
4800	Aug. 5	2403.91	(− 75) 1	(− 44) 1	− 57 5	−11.4
4806	Aug. 25	2423.68	(− 76) 3	....	+ 39 7	−10.9
4809	Aug. 26	2424.68	(−100), +32 11*	+ 38 3	+ 34 11	− 9.8
4874	Sept. 27	2456.70	(−100), (+3)*	− 6 2	− 5 12	−11.5
4913	Oct. 6	2465.74	(− 74) 2	....	−154 7	− 9.1
4919	Oct. 8	2467.69	− 65 13	(− 71) 1	− 66 22	−10.7
4931	Oct. 25	2484.66	−100 12, ?*	(0) 1	− 7 12	....
5201	1948 June 16	2719.94	−115 *Hα*	− 46 1	− 48 3	− 8.1 *Na* I
5207	June 17	2720.87	?*	− 24 4	− 21 15	−12.6
5272	Aug. 15	2779.75	− 88 16	....	+ 38 11	− 9.3
5274	Aug. 16	2780.67	−114 *Hα*	....	(+ 38) 2	− 7.5 *Na* I
5311	Sept. 11	2806.73	− 85 13, +5 9	+ 28 3	+ 28 8	−11.4

* See Fig. 2.

RADIAL VELOCITIES

All stellar lines except certain components of the hydrogen lines appear to yield the same velocities. For example, lines of individual elements on plate Ce 4732 yield the results in Table 2.

TABLE 2

RADIAL VELOCITIES MEASURED ON PLATE Ce 4732

(Km/Sec)

Element	Velocity and No. of Lines	Element	Velocity and No. of Lines
H	+38.7 (7), −94 (6)	*Si* II	+38.4 (5)
He	+39.4 (2)	*Ti* II	+40.4 (5)
Mg II	+38.0 (1)	*Fe* II	+39.1 (15)
Ca II	+40.1 (2), −9.4 (2)*	*M* II	+39.1 (29)

* Interstellar.

The radial velocities of *He* I and *M* II (ionized metals) in Table 1 are well represented by an elliptic orbit (see Fig. 1). The orbital elements computed by Miss Louise Lowen are in Table 3. This orbit represents the observations of Swings and Struve[3] in 1942 within the errors of measurement. To represent my single low-weight plate of 1924, a correction to the period of about +0.005 day would be required.

HYDROGEN LINES

There appear to be two independent sets of dark hydrogen lines, both of variable intensity. Set A yields the same velocity as the lines of *M* II and *He* I; set B has a nearly constant displacement not far from −95 km/sec. At $H\alpha$ and $H\beta$, B is regularly dominant, but at lines of shorter wave length this is not always so. Set A, in fact, seems to have the slower decrement on plates where it is well separated from B. The apparently slower decrement may be due to superposed hydrogen emission, which tends to weaken the longward lines of A but not those of B. On this hypothesis the lines of B would be formed in an outlying absorbing layer that envelops the whole system, while the lines of A arise in a stellar atmosphere along with those of *M* II and *He* I.

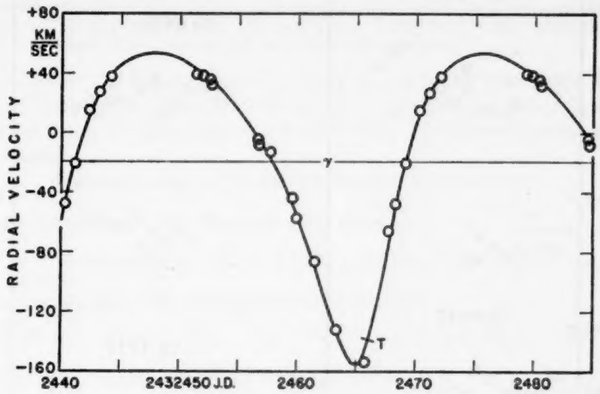

FIG. 1.—Velocity-curve of HD 187399 from measures of metallic lines

TABLE 3

ORBITAL ELEMENTS OF HD 187399

$P = 27.97$ days	$K = 104.5$ km/sec
$T =$ JD 2432465.98	$\gamma = -18.9$ km/sec
$\omega = 210\overset{\circ}{.}7$	$a \sin i = 37{,}600{,}000$ km
$e = 0.35$	$f(m) = 2.72$

Mean displacements of one or both sets are recorded for most plates in Table 1. On other plates the results are complicated by a relative displacement from line to line along the Balmer series. Several of the more striking cases are plotted in Figure 2. It seems probable that some of the complicated details have their explanation in the various degrees of blending of sets A and B and of the varying influence of hydrogen emission.

The bright $H\beta$ line is wide, poorly defined, and mutilated by absorption components; hence its center is difficult to measure. The measured velocities on ten plates range from +33 to −47 km/sec, with a mean of +2 km/sec. The overexposed $H\alpha$ line on one plate yielded a value of +7 km/sec. Because the absorption components lie chiefly in the shortward half of the line, the measurements of the emission may have a systematic positive error. Hence it is quite possible that the true center of the emission corresponds in position to the velocity of the center of mass of the binary system, $\gamma = -19$ km/sec.

The facts suggest that the binary orbit is enveloped by a cloud of incandescent hydrogen whose outer absorbing layers are expanding at the rate of about 75 km/sec. The system seems to resemble that of β Lyrae in certain respects.

In a number of Be stars, the bright hydrogen lines do not oscillate with the dark lines and thus may originate in a cloud partly independent of the binary stellar system. This circumstance could probably best be studied by means of special observations of the strong *Hα* line.

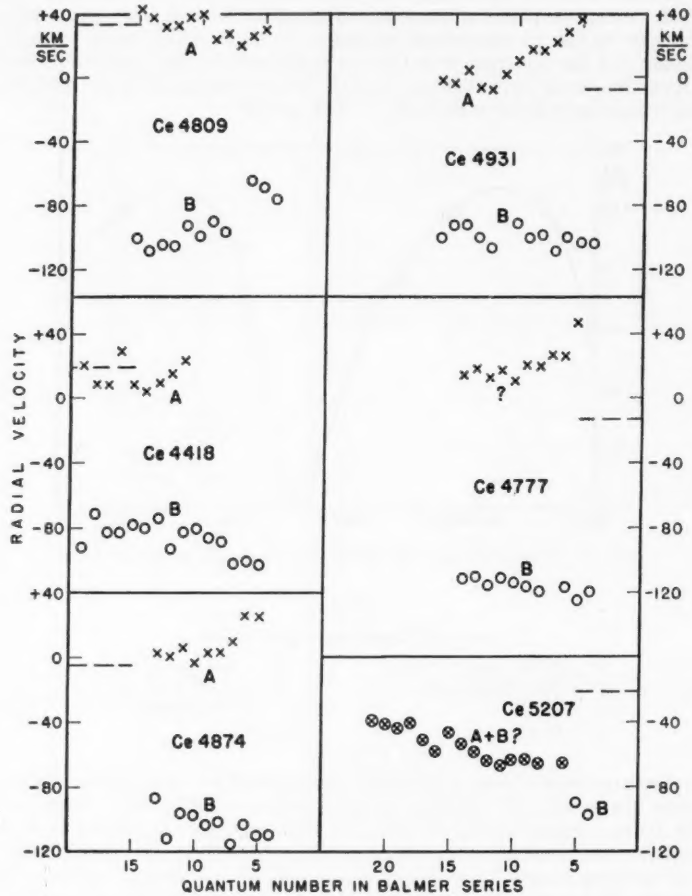

FIG. 2.—Radial velocities of two sets of dark hydrogen lines on various plates. The velocity yielded by the stellar lines of ionized metals is indicated by the short dashed lines at the edge of each diagram.

SPECTROSCOPIC OBSERVATIONS OF TW DRACONIS*

BURKE SMITH
McDonald Observatory
Received March 29, 1949

ABSTRACT

New circular elements have been derived. The epoch of total eclipse as determined from the spectrographic material is 0.146 day later than that computed from Kordylewski's light-minimum. The rotation effect is found to be small. A few lines of the secondary were observed.

The variability of TW Draconis, $\alpha = 15^{h}32^{m}.4$, $\delta = +64°14'$ (1900), Sp. A6 + K2, was discovered in 1910 by Miss Cannon.[1] The normal magnitude is 7.8, but during principal eclipse, which is total, the light diminishes to 8.9 mag. The light-elements were given by Graff[2] in 1913 as

$$\text{Primary min.} = \text{JD } 2418906.453 + 2.80654E\ .$$

A more recent determination by Kordylewski[3] gives

$$\text{Primary min.} = \text{JD } 2423711.321 + 2.80664E\ .$$

According to Gaposchkin,[4] the photometric elements are

$$A_1 = 2.55\ , \quad A_2 = 0.08\ , \quad L_b = 0.89\ , \quad r_b = 0.21\ , \quad k = 0.65\ ,$$

$$i = 85^{\circ}.6\ , \quad \text{Ratio of surface brightnesses} = 19.9\ .$$

During June and July, 1947, fifty-five spectrograms of this star were obtained with the 82-inch McDonald reflector, equipped with the standard Cassegrain spectrograph and 500-mm camera. The dispersion was 55 A/mm at $H\gamma$, and the emulsion was Eastman 103*a*-O. Table 1 shows the list of star lines and Table 2 the measured velocities. Only the spectrum of the primary is visible, except on two plates, Nos. 5384 and 5385, which show a few lines belonging to the secondary. Since the light diminishes to 0.115 of the normal during totality, the spectrum of the secondary is very faint. The spectral lines generally are diffuse, but an average of twenty-five lines per plate was measured, except on poor plates. The probable error per plate, for all but the poorest plates, varied from about ± 2.2 to ± 4.3 km/sec.

Table 2, fifth column, shows the measured velocities. When plotted, however, the scatter seems to be larger than one would expect from the probable errors. A preliminary orbit was computed, and the residuals, $V_o - V_c$, are shown in Table 2, sixth column, except for eclipse points, and are plotted in Figure 1 against the time in days. It will be noted that the grouping of points suggests that there were systematic errors present when the plates were obtained, and this is confirmed by the appearance of the lines of the comparison spectrum, which show a slight coma on plates taken between June 14

* *Contributions from the McDonald Observatory, University of Texas,* No. 169.

[1] *A.N.*, **185**, 255, 1910.

[2] *A.N.*, **196**, 395, 1913.

[3] *Acta astr.*, Ser. c, **2**, 59, 1934.

[4] *Variable Stars* ("Harvard Observatory Monographs" No. 5 [Cambridge, Mass.: Harvard College Observatory, 1938]), p. 72.

and July 5. The measured velocities were therefore corrected on the basis of the smooth curve shown in Figure 1 and the adjusted velocities are tabulated in Table 2, seventh column, and plotted in Figure 2.

The phase was computed from the epoch JD 2432340.482 with a period of 2.806 days. Mid-eclipse would then occur at JD 2432341.885, which is in agreement with the two plates showing lines of the secondary spectrum, but is 0.146 day later than the epoch of minimum light as computed from the light-elements of Kordylewski.

According to Baker[5] the eclipse phase lasts 0.460 day. Eleven eclipse plates, taken between phases 1.2 and 1.6 days, were accordingly omitted in computing the orbit, leaving a total of forty-four plates. From spectrographic orbits published by Plaskett,[6] and Pearce,[7] and the plot of velocities in Figure 2 it appears that e is very small. A circular orbit was therefore computed, using the adjusted velocities shown in Table 2, eighth column. The systemic velocity, γ, and semi-amplitude, K, were determined by setting up forty-four equations of the form

$$\text{Adjusted vel.} = \gamma + K \sin\left(\frac{360^\circ}{P} \times \text{phase}\right)$$

TABLE 1

LIST OF STAR LINES

Element	λ	Element	λ	Element	λ	Element	λ
Fe I	3856.37	*He* I	4009.27	*Fe* I	4143.50	*Sc* II	4314.08
Fe I	3878.58	*Fe* I	4045.82	*Mg* I	4167.27	*Fe* I	4325.76
Fe I	3902.95	*Fe* I	4057.36	*Fe* II	4178.85	$H\gamma$	4340.47
Ti II	3913.46	*Fe* I	4063.60	*Fe* I	4199.10	*Fe* II	4351.76
V II	3916.42	*Fe* I	4066.98	*Sr* II	4215.52	*Fe* I	4383.55
Ca II	3933.67	*Ni* II	4067.05	*Ca* I	4226.73	*Ti* II	4394.06
Fe I	3956.68	*Sr* II	4077.71	*Fe* II	4233.17	*Ti* II	4395.04
Fe I	3997.39	$H\delta$	4101.74	*Fe* I	4235.94	*Fe* I	4404.75
Cr II	4003.33	*Fe* I	4118.55	*Fe* I	4260.48	*Ti* II	4399.77
Fe I	4005.25	*Fe* I	4132.06	*Fe* I	4299.24	*Mg* II	4481.23

and solving for γ and K by least squares, which gave

$$\gamma = +2.75 \text{ km/sec}, \qquad K = 61.23 \pm 0.85 \text{ km},$$

$$a \sin i = 2{,}365{,}000 \text{ km}, \qquad \frac{m_2^3}{(m_1 + m_2)^2} \sin^3 i = 0.068\odot .$$

The smooth curve in Figure 2 is based on these elements. The rotation effect is evidently small. For comparison the solutions by Plaskett and Pearce are shown in Table 3.

Although eighteen lines were measured for radial velocity on the two plates which show the secondary spectrum, there are only a few lines which are clear enough to permit classification of the spectrum. The most striking feature is the strength of *Fe* I. The plates are very weak on the violet side of λ 4325, but the *Ca* II K line is visible. $H\gamma$ is present but is distinctly weaker than *Fe* I 4325 and 4383. No other *H* line is seen, and the G band is barely visible.

I am much indebted to Dr. O. Struve for having obtained the spectrograms and for his kind advice and encouragement.

[5] *Laws Obs. Bull.*, No. 33, 1924.

[6] *Pub. Dom. Ap. Obs., Victoria*, **1**, 145, 1922..

[7] *Proc. December meeting A.A.S.*, 1937.

TABLE 2

RADIAL VELOCITIES

PLATE* CQ	DATE U.T. (1947)	PHASE		MEASURED VELOCITIES (KM/SEC)	RESIDUALS $V_o - V_e$ (KM/SEC)	ADJUSTED VELOCITIES (KM/SEC)	NO. LINES MEASURED
		In Days	In Period				
5354	June 6 3:04	2.146	0.765	−55.4	+ 4.2	−45.1	20
5355	6 3:25	2.160	.770	−72.2	−12.7	−61.9	25
5356	6 3:48	2.176	.776	−64.1	− 4.9	−53.8	20
5367	7 2:38	0.322	.115	+32.2	−11.4	+41.2	25
5368P	7 2:58	0.336	.120	+35.1	−10.0	+44.1	17
5369	7 3:23	0.353	.126	+37.8	− 9.0	+46.8	25
5382P	8 2:45	1.327	.473	+14.5	....	+21.5	20
5384P	8 4:03	1.381	.492	−25.5	....	−18.5	16
5385P	8 5:17	1.432	.510	−25.1	....	−18.1	18
5398	9 3:01	2.338	.833	−55.0	− 3.4	−49.2	23
5399	9 3:22	2.352	.839	−45.8	+ 4.8	−40.0	25
5400	9 3:48	2.370	.844	−45.6	+ 3.6	−39.8	24
5417	10 2:41	0.517	.184	+50.3	− 9.3	+54.3	18
5418	10 3:01	0.530	.189	+55.7	− 4.5	+59.7	29
5419	10 3:22	0.545	.194	+50.0	−11.0	+54.0	20
5420	10 3:43	0.560	.200	+61.8	+ 0.1	+65.8	21
5440	11 2:54	1.526	.544	− 9.8	....	− 8.2	29
5441	11 3:24	1.547	.552	−14.5	....	−12.9	30
5442	11 3:52	1.566	.558	− 6.5	....	− 4.9	23
5455	12 2:49	2.522	.900	−38.4	− 4.0	−37.9	24
5456	12 3:24	2.547	.908	−22.1	+ 9.4	−21.6	18
5457	12 4:12	2.580	.998	−35.4	− 7.6	−34.9	23
5480P	14 3:19	1.736	.619	−54.6	−15.3	−56.8	19
5481P	14 4:15	1.775	.632	−41.1	+ 2.2	−43.3	22
5495P	16 2:45	0.907	.323	+58.1	0.0	+53.1	18
5527	20 2:45	2.100	.749	−62.7	− 2.8	−71.2	32
5528	20 3:10	2.117	.754	−53.9	+ 6.0	−62.4	25
5529	20 3:36	2.135	.761	−48.2	+11.6	−56.7	26
5545	21 2:45	0.293	.104	+49.7	+ 9.1	+40.5	22
5546	21 3:06	0.304	.108	+49.3	+ 7.5	+40.1	24
5574	22 2:52	1.297	.463	+45.6	....	+35.8	21
5575	22 3:45	1.334	.475	+32.2	....	+23.4	21
5587	23 2:46	2.293	.818	−49.3	+ 5.2	−59.3	24
5588P	23 3:11	2.311	.824	−53.3	+ 0.1	−63.3	15
5589	23 3:37	2.329	.830	−38.9	+13.2	−48.9	23
5602	24 3:16	0.508	.181	+68.1	+ 9.1	+58.6	18
5603	24 3:57	0.537	.191	+82.2	+21.6	+72.7	27
5613	25 2:51	1.491	.532	−17.1	....	−27.5	22
5647P	27 4:28	0.751	.268	+64.1	− 0.2	+56.1	21
5648	27 5:05	0.777	.277	+76.4	+12.6	+68.4	25
5662	28 4:41	1.760	.628	−23.8	+18.2	−30.8	24
5674P	30 2:52	0.878	.313	+73.0	+12.8	+68.5	13
5716	July 3 2:50	1.070	.381	+47.6	+ 3.2	+46.7	25
5737	4 2:44	2.066	.736	−66.6	− 7.0	−65.6	27
5738	4 3:06	2.081	.742	−64.5	− 4.7	−63.5	29
5763	5 2:40	0.256	.091	+37.0	+ 0.7	+39.5	29
5764	5 3:00	0.270	.096	+32.8	− 5.1	+35.3	28
5785	6 3:09	1.276	.455	+26.1	....	+29.6	29
5799	7 2:41	2.257	.804	−69.7	−13.3	−63.7	26
5800	7 3:01	2.271	.810	−56.2	− 0.5	−50.2	28
5842	9 3:08	1.470	.524	−31.2	....	−21.7	29
5867	10 2:37	2.448	.872	−41.7	+ 0.6	−30.7	29
5868	10 2:57	2.462	.878	−44.6	− 3.6	−33.6	26
5869	10 3:22	2.479	.883	−40.2	− 0.9	−29.2	26
5885	11 4:26	0.717	0.256	+51.8	−12.9	+63.8	23

* The letter "P" in this column denotes poor spectrogram.

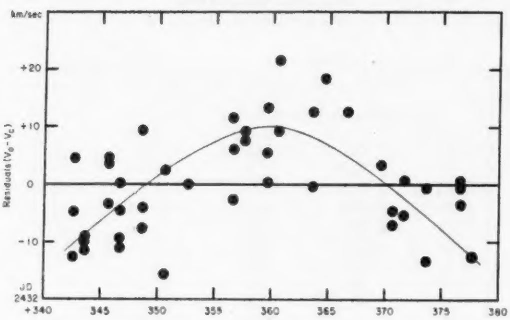

FIG. 1.—Residuals from preliminary orbit

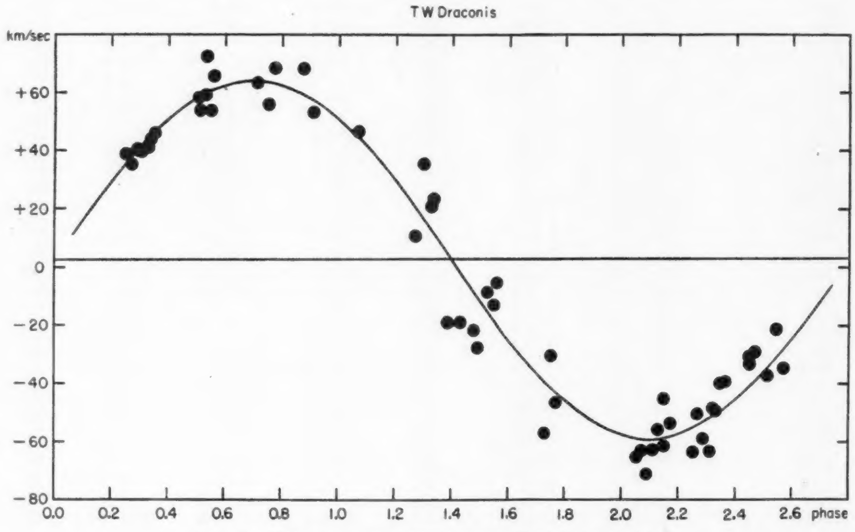

FIG. 2.—Velocity-curve of TW Draconis (phase in days)

TABLE 3

	Plaskett	Pearce (2 Solutions)			Plaskett	Pearce (2 Solutions)	
No. of plates	14	14	33	l	0.054	0.021	0.027
γ (km/sec)	− 0.34	+ 0.6	+ 2.6	$a \sin i$	2,535,000	....	....
K (km)	65.78	62.8	63.5	P (days)	....	2.806594	2.806689

ANOMALOUS SPECTRA OF STARS OF CLASS A

MIRIAM E. WALTHER
Harvard College Observatory
Received April 15, 1949

ABSTRACT

Objective-prism plates with a dispersion of 95 A/mm at $H\gamma$ have revealed 41 peculiar A stars and 8 metallic-line A stars. The material examined shows that, at low galactic latitudes, 13 per cent of the A stars between magnitudes 5.5 and 9.5 have spectra characterized by abnormal intensity of the lines of chromium, silicon, europium, or strontium.

I. INTRODUCTION

In the course of the classification of objective-prism spectra taken recently at the Harvard Observatory, I have found a number of A stars with anomalous spectra. The plates were taken as part of a program designed to adapt the Morgan-Keenan-Kellman system of spectral classification to objective-prism spectra. The spectra, taken with the 12-inch Metcalf doublet (the MA) equipped with a crown-glass objective prism of 12°, have a dispersion of 95 A/mm at $H\gamma$. Experiment showed that Eastman emulsion II*a*-O and development in DK20 for 15 minutes at 65° gave spectra of highest quality. Three luminosity classes can be assigned to most spectra obtained in good seeing, but a detailed luminosity classification of the A stars is possible only on plates of superior quality. On the other hand, certain peculiar features are very marked, and these are easily distinguished from luminosity effects on all plates.

II. THE PECULIAR A STARS

The spectra of the peculiar A stars (as distinguished from the metallic-line stars) appearing on the MA plates fall into three groups, which are characterized by the element that gives rise to the most marked anomalous feature. These groups—the silicon, the chromium-europium, and the strontium stars—are represented by prototypes which have been described in detail by Morgan.[1]

Table 1 contains a list of the 41 peculiar A stars detected on the MA plates; only 2 of these stars were previously known to be peculiar. The first five columns of the table require no explanation. The photovisual magnitude in the sixth column is taken from the *Henry Draper Catalogue* when the star is included in that catalogue; otherwise it is taken from the BD catalogue. The new spectral type is based on the intensity of the K line relative to the near-by Balmer lines. Since this line is weak in nearly every case, all the stars, with one exception, have been designated either B9 or A0. This classification is not altogether satisfactory, since it conveys very little information about the general appearance of the spectrum. The descriptions in the notes which follow the table are more informative. Following to some extent the notation adopted by Deutsch,[2] I define, below, the symbols describing the peculiar features listed in the table:

"*Cr*" means that λ 4077 and λ 4171 of *Cr* II are strong.

"*Sr*" means that λ 4077 and λ 4215 of *Sr* II are strong.

"λ 4200" means that this unidentified line is strong.

"*Eu*" means that *Eu* I is implied by the fact that the general features of the spectrum match a typical chromium-europium star.

"*Si*" indicates that the blend at λλ 4128–4131 is strong and that the general features of the spectrum correspond to a typical silicon star.

[1] Morgan, Keenan, and Kellman, *An Atlas of Stellar Spectra* (Chicago: University of Chicago Press, 1943); W. W. Morgan, *Ap. J.*, **77**, 77, 1933; *ibid.*, **74**, 24, 1931.

[2] *Ap. J.*, **105**, 297, 1946.

TABLE 1

LIST OF PECULIAR A STARS

MEW No.	HD No.	BD No.	α (1900)	δ (1900)	m_{pv}	HD Type	MEW Type	Peculiar Features
1	5797	+59° 163	0h 54m.5	+59° 55′	8.8	A0	A0p	*Cr, Eu, Sr*
2	....	+57 184	0 57.0	+57 43	9.0	......	B9p	*Si*
3	7370	+60 194	1 8.8	+60 20	8.66	A	B9p	*Cr, Eu*
4	17775	+61 495	2 46.1	+61 28	8.8	A0	A0p	*Cr, Eu*
5	....	+58 538	2 50.7	+58 50	9.0	......	B9p	*Si*
6	18473	+59 582	2 53.1	+59 17	7.35	A0	B9p	*Si*, λ 4200
7	....	+59 597	3 1.4	+60 4	9.2	......	B9p	*Si*, λ 4200
8	19653	+60 640	3 4.8	+60 26	8.9	A0	B9p	*Cr, Eu, Sr*
9	22374	+22 518	3 31.0	+22 54	6.69	A0p	B9p	*Cr, Eu*
10	29580	+44 1006	4 34.4	+44 19	8.0	B9	B9p	*Si*, λ 4200
11	30584	+44 1036	4 43.8	+44 47	8.0	B9	B9p	*Si*, λ 4200
12	....	+43 1092	4 43.9	+43 40	9.0	......	B9p	*Si*, λ 4200
13	35479	+29 893	5 19.9	+29 54	8.06	B9	B9p	*Si*, λ 4200
14	44636	+15 1175	6 17.7	+15 55	8.7	B9	B9p	*Cr, Eu*
15	44738	+14 1276	6 18.3	+14 10	7.3	A0p	A0p	*Si*, λ 4200
16	49713	− 1 1395	6 44.7	− 1 13	7.7	A0	B9p	*Cr, Eu*
17	171279	− 7 4623	18 28.8	− 7 47	7.22	A0	B9p	*Cr, Eu*
18	....	+14 3854	19 12.0	+14 27	8.7	......	A0p	*Cr, Eu*
19	182381	+15 3798	19 19.3	+15 49	7.42	A2	B9p	λ 4128, λ 4131
20	189394	+34 3817	19 54.7	+34 14	8.2	A0	B9p	λ 4128, λ 4131
21	190275	+37 3735	19 59.1	+37 32	7.16	A2	A5p	λ 4144, λ 4272
22	192606	+34 3934	20 10.6	+35 6	8.42	A2	B9p	*Si*, λ 4200
23	193344	+35 4059	20 14.7	+35 56	8.0	B9	B9p	*Cr, Eu*
24	196178	+46 2977	20 30.6	+46 21	5.59	B9	B8p	*Si*, λ 4200:
25	197374	+43 3687	20 38.2	+43 28	8.5	A0	B9p	*Si*
26	....	+29 4202	20 46.6	+29 26	8.8	......	A0p	*Cr, Eu*
27	....	+45 3303	20 47.6	+45 40	9.2	......	B9p	*Cr, Eu*
28	200177	+48 3260	20 56.8	+48 17	7.08	A0	B9p	*Cr, Eu*
29	200311	+43 3786	20 57.6	+43 19	7.9	A0	B9p	*Si*, λ4200
30	200369	+46 3144	20 58.0	+46 48	8.9	A2	A0p	*Cr, Eu*
31	201174	+44 3701	21 2.8	+44 52	8.5	A2	A0p	*Cr, Eu, Sr*
32	208340	+52 3056	21 50.6	+52 30	8.7	A0	B9p	*Cr, Eu*
33	....	+45 3736	21 52.7	+45 40	8.7	......	B9p	*Cr, Eu*
34	209308	+53 2766	21 57.3	+53 41	9.3	B9	B9p	*Si*, λ 4200:
35	209515	+43 4119	21 58.9	+44 10	5.52	A0	B9p	*Cr, Eu*
36	209664	+44 4031	22 0.0	+44 47	8.6	A	B9p	*Cr, Eu:*
37	210071	+55 2679	22 2.7	+55 51	6.22	B9	A0p	*Cr, Eu:*
38	....	+52 3127	22 6.7	+52 19	9.4	......	B9p	*Cr, Eu:*
39	219855	+57 2719	23 14.0	+57 38	8.0	A0	B9p	λ 4128, λ 4131
40	220147	+61 2430	23 16.4	+61 52	7.6	A0	B9p	*Cr, Eu*
41	221568	+57 2758	23 28.1	+57 21	8.0	A0	A0p	*Cr, Eu*

NOTES TO TABLE 1

1. On one of the better plates both *Sr* II 4077 and *Sr* II 4215 are very strong, while on another plate of nearly equal quality these lines are weaker, especially λ 4215, which is very weak or entirely absent. This suggests that the star is a spectrum variable.

8. The spectrum of this star resembles that of χ Serpentis, though the feature at λλ 4128–4131 is stronger. Except for the Balmer lines, the *Sr* II lines λ 4077 and λ 4215 are the most prominent features in the spectrum. The line at λ 4161, which may possibly be due to *Sr* II, is present. The weakening of λλ 4077, 4161, and 4215 on two of the four plates, all of relatively high quality, suggests that this star is a spectrum variable. When *Sr* II 4215 is compared with *Cr* II 4171, it is found that it appears considerably stronger on two plates and equal or slightly stronger on the other two.

9. Certain changes indicate spectral variability, though neither of the two spectra available is of sufficient quality to establish variability.

15. The lines λ 4026 and λ 4077 also appear, but they are not strong.

17. The spectrum of this chromium-europium star is similar to that of BD − 18°3789 at phase 0.38 day. Strong lines appear at λλ 4077, 4128–4131, 4171; a fainter one seems to be present at λ 4179. The char-

NOTES TO TABLE 1—*Continued*

acteristic asymmetry of $H\gamma$, $H\delta$, and $H\epsilon$, which is produced by blends on the red side of these lines, is very marked. The K line is very weak, corresponding approximately to class B9.

19. Inferior spectrum. *He* I 4026 present.

21. The peculiarities of the spectrum of this star are so unusual that it is not possible to place it in any of the groups described previously. The K line is weak relative to the general development of the spectrum; it corresponds approximately to class A5. The metallic lines are, in general, strong, corresponding to class A7 or F0. A blend at λ 4272 and a line at λ 4144 are even stronger than the corresponding features in the F0 stars. The unusual strength of these latter two features makes one suspect that the spectrum is a composite, but it is hard to understand what types could combine to produce this anomaly. The spectrum appears on four plates.

23. The spectrum resembles very much that of BD−18°3789 at the phase 0.38 day, where the *Cr* II lines at λ 4077 and λ 4171 and the line at λ 4179 are at maximum strength. The blend at λλ 4128–4131 is strong; the K line is very weak.

33. The spectrum, with peculiarities at λλ 4063, 4077, 4128–4131, and 4171, resembles that of BD−18°3789. The relative intensity of λ 4063 and λ 4077 is not the same on two of the plates. While the spectra on these plates are not comparable, it is almost certain that they give evidence of variation.

36, 37, 38. The inferior quality of the spectra of these stars permits only an indication of the type of peculiarity; hence the classification should be considered provisional.

39. The blend at λλ 4128–4131 is not very strong but probably sufficiently so to qualify this star as peculiar.

41. There is some indication that the intensities of λ 4171 and the K line vary, but this observation is subject to confirmation.

The classifications given are provisional and subject to modification when slit spectra are available.

Peculiarities occurring in the spectra of A stars are immediately apparent, but it is often difficult to identify the ions responsible for the peculiarities in a given spectrum. Certain peculiarities are so pronounced that they may be detected even when the quality of the spectrum is inferior. This is especially true of the blend at λλ 4128–4131, which is so frequently recorded in the *Henry Draper Catalogue* as the only peculiar feature. The high percentage of silicon stars doubtless arises, in part at least, from the fact that λλ 4128–4131 appears when many of the other fainter features, such as λ 4077 and λ 4171, are washed out. Data from the *Henry Draper Catalogue* reveal that 114 of the 188 peculiar A stars in this catalogue belong to the group of silicon stars.

In general, the strength of the blend near λ 4130 is attributed to the silicon doublet at λ 4128 and λ 4131. Certainly, one can assume this to be true when the remainder of the spectrum resembles a typical silicon star, such as BD+33°1008 Aurigae, in which λ 4200 is strong and *Ca* II K corresponds to class B9. On the other hand, one of the stronger europium lines, *Eu* II 4129, may contribute to the strength of the blend at λλ 4128–4131. Actually, none of the strongest lines of europium, at λλ 3930, 4129, and 4205, has been detected in any of the spectra thus far examined. However, when both λλ 4128–4131 and λ 4171 appear as prominent features and the spectrum resembles that of a typical chromium-europium star like 78 Vir, the existence of features due to europium is implied. I have, therefore, designated a star as belonging to the chromium-europium group if the spectrum resembles that of 78 Vir.

The intensity of the feature at λλ 4128–4131 differs greatly from one silicon star to the next. In fact, in accordance with Morgan's previous observation,[3] it appears from the MA plates that the intensity of the feature at λλ 4128–4131 in the silicon stars deviates only in various degrees from that of a normal A star. In the case of some stars it was difficult to decide whether or not they should be classified as peculiar; in others the peculiarities are very pronounced. Most of the doubtful cases have not been included in Table 1. The chromium-europium and strontium stars, on the other hand, seem more likely to form discrete groups.

It would be well to emphasize that there exists very little possibility of confusing the

[3] *Pub. Yerkes Obs.*, **7**, Part III, 7, 1934.

highly luminous A stars with the chromium-europium stars. In the spectra of both types there are features at approximately λ 4130 and λ 4171, but they have distinctly different appearances in the two types. In the chromium-europium star, λλ 4128–4131 is definitely a strong blend, and λ 4171 is a fairly narrow line due to *Cr* II. On the other hand, in the supergiant the blend at λλ 4128–4131 is relatively weaker and narrower, and the feature near λ 4171 consists of two strong *Fe* II lines at λ 4173 and λ 4178. The line at λ 4077, which is strong in the chromium-europium stars, is so faint that it is hardly visible in the supergiants of classes A0 and A2. The hydrogen lines also are very different in the two types of stars under consideration. They are narrow and weak in the highly luminous stars; in the chromium-europium stars they are wide and strong, and some appear asymmetric. The K line, on the other hand, is relatively stronger in the supergiants than in the peculiar A stars of corresponding spectral type. Only on inferior plates could these spectral features be so distorted that the difference would not be evident.

Table 1 includes three stars that seem likely to be spectrum variables and two others that show indications of variability. Two of the first three, BD+59°163 and BD+60°640, belong to the chromium-europium-strontium group. For both of them it is the strong strontium lines at λ 4077 and λ 4215 which give evidence of variability. The third one, BD+45°3736, appears to be a spectrum variable similar to BD−18°3789.[4] In the case of the other two stars—BD+22°518 and BD+57°2758, both chromium-europium stars—the observations are less convincing. For each of the stars the spectral variations should be confirmed with slit spectra which show more detail. In general, objective-prism plates are not satisfactory for studying spectral variations, especially when these variations are not very pronounced.

III. FREQUENCY OF PECULIAR A STARS

Of the A0 and A2 stars brighter than the sixth magnitude (app. m_{pv}), the *Henry Draper Catalogue* lists 11 per cent as peculiar. The frequency of A stars in the *HD Catalogue* decreases to 3 per cent for stars between 6.0 and 7.0 mag., and to less than 1 per cent for stars between 7.0 and 8.0 mag. This rapid decrease in frequency is certainly a selection effect. The MA plates reveal that many more of the faint early A stars, including classes B9–A3, are peculiar. All the regions listed in Table 2 are very close to the galactic circle. In the fourth column there is given for each of the regions the total number of stars classified on the MA plates in the spectral classes B9, A0, A1, A2, and A3; in the last column are the corresponding counts of the peculiar A stars. Table 2 does not include all the peculiar A stars in Table 1, since some of them are in regions for which the classifications are not complete. The stars range in magnitude from 5.5 to 9.0, but the material is probably only relatively complete down to 8.5. Although it would be difficult to be certain that the counts are complete to any given magnitude, it is reasonable to assume that the classifications and counts are comparable in the degree of completeness for both the total number of B9–A3 stars and the number of peculiar A stars. From these data it follows that 13 per cent of the A stars at low galactic latitudes are peculiar. Since the data are rather scanty, the actual percentage must be recognized as preliminary.

IV. METALLIC-LINE A STARS

Although the metallic-line A stars have been noted for their peculiarities since the earliest work on spectral classification at Harvard, Titus and Morgan[5] were the first to recognize that these stars form a fairly homogeneous group. Usually, though not always, Miss Cannon classified these stars as composites. Miss Maury first described the characteristics of the composite spectra.[6] These puzzling spectra usually represent a

[4] Deutsch, *op. cit.*, p. 285.

[5] *Ap. J.*, **92**, 259, 1940.

[6] *Harvard Ann.*, **28**, Part I, 48–49, 1897.

combination of a late-type and an early-type star with strong hydrogen lines. When these lines appear in a spectrum which is otherwise a later type, the K line is invariably narrow and obscure. If the hydrogen lines are very strong, the K line appears as a shallow band, sometimes having a fine central core. The lines characteristic of the late type disappear from the ultraviolet, while they are strong in the interval from $H\beta$ to $H\delta$. In the metallic-line A stars, on the other hand, the metallic lines appear throughout the whole spectral range used. The K line in the two types of spectra is entirely different. In the composite spectrum the K line is broad and fuzzy, while in the metallic-line A stars it is sharp and distinct. These characteristics usually suffice for distinguishing these two types of spectra.

TABLE 2

COUNTS OF A STARS IN THE MILKY WAY

Region	Co-ordinates of Region Center		Total No. of B9–A3 Stars	No. of Peculiar A Stars
	α (1900)	δ (1900)		
SA 8	1^h03^m	+60°0′	26	2
SA 9	3 08	+60.5	23	6
SA 24	4 45	+45.0	23	3
SA 49	5 27	+29.7	7	1
Scutum Cloud	18 38	− 7.0	2	1
SA 110	18 39	+ 0.1	10	0
SA 87	19 13	+15.0	17	2
SA 64	20 00	+30.5	12	0
Cygnus Cloud	20 08	+36.0	12	3
SA 40	20 45	+45.0	30	7
SA 65	20 58	+30.2	10	1
SA 41	21 52	+45.2	30	3
	22 01	+53.9	39	3
SA 19	23 25	+60.0	21	3
Total			262	35

The criteria that I have used in distinguishing the metallic-line A stars from other anomalous A stars follow closely those set forth in a recent report from the Yerkes Observatory.[7] Since the present study was nearly completed at the time that this report came out, I did not find it possible to use the list of standards published. While there seem to be fundamental differences between the metallic-line and peculiar A stars, there is occasionally a star whose spectral features at low dispersion do not place it definitely in either category. Two of these stars whose classifications are uncertain are included in Table 3, which lists the metallic-line stars discovered on the MA plates. My two classifications depend, respectively, on the relative intensities of H and K and on the strength of the other metallic lines. The notes following the table indicate precisely what the observed peculiarities are.

Most of the stars in the spectral range A0–F0 are classified primarily on the basis of the relative strength of K and H + $H\epsilon$; consequently, many classifications do not depend on the rest of the spectrum. Unless the spectra are of superior quality, it is unlikely that the anomalous strengths of the metallic lines would be apparent. It follows that many of the metallic-line A stars may not be detected.

For the stars listed in Table 3, the feature at λ 4077 is strong in every spectrum except in that of BD+59°621, in which it does not appear. If λ 4215 were also strengthened,

[7] N. G. Roman, W. W. Morgan, and O. J. Eggen, *Ap. J.*, **107**, 107, 1948.

one might be inclined to assign these stars to the strontium group of peculiar stars. The line λ 4215, however, appears normal in every star in which λ 4077 is strengthened. Several of the stars, notably BD+30°3875, BD+43°3789, and BD+28°787, substantiate the reciprocal relation between *Ca* II K and λ 4077 recognized by Weaver.[8]

References[7] are occasionally made to spurious absolute-magnitude effects apparent in the metallic-line A stars, but in no case are the features which show these effects specified.

TABLE 3

LIST OF METALLIC-LINE A STARS

MEW No.	HD No.	BD No.	α (1900)	δ (1900)	m_{pv}	HD Type	MEW Type (K Line)	MEW Type (Metallic Lines)
1	19342	+58° 564	$3^h\ 1^m.6$	+58° 22′	8.0	A2	A7	F0
2	20095	+59 621	3 8.7	+59 37	8.4	A0	B9	A5?
3	22538	+18 517	3 32.4	+19 1	7.67	A0	A5	F0
4	26039	+16 559	4 2.3	+16 16	7.52	B9	B9	A2?
5	35035	+28 787	5 16.7	+28 22	7.36	A3	A3	F0
6	43682	+16 1080	6 12.4	+15 59	8.3	A2	A5	F0
7	190537	+30 3875	20 0.3	+30 57	6.87	A2	A3	F0
8	200407	+43 3789	20 58.2	+43 47	6.72	A2	A5	F0

NOTES TO TABLE 3

1. *Sr* II 4077 and the blend λλ 4030–4034 are relatively strong for class F0. The ratio λ 4417: λ 4481 seems to indicate class V.

2. Although the K line is weak, corresponding to class B9, there are many other features which indicate a much later type. In the interval between $H\delta$ and $H\epsilon$ the lines and blends match those of an F0 star, except that λ 4077 does not appear. The lines between $H\gamma$ and $H\delta$ are faint, and it is not certain whether they correspond to those of an F star or not. While the lines between $H\beta$ and $H\gamma$ are faint, their positions seem to coincide with the lines of an F0 spectrum. Except for the failure of λ 4077 to appear, this star would qualify reasonably well as an early metallic-line A star. It is possible that this enigmatic spectrum is a composite.

4. The spectrum lies near the edge of the plate and is underexposed. The K line is very weak or absent; the metallic lines indicate spectral type A2 or later. The line λ 4077 is rather strong.

6. The quality of the spectrum prevents definite classification as a metallic-line star. The K line corresponds to A5, while the remainder of the spectrum corresponds nearly to class F0, though λ 4077 is abnormally strong.

7. *Sr* II 4077 is very strong. From the ratios λ 4444:λ 4481 and λ 4417:λ 4481 the star appears to belong to class V.

For the stars in Table 3 the usual ratios employed by Morgan, Keenan, and Kellman[9] in the luminosity classification of F0 stars indicate luminosity class V. In every case in which the ratio λ 4417:λ 4481 could be estimated, it corresponded to luminosity class V.

I wish to thank Dr. Harlow Shapley, Dr. Bart J. Bok, and Dr. Armin Deutsch for their encouragement and advice. It is also a pleasure to acknowledge the financial assistance that several fellowships have provided for my studies. During the first year I held the Edward C. Pickering Fellowship and a National Fellowship of the Kappa Kappa Gamma Sorority. The second and third years were financed, respectively, by an American Association of University Women Fellowship and by the Alice Freeman Palmer Fellowship.

[8] *Pub. A.S.P.*, **58**, 246, 1946.

[9] *Op. cit.*

THE FOX-HERZBERG SYSTEM OF THE C_2 MOLECULE

JOHN G. PHILLIPS
Yerkes Observatory
Received February 28, 1949

ABSTRACT

Nine new bands have been observed in the spectrum of the C_2 molecule between 2370 A and 3855 A. They are degraded to the red and do not have pronounced heads. The wave lengths of the heads are included in Table 11. An analysis of the bands has shown that they are additional members of the Fox-Herzberg system ($B^3\Pi_g - X^3\Pi_u$). Their discovery makes possible a more complete discussion of the molecular constants of the $B^3\Pi_g$ state. The resulting rotational constants, B'_e and α'_e, are 1.1922 cm^{-1} and 0.0242 cm^{-1}, respectively. The vibrational quanta are included in Table 15, and the resulting vibrational constants in Table 14. Since the vibrational quanta show an anomalous change with increasing vibrational number, extrapolations to higher vibrational levels have little significance when made on the basis of these constants.

A. INTRODUCTION

During an investigation carried out recently in this laboratory on the spectrum of the C_2 molecule, a number of faint bands were found between 2370 A and 2855 A which have not been previously mentioned in the literature. A low-dispersion spectrogram of this region is reproduced in Figure 1, spectrum *a*. The heads of the more prominent of the bands are shown. The bands degrade to the red and do not have pronounced heads. An enlargement of a high-dispersion spectrogram of a portion of the band at 2772 A is shown in Figure 1, spectrum *b*. At this dispersion the fine structure of the band is well resolved. The lines are readily grouped into two series of triplets, forming the *R* and *P* branches, identified in the figure by the short and long leading lines. Furthermore, there is a regular alternation in the spacing of the components of successive triplets in each series, alternate triplets showing the same relative spacing. All the bands identified in spectrum *a*, Figure 1, have the same structure as the 2772 A band.

The triplet structure of the bands and the alternation, or "stagger," of the spacing of the component lines of the triplets are characteristics of bands of the C_2 molecule arising from transitions between triplet energy levels. Triplet systems that have been observed are the Swan system ($A^3\Pi_g - X^3\Pi_u$) and the Fox-Herzberg system ($B^3\Pi_g - X^3\Pi_u$). Four bands of the latter system, namely, the (0–3), (0–4), (0–5), and (0–6) bands at 2855 A, 2987 A, 3129 A, and 3283 A, respectively, were found and analyzed by Fox and Herzberg[1] in 1937. They are degraded to the red and do not have pronounced heads. The similarity in appearance and structure of the new bands and the four previously identified bands of the Fox-Herzberg system and the fact that they are found in the same spectral region suggest that the new bands are further members of this system. If this is actually the case, the new bands would be of considerable interest, since undoubtedly some of them would arise from excited vibrational levels of the $B^3\Pi_g$ state and would thus provide a means for making a more complete determination of the vibrational and rotational constants of this state.

B. EXPERIMENTAL

The apparatus and techniques used to produce the spectrum of the C_2 molecule have been described in a previous publication.[2] The high-dispersion spectra were photographed in the fourth order of the 21-foot grating spectrograph, with a dispersion of 0.625 A per millimeter. The emulsions used were 103*a*-O and 103*a*-O UV. The exposure times varied from 5 hours at 2855 A to 10 hours at 2300 A.

[1] J. G. Fox and G. Herzberg, *Phys. Rev.*, **52**, 638, 1937.

[2] John G. Phillips, *Ap. J.*, **107**, 389, 1948.

C. ANALYSIS OF THE NEW BANDS

For reasons given in the introduction it was suspected that the new bands were further members of the Fox-Herzberg system. If this was actually so, the band heads of the nine most prominent bands could be used to determine the vibrational transitions involved. Little error was made in using the band heads, since the rotational lines in the neighborhood of the heads were very weak, indicating that the band origins were very close to the heads. The order of magnitude of the vibrational quanta of the upper state could be predicted in advance, since an approximate proportionality exists between the vibrational and rotational quanta of a given electronic state, according to which a state with smaller rotational quanta will have smaller vibrational quanta. Thus, since Fox and Herzberg[1] found that the constant B_0' of the $B^3\Pi_g$ state was 1.1804 cm^{-1}, while the Swan bands gave $B_e'' = 1.6326$ cm^{-1} and $\omega_e'' = 1641.35$ cm^{-1} for the $X^3\Pi_u$ state,[3] it could be predicted that ω_e' of the $B^3\Pi_g$ state was approximately 1000 cm^{-1}. With this as a guide, it was found that it was indeed possible to find a consistent set of vibrational numbers for all the nine bands. These tentative numbers are included in Figure 1, spectrum *a*.

The tentative vibrational analysis was then verified by searching for combination differences between the *R* and *P* branches of each new band that were in agreement with corresponding combination differences found for Swan bands with the same lower vibrational state. This search was successful in all cases, proving conclusively that the identifications of the lower states that are involved are correct. The relative numbering of the upper vibrational levels must also be correct, since, as will be shown later, the resulting vibrational quanta of the upper state fit into a smooth series. The only uncertainty that remains is that the absolute vibrational numbering of the upper state may be in error and that they should all be increased by one or two units. However, it will be shown later that this is unlikely.

a) ROTATIONAL ANALYSIS

The rotational quantum numbers of the lines of each band were found by the process described above. Tables 1–9 give the measured lines of each band, and their *J*-values. The assignment of the red, central, and violet components of each triplet to the $^3\Pi_0 - {}^3\Pi_0$, $^3\Pi_1 - {}^3\Pi_1$, and $^3\Pi_2 - {}^3\Pi_2$ subbands, respectively, was made unambiguously from a comparison of the corresponding combination differences of the Swan system. As an illustration of the degree of agreement found, combination differences of the lower states of the (1–2) and (2–2) bands are compared in Table 10 with those obtained previously[3] for the (0–2) Swan band. In this table, columns headed $\Delta_2F_1''(J)$ are to be compared with one another, etc.

With the rotational analyses known, the usual methods were used to find the rotational constants and band origins of each of the nine bands. Three steps were taken, as follows:

1. Using the method previously described in the study of the Swan bands,[3] approximate rotational constants of the upper and lower states of each band were found, using the following equation:

$$\frac{\Delta_2 F_m(J)}{J+\frac{1}{2}} = 4\bar{B}_v - 8\bar{D}_v\left(J+\tfrac{1}{2}\right)^2 .$$

2. The band origins, ν_0, were found through the use of the equation

$$R_m(J-1) + P_m(J) - 2\,\overline{(B_v'-B_v'')}\,J^2 + 2\,\overline{(D_v'-D_v'')}\,J^2(J+1)^2$$
$$= 2\nu_0 + 2\,(B_v'-B_v'')_{\text{corr}}\,J^2 - 2\,(D_v'-D_v'')_{\text{corr}}\,J^2(J+1)^2 .$$

[3] Phillips, *ibid.*, **108**, 434, 1948.

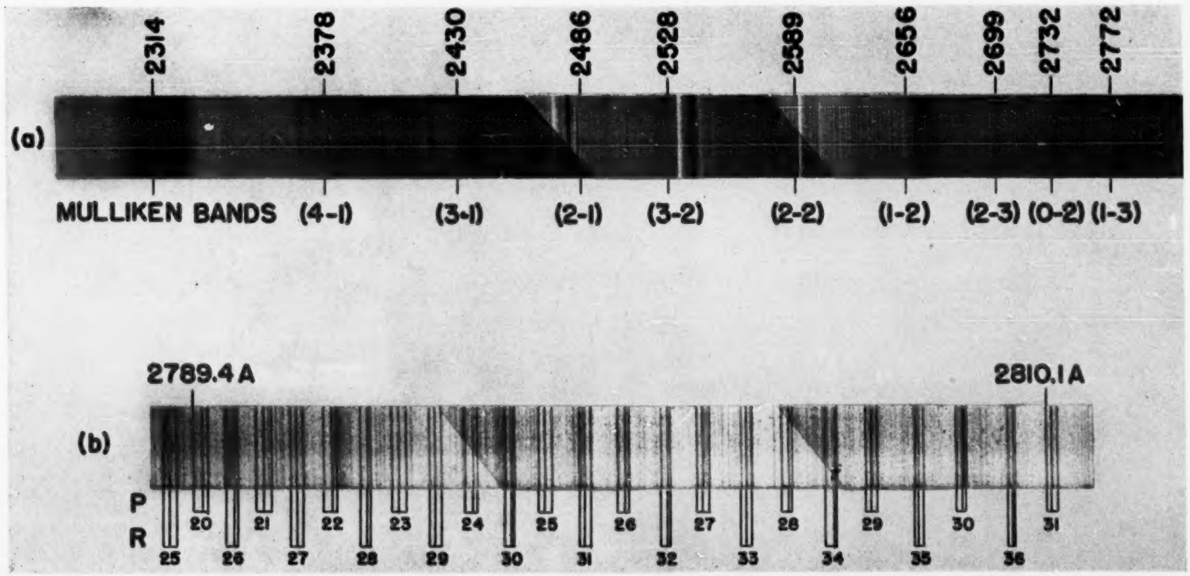

FIG. 1.—The ultraviolet spectrum of the C_2 molecule. *a*, Low-dispersion spectrum, showing the heads and vibrational transitions of the nine new bands. The three absorption bands are produced by benzene vapor. *b*, High-dispersion spectrum of a portion of the 2772 A band.

TABLE 1

WAVE NUMBERS OF THE LINES IN THE (1–3) BAND
($\nu_0 = 36{,}058.97$ Cm^{-1})

J	$^3\Pi_0-{}^3\Pi_0$		J	$^3\Pi_1-{}^3\Pi_1$		J	$^3\Pi_2-{}^3\Pi_2$	
	$R_3(J)$	$P_3(J)$		$R_2(J)$	$P_2(J)$		$R_1(J)$	$P_1(J)$
	Cm^{-1}	Cm^{-1}		Cm^{-1}	Cm^{-1}		Cm^{-1}	Cm^{-1}
4....	36,053.60	36,027.29	5....	....	36,034.58	6...	36,067.46	....
5....	052.32	021.49	6....	36,056.51	026.33	7...	064.31	36,034.11
6....	048.37	013.23	7....	053.60	019.09	8...	060.20	025.52
7....	044.92	36,005.53	8....	048.97	009.36	9...	055.22	015.98
8....	039.46	35,995.64	9....	044.15	36,000.28	10...	049.66	36,005.53
9....	034.58	985.95	10....	037.81	35,989.26	11...	043.12	35,994.61
10....	027.29	974.25	11....	031.43	978.26	12...	035.99	982.83
11....	020.51	962.76	12....	023.30	965.54	13...	027.84	969.99
12....	011.70	949.25	13....	015.27	953.01	14...	019.09	956.80
13....	36,003.01	936.12	14....	36,005.53	938.55	15...	36,009.36	942.44
14....	35,992.48	921.02	15....	35,995.64	924.26	16...	35,999.11	927.60
15....	982.05	906.01	16....	984.11	908.02	17...	987.67	911.58
16....	969.99	889.24	17....	972.77	892.14	18...	975.76	895.10
17....	957.62	872.43	18....	959.45	874.29	19...	962.76	877.42
18....	943.85	854.02	19....	946.51	856.73	20...	949.25	859.37
19....	929.86	835.51	20....	931.50	837.09	21...	934.35	840.02
20....	914.40	815.49	21....	916.86	817.97	22...	919.24	820.33
21....	898.65	795.24	22....	900.08	796.60	23...	902.69	799.25
22....	881.57	773.54	23....	883.83	775.85	24...	885.98	777.99
23....	864.04	751.48	24....	865.30	752.74	25...	867.77	755.21
24....	845.30	728.24	25....	847.43	730.38	26...	849.41	732.35
25....	826.06	704.44	26....	827.17	705.58	27...	829.49	707.89
26....	805.69	679.62	27....	807.71	681.64	28...	809.55	683.40
27....	784.65	654.04	28....	785.66	655.08	29...	787.86	657.23
28....	762.69	627.62	29....	764.62	629.55	30...	766.27	631.21
29....	739.86	600.31	30....	740.78	601.30	31...	742.80	603.26
30....	716.28	572.31	31....	718.09	574.11	32...	719.70	575.62
31....	691.71	543.27	32....	692.52	544.04	33...	694.52	546.02
32....	666.53	513.63	33....	668.22	515.37	34...	669.81	516.87
33....	640.19	482.84	34....	641.33	483.54	35...	643.74	485.43
34....	613.38	451.60	35....	614.97	453.24	36...	616.04	454.73
35....	585.28	419.06	36....	585.93	420.38	37...	587.47	422.45
36....	556.84	386.20	37....	558.40	387.80	38...	559.55	388.78
37....	527.02	352.00	38....	527.53	352.59	39...	529.06	354.06
38....	497.00	317.55	39....	498.41	319.02	40...	499.50	320.12
39....	465.34	281.53	40....	465.80	282.05	41...	467.28	283.54
40....	434.14	245.54	41....	435.04	246.98	42...	436.08	247.99
41....	399.73	207.77	42....	400.61	208.77	43...	402.03	210.17
42....	366.89	170.51	43....	368.29	171.47	44...	369.25	172.46
43....	331.54	130.10	44....	332.06	130.97	45...	333.30	132.38
44....	296.67	091.24	45....	298.09	092.71	46...	299.08	093.64
45....	259.68	....	46....	260.14	....	47...	261.44	....
46....	223.19	....	47....	224.53	....	48...	225.44	....
47....	184.33	....	48....	184.73	....	49...	185.99	....
48....	146.29	....	49....	147.60	....	50...	148.38	....
49....	105.64	....	50....	106.07	....	51...	106.88	....

TABLE 2

WAVE NUMBERS OF THE LINES IN THE (0–2) BAND
($\nu_0 = 36{,}593.78$ Cm^{-1})

J	$^3\Pi_0-{}^3\Pi_0$		J	$^3\Pi_1-{}^3\Pi_1$		J	$^3\Pi_2-{}^3\Pi_2$	
	$R_3(J)$	$P_3(J)$		$R_2(J)$	$P_2(J)$		$R_1(J)$	$P_1(J)$
	Cm^{-1}	Cm^{-1}		Cm^{-1}	Cm^{-1}		Cm^{-1}	Cm^{-1}
5	....	....	6	....	36,560.75	7	....	36,569.44
6	....	....	7	36,589.14	553.56	8	36,596.00	560.75
7	36,580.51	36,540.97	8	584.54	544.27	9	591.16	551.11
8	575.32	530.38	9	580.03	535.43	10	585.77	540.97
9	570.50	521.00	10	573.90	524.43	11	579.42	529.86
10	563.56	509.36	11	567.69	513.55	12	572.51	518.20
11	557.02	497.97	12	559.84	501.17	13	564.63	505.71
12	548.45	484.83	13	552.11	488.53	14	556.10	492.55
13	540.09	471.92	14	542.66	474.26	15	546.70	478.45
14	529.86	....	15	533.13	....	16	536.63	....
15	519.68	441.82	16	521.78	444.09	17	525.54	....
16	507.87	425.55	17	510.83	428.49	18	513.90	431.57
17	496.04	408.84	18	497.97	410.83	19	501.17	414.16
18	482.42	390.77	19	{485.59, 484.83}	393.51	20	488.06	396.28
19	....	372.49	20	....	374.13	21	473.66	377.20
20	....	352.53	21	....	{355.51, 354.81}	22	....	357.75
21	438.50	332.58	22	439.90	334.06	23	442.81	336.91
22	421.95	311.32	23	424.31	313.66	24	426.50	315.96
23	404.82	289.60	24	405.89	290.92	25	408.84	293.58
24	386.47	266.71	25	388.67	268.94	26	390.77	271.03
25	367.69	243.36	26	368.86	244.60	27	371.28	247.02
26	347.76	218.87	27	349.81	220.93	28	351.75	222.86
27	327.29	193.80	28	328.35	194.87	29	330.62	197.18
28	305.85	167.69	29	307.78	169.70	30	309.59	171.40
29	283.70	141.00	30	284.57	141.92	31	286.72	144.10
30	260.57	113.28	31	262.45	115.17	32	264.10	116.80
31	236.72	084.77	32	237.62	085.67	33	239.63	087.72
32	212.13	055.75	33	213.89	057.50	34	215.35	059.02
33	186.49	36,025.52	34	187.26	36,026.33	35	189.23	36,028.28
34	160.34	35,994.61	35	161.99	35,996.48	36	163.39	35,997.93
35	132.95	962.76	36	133.68	963.62	37	135.52	965.54
36	105.07	....	37	106.75	....	38	108.09	....

TABLE 3

WAVE NUMBERS OF THE LINES IN THE (2–3) BAND

($\nu_0 = 37{,}038.52\ Cm^{-1}$)

J	$^3\Pi_0 - {}^3\Pi_0$		J	$^3\Pi_1 - {}^3\Pi_1$		J	$^3\Pi_2 - {}^3\Pi_2$	
	$R_3(J)$	$P_3(J)$		$R_2(J)$	$P_2(J)$		$R_1(J)$	$P_1(J)$
	Cm^{-1}	Cm^{-1}		Cm^{-1}	Cm^{-1}		Cm^{-1}	Cm^{-1}
7....	....	....	8...	....	....	9....	37,032.15	36,993.60
8....	....	....	9...	....	....	10....	025.99	982.80
9....	37,011.27	36,963.64	10...	37,014.03	36,966.67	11....	019.00	971.58
10....	37,003.51	951.26	11...	37,007.14	955.14	12....	011.27	959.34
11....	36,995.64	939.25	12...	36,998.42	941.85	13....	37,002.59	945.90
12....	....	925.26	13...	989.70	928.75	14....	36,993.19	932.29
13....	976.54	911.29	14...	979.00	913.62	15....	982.80	917.17
14....	965.39	895.48	15...	968.78	898.58	16....	971.58	901.52
15....	954.02	879.68	16...	955.93	881.53	17....	959.34	884.90
16....	940.96	862.07	17...	943.82	865.28	18....	946.61	867.62
17....	927.81	844.43	18...	929.58	846.25	19....	932.29	849.18
18....	913.02	825.50	19...	915.59	827.50	20....	918.01	830.32
19....	897.97	805.69	20...	899.23	807.25	21....	902.19	809.85
20....	881.53	784.50	21...	883.79	787.14	22....	885.92	789.36
21....	864.32	763.28	22...	865.82	764.85	23....	868.28	767.01
22....	846.25	740.52	23...	848.37	742.55	24....	850.31	744.73
23....	827.50	717.35	24...	828.51	718.51	25....	830.90	720.77
24....	807.25	692.84	25...	809.39	694.95	26....	811.20	696.73
25....	786.65	667.85	26...	787.99	668.92	27....	789.91	671.03
26....	764.85	641.64	27...	767.01	643.78	28....	768.54	645.37
27....	742.55	....	28...	743.40	....	29....	745.26	617.73
28....	718.92	....	29...	720.77	....	30....	722.24	....
29....	694.54	....	30...	695.41	....	31....	697.22	....
30....	669.29	....	31...	671.03	....	32....	672.43	....
31....	643.02	....	32...	643.78	....	33....	645.37	....
32....	....	....	33...	617.73	....	34....	619.06	....

TABLE 4

WAVE NUMBERS OF THE LINES IN THE (1–2) BAND
($\nu_0 = 37{,}630.36$ Cm^{-1})

J	$^3\Pi_0-{}^3\Pi_0$		J	$^3\Pi_1-{}^3\Pi_1$		J	$^3\Pi_2-{}^3\Pi_2$	
	$R_3(J)$	$P_3(J)$		$R_2(J)$	$P_2(J)$		$R_1(J)$	$P_1(J)$
	Cm^{-1}	Cm^{-1}		Cm^{-1}	Cm^{-1}		Cm^{-1}	Cm^{-1}
5	....	37,592.20	6	....	37,597.68	7	37,635.12	37,605.13
6	37,618.35	583.60	7	....	589.34	8	630.68	595.85
7	615.12	575.60	8	37,619.05	579.97	9	625.40	586.05
8	609.36	565.51	9	614.02	570.17	10	619.65	575.60
9	604.12	555.59	10	607.31	558.96	11	612.62	562.76
10	596.59	543.47	11	600.57	547.54	12	605.13	552.00
11	589.34	531.63	12	592.20	534.40	13	596.59	538.97
12	579.97	517.79	13	583.60	521.34	14	587.42	525.14
13	570.87	504.00	14	573.24	506.35	15	577.27	510.27
14	559.85	488.38	15	563.05	491.62	16	566.38	494.93
15	548.94	472.86	16	550.98	474.89	17	554.49	478.40
16	536.12	455.54	17	538.97	458.41	18	541.99	461.47
17	523.32	438.12	18	525.14	439.90	19	528.32	443.10
18	508.87	419.09	19	511.57	421.81	20	514.14	424.33
19	494.23	399.94	20	495.81	401.53	21	498.71	404.41
20	478.02	379.15	21	480.48	381.64	22	482.84	383.91
21	461.47	358.13	22	463.03	359.49	23	465.68	362.24
22	443.68	335.70	23	446.01	338.05	24	448.12	340.14
23	425.41	312.91	24	426.66	314.11	25	429.14	316.59
24	405.80	288.80	25	407.98	290.97	26	409.90	292.89
25	385.73	264.22	26	386.83	265.26	27	389.13	267.55
26	364.43	238.35	27	366.48	240.38	28	368.27	242.15
27	342.47	211.90	28	343.50	212.91	29	345.66	215.03
28	319.53	184.43	29	321.37	186.37	30	323.06	187.99
29	295.77	156.19	30	296.64	157.10	31	298.70	159.13
30	271.09	127.06	31	272.86	128.82	32	274.47	130.37
31	245.51	096.99	32	246.33	097.78	33	248.27	099.76
32	219.14	066.04	33	220.86	067.91	34	222.39	069.32
33	191.79	034.33	34	192.50	035.03	35	195.26	036.91
34	163.59	37,001.85	35	165.20	37,003.51	36	166.26	37,004.92
35	134.42	36,968.20	36	135.05	36,968.78	37	136.64	36,971.58
36	104.66	934.03	37	106.13	935.60	38	107.40	936.54
37	073.63	898.58	38	074.12	899.23	39	075.67	900.66
38	042.18	862.75	39	043.62	864.32	40	044.67	865.28
39	37,009.37	825.50	40	37,009.92	825.99	41	37,011.27	827.50
40	36,976.54	787.99	41	36,977.50	789.36	42	36,978.50	790.41
41	940.96	748.97	42	941.85	749.38	43	943.26	750.93
42	906.33	710.20	43	907.88	711.12	44	908.89	712.08
43	869.85	668.45	44	870.34	669.29	45	871.74	670.64
44	833.38	627.86	45	834.77	629.40	46	835.68	630.29
45	794.88	585.30	46	795.34	585.77	47	796.67	586.96
46	756.71	542.66	47	758.01	544.27	48	758.90	545.15
47	716.43	....	48	716.81	....	49	718.05	....
48	676.61	....	49	677.86	....	50	678.72	....
49	634.25	....	50	634.25	....	51	635.64	....
50	593.08	....	51	594.31	....	52	595.09	....
51	548.45	....	52	549.03	....	53	550.13	....
52	505.71	....	53	506.98	....	54	507.87	....

TABLE 5

WAVE NUMBERS OF THE LINES IN THE (2–2) BAND
(ν_0 = 38,609.86 Cm^{-1})

J	$^3\Pi_0-{}^3\Pi_0$		J	$^3\Pi_1-{}^3\Pi_1$		J	$^3\Pi_2-{}^3\Pi_2$	
	$R_3(J)$	$P_3(J)$		$R_2(J)$	$P_2(J)$		$R_1(J)$	$P_1(J)$
	Cm^{-1}	Cm^{-1}		Cm^{-1}	Cm^{-1}		Cm^{-1}	Cm^{-1}
5	....	38,571.28	6	....	38,575.52	7	....	38,583.01
6	38,596.17	562.51	7	38,601.36	567.95	8	38,608.05	573.99
7	592.76	554.39	8	596.17	557.93	9	602.31	563.71
8	586.33	543.42	9	590.81	548.00	10	596.17	552.93
9	580.48	532.72	10	583.62	536.28	11	588.55	541.08
10	572.34	520.41	11	576.33	524.39	12	580.48	528.53
11	564.52	507.91	12	567.07	510.70	13	571.28	514.83
12	554.39	493.47	13	557.93	497.02	14	561.48	500.55
13	544.52	479.19	14	546.90	481.46	15	550.53	485.05
14	532.74	462.88	15	535.88	465.96	16	538.94	469.02
15	520.90	446.54	16	522.89	448.52	17	526.18	451.73
16	507.27	428.29	17	510.09	431.22	18	512.79	433.89
17	493.47	410.08	18	495.23	411.82	19	498.17	414.51
18	478.02	390.04	19	480.63	392.78	20	482.95	395.05
19	462.29	369.92	20	463.84	371.60	21	466.49	374.16
20	445.02	348.21	21	447.41	350.69	22	449.50	352.80
21	427.33	326.17	22	428.69	327.17	23	431.22	329.94
22	408.25	302.59	23	410.48	304.85	24	412.42	306.79
23	388.73	278.59	24	390.04	279.85	25	392.15	282.08
24	367.77	253.16	25	369.92	255.38	26	371.60	257.12
25	346.24	227.39	26	347.39	228.50	27	349.48	230.58
26	323.57	200.26	27	325.54	202.26	28	327.53	203.85
27	300.14	172.42	28	301.11	173.43	29	302.96	175.42
28	275.60	143.56	29	277.49	145.48	30	278.94	146.97
29	250.27	113.80	30	251.21	114.76	31	253.16	116.48
30	223.86	083.15	31	225.74	084.93	32	227.05	086.24
31	196.71	051.56	32	197.53	052.35	33	199.22	054.05
32	168.55	38,019.04	33	170.29	38,020.84	34	171.50	38,022.00
33	139.39	37,985.53	34	140.06	37,986.28	35	141.73	37,987.85
34	109.48	951.32	35	111.06	952.91	36	112.15	954.07
35	077.49	915.88	36	078.96	916.53	37	080.49	918.05
36	046.49	879.86	37	048.13	881.37	38	049.14	882.46
37	38,013.44	841.51	38	38,014.02	843.02	39	38,015.49	844.44
38	37,979.95	804.55	39	37,981.45	806.09	40	37,982.40	807.11
39	944.88	765.27	40	945.43	765.90	41	946.80	767.21
40	909.57	725.69	41	910.96	727.16	42	911.83	728.07
41	872.49	684.52	42	873.07	685.19	43	874.39	686.33
42	835.36	643.17	43	836.79	....	44	837.66	....
43	796.45	....	44	796.90	....	45	798.10	....
44	757.47	....	45	758.84	....	46	759.63	....
45	716.66	....	46	717.03	....	47	718.12	....
46	675.83	....	47	677.11	....	48	677.92	....

TABLE 6

WAVE NUMBERS OF THE LINES IN THE (3–2) BAND
($\nu_0 = 39{,}542.94$ Cm^{-1})

J	$^3\Pi_0-{}^3\Pi_0$		J	$^3\Pi_1-{}^3\Pi_1$		J	$^3\Pi_2-{}^3\Pi_2$	
	$R_3(J)$	$P_3(J)$		$R_2(J)$	$P_2(J)$		$R_1(J)$	$P_1(J)$
	Cm^{-1}	Cm^{-1}		Cm^{-1}	Cm^{-1}		Cm^{-1}	Cm^{-1}
16....	....	39,355.20	17...	....	39,357.91	18....	....	39,359.78
17....	....	335.99	18...	....	337.64	19....	....	340.38
18....	....	315.20	19...	....	317.74	20....	....	319.84
19....	....	293.98	20...	....	295.61	21....	....	298.04
20....	39,365.95	271.37	21...	39,368.38	273.76	22....	39,370.38	275.61
21....	347.29	248.28	22...	348.56	249.62	23....	350.89	251.82
22....	327.03	223.59	23...	329.20	225.88	24....	330.98	227.56
23....	306.22	198.62	24...	307.40	199.79	25....	309.48	201.77
24....	284.00	172.05	25...	286.09	174.19	26....	287.55	175.66
25....	261.29	145.02	26...	262.30	146.00	27....	264.29	147.98
26....	237.15	116.69	27...	239.09	118.39	28....	240.61	119.94
27....	212.41	087.46	28...	213.28	088.48	29....	215.14	090.15
28....	186.27	057.16	29...	188.65	058.99	30....	189.57	060.28
29....	159.48	39,026.06	30...	160.33	39,027.02	31....	162.07	39,028.94
30....	131.56	38,993.80	31...	133.42	38,995.70	32....	134.50	38,996.92
31....	102.61	960.83	32...	103.60	961.55	33....	105.08	963.18
32....	072.84	926.77	33...	074.69	928.32	34....	075.68	929.51
33....	042.04	891.63	34...	042.74	892.30	35....	044.25	893.75
34....	39,010.15	855.60	35...	39,011.95	857.28	36....	39,012.80	858.41
35....	38,977.43	818.50	36...	38,978.04	819.18	37....	38,979.50	820.46
36....	943.73	780.76	37...	....	782.28	38....	946.45	783.17
37....	908.90	741.50	38...	908.90	742.12	39....	910.68	743.45
38....	873.26	701.86	39...	874.80	703.25	40....	875.78	704.39
39....	836.21	660.70	40...	836.79	661.25	41....	837.87	662.37
40....	799.22	....	41...	800.15	....	42....	801.12	....
41....	759.73	....	42...	760.21	....	43....	761.28	....
42....	720.38	....	43...	721.64	....	44....	722.55	....
43....	769.46	....	44...	679.46	....	45....	680.73	....
44....	637.98	....	45...	639.29	....	46....	639.92	....
45....	594.89	....	46...	594.89	....	47....	596.17	....

TABLE 7

WAVE NUMBERS OF THE LINES IN THE (2–1) BAND
($\nu_0 = 40{,}204.49$ Cm^{-1})

J	$^3\Pi_0 - {^3\Pi_0}$		J	$^3\Pi_1 - {^3\Pi_1}$		J	$^3\Pi_2 - {^3\Pi_2}$	
	$R_3(J)$	$P_3(J)$		$R_2(J)$	$P_2(J)$		$R_1(J)$	$P_1(J)$
	Cm^{-1}	Cm^{-1}		Cm^{-1}	Cm^{-1}		Cm^{-1}	Cm^{-1}
4....	....	40,172.90	5...	40,204.10	....	6....	....	....
5....	40,194.57	166.33	6...	200.03	40,170.01	7....	....	40,177.14
6....	190.16	156.62	7...	195.81	162.11	8....	40,201.89	167.69
7....	186.25	147.84	8...	190.16	151.56	9....	195.81	156.62
8....	179.53	136.57	9...	184.17	141.90	10....	189.14	146.11
9....	174.05	125.99	10...	176.58	129.53	11....	181.39	133.90
10....	164.83	113.00	11...	168.80	117.27	12....	172.90	120.89
11....	156.62	100.20	12...	159.20	102.53	13....	163.43	106.86
12....	146.11	085.17	13...	149.62	088.75	14....	153.20	092.16
13....	135.77	070.34	14...	137.96	072.65	15....	141.90	076.24
14....	123.41	053.41	15...	126.52	056.62	16....	129.53	059.68
15....	110.94	036.59	16...	113.00	038.64	17....	116.25	041.81
16....	096.79	40,017.92	17...	099.60	020.77	18....	102.53	023.40
17....	082.55	39,999.13	18...	084.17	40,000.84	19....	087.19	40,003.92
18....	066.33	978.49	19...	068.95	39,981.19	20....	071.24	39,983.36
19....	049.91	957.66	20...	051.45	959.25	21....	054.18	961.86
20....	031.92	935.28	21...	034.31	937.72	22....	036.59	939.83
21....	40,013.62	912.44	22...	40,014.96	913.77	23....	40,017.44	916.23
22....	39,993.78	888.12	23...	39,995.93	890.38	24....	39,997.84	892.25
23....	973.40	863.31	24...	974.59	864.57	25....	976.89	866.79
24....	951.61	837.12	25...	953.78	839.22	26....	955.48	840.95
25....	929.30	810.43	26...	930.55	811.56	27....	932.57	813.54
26....	905.59	782.35	27...	907.52	784.33	28....	909.23	785.91
27....	881.31	753.62	28...	882.34	754.61	29....	884.14	756.54
28....	855.81	723.71	29...	857.70	725.62	30....	859.07	727.09
29....	829.52	693.02	30...	830.40	693.92	31....	832.22	695.69
30....	802.05	661.19	31...	803.86	663.07	32....	805.16	664.32
31....	773.81	628.64	32...	774.57	629.49	33....	776.28	631.14
32....	744.49	594.99	33...	746.14	596.65	34....	747.41	597.87
33....	714.13	560.06	34...	714.89	561.12	35....	716.58	562.62
34....	683.04	524.89	35...	684.82	526.51	36....	685.90	527.56
35....	650.06	....	36...	651.43	488.34	37....	652.92	490.38
36....	617.65	....	37...	619.21	452.52	38....	620.21	453.59
37....	583.39	....	38...	584.06	....	39....	585.42	....
38....	548.51	....	39...	550.01	....	40....	550.96	....
39....	512.21	....	40...	512.83	....	41....	513.97	....
40....	475.40	....	41...	476.79	....	42....	477.78	....

TABLE 8

Wave Numbers of the Lines in the (3–1) Band
($\nu_0 = 41{,}137.86\ Cm^{-1}$)

J	$^3\Pi_0 - ^3\Pi_0$		J	$^3\Pi_1 - ^3\Pi_1$		J	$^3\Pi_2 - ^3\Pi_2$	
	$R_3(J)$	$P_3(J)$		$R_2(J)$	$P_2(J)$		$R_1(J)$	$P_1(J)$
	Cm^{-1}	Cm^{-1}		Cm^{-1}	Cm^{-1}		Cm^{-1}	Cm^{-1}
4	....	41,104.93	5	....	....	6	....	41,118.18
5	....	098.39	6	....	....	7	....	109.17
6	41,122.07	088.82	7	....	41,094.12	8	....	099.79
7	117.54	080.04	8	41,121.21	083.60	9	41,126.75	088.82
8	110.49	068.50	9	114.87	072.99	10	119.60	077.41
9	103.71	057.39	10	106.79	060.35	11	111.37	064.81
10	094.62	043.72	11	098.39	047.65	12	102.36	051.44
11	085.71	030.58	12	088.28	033.04	13	092.13	036.85
12	074.55	41,014.98	13	077.93	018.37	14	081.19	021.45
13	063.52	40,999.50	14	065.70	41,001.70	15	069.11	41,004.99
14	050.34	981.99	15	053.43	40,985.03	16	056.26	40,987.83
15	037.17	964.41	16	039.09	966.31	17	042.14	969.30
16	022.05	944.92	17	024.81	947.69	15	027.29	950.09
17	41,006.71	925.35	18	41,008.46	926.97	19	41,011.13	929.57
18	40,989.63	903.79	19	40,992.19	906.33	20	40,994.37	908.44
19	972.32	882.02	20	973.78	883.50	21	976.26	885.93
20	953.17	858.55	21	955.55	860.92	22	957.48	862.79
21	933.76	834.79	22	935.07	836.09	23	937.33	838.31
22	912.71	809.71	23	914.92	811.94	24	916.59	813.64
23	891.18	783.46	24	892.35	784.68	25	894.45	786.74
24	868.05	755.97	25	870.14	758.13	26	871.69	759.64
25	844.46	728.07	26	845.58	729.13	27	847.53	731.09
26	819.50	698.64	27	821.39	700.58	28	822.79	701.97
27	793.79	668.72	28	794.74	669.68	29	796.64	671.40
28	766.60	637.42	29	768.53	639.27	30	769.79	640.46
29	738.75	605.41	30	739.68	606.31	31	741.37	607.91
30	709.76	572.09	31	711.52	573.86	32	712.71	574.99
31	679.90	537.82	32	680.75	538.67	33	682.24	540.30
32	648.91	502.78	33	650.63	504.39	34	651.67	505.42
33	617.10	466.48	34	617.76	467.23	35	619.31	468.64
34	584.03	429.37	35	585.55	430.99	36	586.57	431.99
35	549.90	....	36	550.64	....	37	551.91	....
36	515.02	....	37	516.58	....	38	517.45	....
37	478.78	....	38	479.55	....	39	480.60	....
38	441.91	....	39	443.38	....	40	444.32	....

TABLE 9

WAVE NUMBERS OF THE LINES IN THE (4–1) BAND

($\nu_0 = 42{,}032.78$ Cm^{-1})

J	$^3\Pi_0-{}^3\Pi_0$		J	$^3\Pi_1-{}^3\Pi_1$		J	$^3\Pi_2-{}^3\Pi_2$	
	$R_3(J)$	$P_3(J)$		$R_2(J)$	$P_2(J)$		$R_1(J)$	$P_1(J)$
	Cm^{-1}	Cm^{-1}		Cm^{-1}	Cm^{-1}		Cm^{-1}	Cm^{-1}
6....	....	41,983.62	7...	....	....	8....	....	....
7....	....	973.96	8...	....	41,977.61	9....	42,019.31	41,982.07
8....	42,002.97	962.04	9...	42,007.36	966.30	10....	011.84	970.48
9....	41,995.70	950.39	10...	41,998.31	953.80	11....	42,002.97	957.32
10....	986.14	936.61	11...	989.91	940.18	12....	41,993.41	943.52
11....	976.54	922.46	12...	979.13	925.17	13....	982.79	928.56
12....	964.73	906.65	13...	968.08	909.97	14....	971.22	912.64
13....	952.83	890.37	14...	955.17	892.37	15....	958.34	895.43
14....	939.07	872.13	15...	942.12	875.02	16....	944.70	877.64
15....	925.17	853.89	16...	927.05	855.57	17....	929.84	858.41
16....	909.09	833.65	17...	911.85	836.41	18....	914.09	838.69
17....	893.01	813.20	18...	894.81	814.79	19....	897.01	817.33
18....	875.02	790.94	19...	877.64	793.28	20....	879.48	796.00
19....	856.80	768.39	20...	858.41	769.68	21....	860.37	772.14
20....	836.41	743.85	21...	838.69	746.31	22....	840.56	747.93
21....	816.01	719.11	22...	817.33	720.34	23....	819.35	722.41
22....	793.80	692.60	23...	796.00	694.79	24....	797.58	696.35
23....	771.12	665.67	24...	772.14	666.84	25....	774.20	668.66
24....	746.75	637.15	25...	748.84	639.18	26....	750.30	640.60
25....	722.00	608.17	26...	722.94	609.07	27....	724.76	610.89
26....	695.55	577.55	27...	697.48	579.48	28....	698.77	580.57
27....	668.66	546.30	28...	669.44	547.20	29....	670.95	548.92
28....	639.98	513.68	29...	641.99	514.72	30....	643.13	516.49
29....	610.89	480.26	30...	611.60	481.05	31....	613.21	482.79
30....	580.57	445.72	31...	582.23	447.32	32....	583.25	448.30
31....	548.92	409.99	32...	549.80	410.76	33....	551.17	412.27
32....	516.49	373.29	33...	518.20	374.99	34....	519.22	375.81
33....	482.79	335.43	34...	483.55	336.38	35....	484.85	337.63
34....	448.30	296.90	35...	449.76	299.05	36....	450.62	299.32
35....	412.27	256.98	36...	413.08	257.66	37....	414.22	258.85
36....	375.81	216.24	37...	376.95	217.82	38....	377.88	218.50
37....	337.63	174.10	38...	337.63	174.68	39....	339.36	175.88
38....	299.05	....	39...	300.38	....	40....	301.25	....
39....	258.85	....	40...	259.36	....	41....	260.37	....
40....	217.82	....	41...	219.33	....	42....	220.06	....
41....	175.88	....	42...	175.88	....	43....	177.05	....

In this equation the approximate $\overline{(B_v' - B_v'')}$ and $\overline{(D_v' - D_v'')}$ were derived from the approximate constants $\overline{B}_v$ and $\overline{D}_v$ found in step 1. The quantities $R_m(J-1)$ and $P_m(J)$ were found by averaging the wave numbers of lines with the same J. Thus everything on the left side of the equation was known. The differences $(B_v' - B_v'')_{\text{corr}}$ and $(D_v' - D_v'')_{\text{corr}}$ are corrections to be added to the approximate differences $\overline{(B_v' - B_v'')}$ and $\overline{(D_v' - D_v'')}$ to give more accurate differences. Since the last term of the equation was small for small J, it was neglected. A plot of the left side of the equation versus J^2 produced a straight line for small J, from which $2\nu_0$ was found by extrapolating to $J = 0$. The origins found in this way are included in Table 11.

TABLE 10

COMPARISON OF COMBINATION DIFFERENCES OF THE LOWER STATE

$\Delta_2 F_i''(J) = R_i(J-1) - P_i(J+1)$

J	(1–2) BAND			(2–2) BAND			(0–2) SWAN BAND		
	$\Delta_2F_1''(J)$ (Cm^{-1})	$\Delta_2F_2''(J)$ (Cm^{-1})	$\Delta_2F_3''(J)$ (Cm^{-1})	$\Delta_2F_1''(J)$ (Cm^{-1})	$\Delta_2F_2''(J)$ (Cm^{-1})	$\Delta_2F_3''(J)$ (Cm^{-1})	$\Delta_2F_1''(J)$ (Cm^{-1})	$\Delta_2F_2''(J)$ (Cm^{-1})	$\Delta_2F_3''(J)$ (Cm^{-1})
12	73.65	79.23	85.34	73.72	79.31	85.33	....	....	85.30
13	79.99	85.85	91.59	79.93	85.61	91.51	....	85.29	91.87
14	86.32	91.98	98.01	86.23	91.97	97.98	85.74	91.98	98.06
15	92.49	98.35	104.31	92.46	98.38	104.45	92.16	98.39	104.35
16	98.87	104.64	110.82	98.80	104.66	110.82	98.84	104.67	110.78
17	104.91	111.08	117.03	105.05	111.07	117.23	105.09	111.05	117.10
18	111.39	117.16	123.38	111.67	117.31	123.55	111.40	117.32	123.46
19	117.66	123.61	129.72	117.72	123.63	129.80	117.65	123.68	129.73
20	123.91	129.93	136.10	124.01	129.94	136.12	123.97	129.94	136.12
21	130.23	136.22	142.32	130.15	136.67	142.43	130.21	136.31	142.35
22	136.47	142.43	148.56	136.55	142.56	148.74	136.54	142.56	148.72
23	142.70	148.92	154.88	142.71	148.84	155.09	142.76	148.73	154.90
24	149.09	155.04	161.19	149.14	155.10	161.34	149.09	155.08	161.29
25	155.23	161.40	167.45	155.30	161.54	167.51	155.28	161.43	167.43
26	161.59	167.60	173.83	161.57	167.66	173.82	161.64	167.54	173.80
27	167.75	173.92	180.00	167.75	173.96	180.01	167.81	173.90	179.99
28	174.10	180.11	186.28	174.06	180.06	186.34	174.06	180.04	186.06
29	180.28	186.40	192.47	180.56	186.35	192.45	180.45	186.33	192.47
30	186.53	192.55	198.78	186.48	192.56	198.71	186.53	192.27	198.73
31	192.69	198.86	205.05	192.70	198.86	204.82	192.50	198.87	204.90
32	198.94	204.95	211.18	199.11	204.90	211.18	199.12	204.92	211.17
33	205.15	211.30	217.29	205.05	211.25	217.23	205.14	211.24	217.26
34	211.36	217.35	223.59	211.37	217.38	223.51	211.36	217.30	223.53
35	217.47	223.72	229.56	217.43	223.52	229.62	217.60	223.60	229.61

3. With the band origins known, the previous equation could be rearranged as follows:

$$\frac{R_m(J-1) + P_m(J) - 2\,\overline{(B_v' - B_v'')}\,J^2 + 2\,\overline{(D_v' - D_v'')}\,J^2(J+1)^2 - 2\nu_0}{J^2} = 2\,(B_v' - B_v'')_{\text{corr}} - 2\,(D_v' - D_v'')_{\text{corr}}\,(J+1)^2 \,.$$

A plot of the left side of the equation versus $(J+1)^2$ gave a straight line, from which $2(B_v' - B_v'')_{\text{corr}}$ and $2(D_v' - D_v'')_{\text{corr}}$ were found from the intercept and slope. The corrected differences $(B_v' - B_v'')$ and $(D_v' - D_v'')$ were then computed by adding these corrections to the approximate differences $\overline{(B_v' - B_v'')}$ and $\overline{(D_v' - D_v'')}$ found in step 1 above.

TABLE 11

Scheme of Band Heads and of Band Origins of the Fox-Herzberg System of C_2 (With Horizontal and Vertical Differences in Cm^{-1})

v'	v''										
	1	$\Delta G_{3/2}$	2	$\Delta G_{5/2}$	3	$\Delta G_{7/2}$	4	$\Delta G_{9/2}$	5	$\Delta G_{11/2}$	6
0			2731.55 A 36593.78 cm^{-1}	1571.64	2855 A* 35022.14 cm^{-1}	1548.07	2987 A* 33474.07 cm^{-1}	1524.48	3129 A* 31949.59 cm^{-1}	1501.40	3283 A* 30448.19 cm^{-1}
$\Delta G_{1/2}$			1036.58		1036.83						
1			2656.33 37630.36	1571.39	2772.07 36058.97		(2896.4)†				
$\Delta G_{3/2}$			979.50		979.55						
2	2486.29 A 40204.49 cm^{-1}	1594.63	2588.97 38609.86	1571.34	2698.79 37038.52						
$\Delta G_{5/2}$	933.37		933.08								
3	2429.89 41137.86	1594.92	2527.90 39542.94								
$\Delta G_{7/2}$	894.92										
4	2378.17 42032.78										

* Analyzed by Fox and Herzberg.

† Band not analyzed.

From the differences $(B_v' - B_v'')$ and $(D_v' - D_v'')$, which were derived in this way for each band, it was possible to find improved constants, B_v and D_v, for the upper and lower vibrational levels that were consistent with these differences and which also gave the best agreement with the constants B_v'' and D_v'' of the lower state, as found previously[3] from a study of the Swan bands. Tables 12 and 13 give the resulting constants. For comparison purposes, the constants of the lower state resulting from the analysis of the Swan bands are included in Table 13.

The analysis of the (0–2) band gave 1.1801 cm^{-1} for B_0'. This was in good agreement with the value of 1.1804 cm^{-1} found by Fox and Herzberg.[1] However, since their de-

TABLE 12

ROTATIONAL CONSTANTS OF THE $B^3\Pi_g$ STATE

v	B_v(Cm^{-1})	ΔB(Cm^{-1})	B_{comp}(Cm^{-1})	O−C (Cm^{-1})	$D_v \cdot 10^6$ (Cm^{-1})	Computed $D_v \cdot 10^6$ (Cm^{-1})	O−C (Cm$^{-1} \cdot 10^6$)
0	1.1803		1.1801	+0.0002	6.1	6.4	−0.3
		0.0241					
1	1.1562		1.1559	+ .0003	6.8	6.7	+ .1
		.0251					
2	1.1311		1.1317	− .0006	7.0	7.0	.0
		.0239					
3	1.1072		1.1075	− .0003	7.5	7.3	+ .2
		0.0234					
4	1.0838		1.0833	+0.0005	7.1	7.6	−0.5

TABLE 13

ROTATIONAL CONSTANTS OF THE $X^3\Pi_u$ STATE

v	B_v(Cm^{-1})	B_v(Cm^{-1}) Swan System	$D_v \cdot 10^6$(Cm^{-1})	$D_v \cdot 10^6$(Cm^{-1}) Swan System
1	1.6071	1.6068	6.4	6.6
2	1.5906	1.5909	6.6	6.6
3	1.5740	1.5740	6.8	6.6

termination was based upon the analysis of two well-observed bands and two incompletely observed bands, their value has undoubtedly greater weight. Accordingly, 1.1803 cm^{-1} was adopted as the most probable value of the constant B_0'.

The third column of Table 12 gives the differences between successive rotational constants of the upper state. These differences are not constant but have a tendency to decrease with increasing v. However, there is a pronounced scatter of the differences, which is greater than the probable error of the determinations. This scatter makes it impossible to fit an exact curve to the data. The best that can be done is to represent the observed constants by the usual linear equation,

$$B_v' = B_e' - \alpha_e' (v' + \tfrac{1}{2}) .$$

By graphical methods it was found that the constant B_e' is 1.1922 cm^{-1} and α_e' is 0.0242 cm^{-1}. The computed B_v''s given by this equation are included in the fourth column of Table 12 and the differences (O − C) in the fifth column.

Similarly, a linear approximation to the constants D_v' gave the equation

$$D_v' = [6.3 + 0.29 (v' + \tfrac{1}{2})] \times 10^{-6}\text{cm}^{-1} .$$

The computed D_v'''s are given in the seventh column of Table 12 and the differences (O − C) in the eighth column. For the sake of convenience the molecular constants in these equations have been collected in Table 14.

The method of Budó[4] was used to investigate the triplet splitting of the vibrational levels of the upper state. For $^3\Pi - {}^3\Pi$ transitions, Budó has shown that the coupling constants, A, could be found from the combination differences. The scatter of the final results was so great that numerical figures cannot be given, but it can be said, in general, that the triplet splitting of the $B^3\Pi_g$ state is much smaller than that of the ground state.

b) VIBRATIONAL ANALYSIS

The determination of the band origins, ν_0, of the nine new bands is described in the previous section. They are included in Table 11, which also includes the origins and heads of the four bands, (0–3), (0–4), (0–5), and (0–6), found by Fox and Herzberg. The table also gives the vibrational quanta as horizontal and vertical differences. The vibrational quanta presented in Table 11 show some large discrepancies. For instance, there are two measured values of $\Delta G''_{3/2}$, namely, 1594.63 and 1594.92 cm^{-1}. A study of the observational data showed that this discrepancy arose through an uncertainty in the origin of the (3–2) band. The head of this band is blended with the strong Hg line at 2536 A and its

TABLE 14

MOLECULAR CONSTANTS OF THE $B^3\Pi_g$ STATE

B_e	1.1922 cm^{-1}	ν_e	40080.41 cm^{-1}
B_0	1.1803 cm^{-1}	ν_{00}	39806.46 cm^{-1}
α	0.0242 cm^{-1}	ω_e	1106.56 cm^{-1}
D_e	6.3×10^{-6} cm^{-1}	$\omega_e x_e$	39.260 cm^{-1}
β	$+0.29\times10^{-6}$ cm^{-1}	$\omega_e y_e$	2.8050 cm^{-1}
r_e	1.5350 A	$\omega_e z_e$	−0.1271 cm^{-1}

accompanying system of ghosts. Therefore, 1594.63 cm^{-1} is to be preferred as the value of $\Delta G''_{3/2}$. This compares favorably with the value 1594.57 cm^{-1} derived from the Swan bands. For the same reason, 933.37 cm^{-1} is to be preferred over 933.08 cm^{-1} as the value of $\Delta G'_{5/2}$.

A similar discrepancy is observed in the case of the quantum $\Delta G''_{5/2}$. The value given by the Swan bands, 1571.38 cm^{-1}, is in close agreement with two of the three determinations, while the value 1571.64 cm^{-1}, found as the difference between the origins of the (0–2) and (0–3) bands, is much too large. A study of the observational data shows that the internal uncertainties in the determinations of the origins of these two bands are of the order of 0.02 cm^{-1}. The only explanation of the discrepancy seems to be that there is a systematic difference between the measurements made in the present study and in that of Fox and Herzberg. Since this possibility exists, no reliance can be placed upon the value of 1036.83 cm^{-1} for $\Delta G'_{1/2}$ found as the difference between the origins of the (1–3) and the (0–3) bands. Accordingly, the value of 1036.58 cm^{-1} is to be preferred. The vibrational quanta finally chosen as being most probably correct are collected in Table 15 and plotted against vibrational number in Figure 2.

The relative numbers assigned to the vibrational levels of the upper state must be correct, otherwise the ΔG-versus-v-curve of Figure 2 would not be smooth. However, the absolute vibrational numbering may be open to question. The locations of band origins in the Deslandres table presented in Table 11 show that the corresponding Condon parabola is very open, as, indeed, might be anticipated from the great difference between the internuclear distances of the upper and lower states. Therefore, if the vibrational numbering of the upper state were too low by one unit, the additional level would be observed only through transitions from it to lower levels with $v'' > 3$, say. By extrapolating from

[4] A. Budó, *Zs. f. Phys.*, **98**, 437, 1936.

the ΔG-versus-v-curve, it is possible to predict quite accurately the wave lengths of the heads that these new bands would have. They were looked for very carefully, and, while the spectrum in that region is very complex, no features were found that would correspond to this prediction. Thus it is improbable that there is an error in the vibrational numbering of the upper state.

TABLE 15

VIBRATIONAL QUANTA IN THE UPPER AND LOWER STATES

v	UPPER STATE $B^3\Pi_g$		LOWER STATE $X^3\Pi_u$	
	$\Delta G'_{v+1/2}=G'(v+1)-G'(v)$	$\Delta_2 G'$	$\Delta G''_{v+1/2}=G''(v+1)-G''(v)$	$\Delta G''_{v+1/2}$ Swan System
0.	1036.58 cm^{-1}		. . . .	. . . .
		57.06 cm^{-1}		
1.	979.52		1594.63 cm^{-1}	1594.57 cm^{-1}
		46.15		
2.	933.37		1571.36	1571.38
		38.45		
3.	894.92		. . . .	. . . .

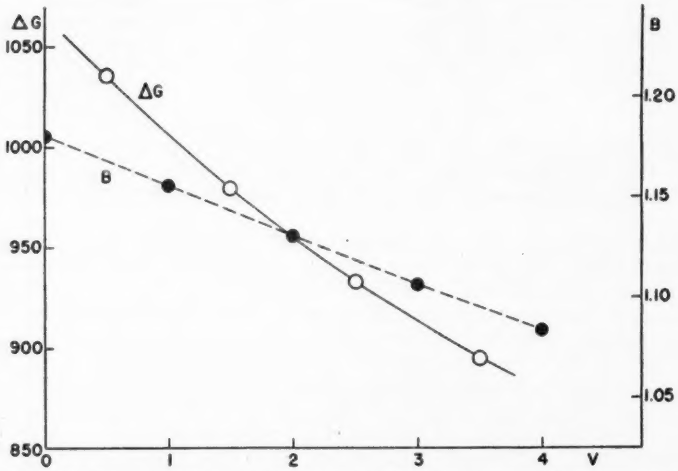

FIG. 2.—B_v and ΔG curves of the upper ($B^3\Pi_g$) state. Observed points on the B_v-curve are indicated by closed circles, and points on the ΔG-curve are given as open circles.

The differences between successive vibrational quanta of the upper state, given in the third column of Table 15, decrease systematically with increasing vibrational number. This is also shown by the upward curvature of the ΔG-versus-v-curve in Figure 2. An equation that would represent the observed quanta accurately would have to have as many terms as there are quanta. The resulting equation for the origins of the nine bands is as follows:

$$\nu_0 = 40080.41 + 1106.56\,(v'+\tfrac{1}{2}) - 39.260\,(v'+\tfrac{1}{2})^2 + 2.8050\,(v'+\tfrac{1}{2})^3 - 0.1271\,(v'+\tfrac{1}{2})^4 - [1641.35\,(v''+\tfrac{1}{2}) - 11.67\,(v''+\tfrac{1}{2})^2]\,\mathrm{cm}^{-1}\,.$$

The constants for the lower state were found previously from the study of the Swan bands. Any extrapolation made to higher vibrational levels on the basis of this equation would be very uncertain, since it is questionable whether the upward curvature of the ΔG-versus-v-curve is maintained for higher v. It is preferable to regard the equation merely as a representation of the observed levels only. The constants of the upper state in the equation are included in Table 14.

The upward curvature of the ΔG-versus-v-curve of the $B^3\Pi_g$ state is quite anomalous. Usually the curve is either linear or shows a downward curvature. Similar upward curvatures have been observed in the case of excited states of a few molecules. An example is *AgH*.[5] There have, in general, been two explanations given for these upward curvatures.

1. The excited state in question is being perturbed by another electronic state. If this is the correct explanation in the present case, the perturbing state must have a lower equilibrium energy than the $B^3\Pi_g$ state in order to produce the observed perturbation. Furthermore, such a vibrational perturbation can occur only if the Kronig selection rules are fulfilled and also if $\Delta\Lambda$ of the two perturbing states is zero. Thus the perturbing state must be a $^3\Pi_g$ state, and its presence would be known through the observation of the band system resulting from transitions to the $X^3\Pi_u$ state. The only observed state fulfilling these conditions is the $A^3\Pi_g$ state, which is the upper state of the Swan system. Therefore, if the anomaly observed in the case of the $B^3\Pi_g$ state is due to a vibrational perturbation, then there exists a strong possibility that the $A^3\Pi_g$ state is the perturbing state. This possibility is strengthened somewhat when the equilibrium internuclear distances of the two states are considered. The equilibrium distance of the $A^3\Pi_g$ state is 1.2660 A, while that of the $B^3\Pi_g$ state is 1.5350 A. Thus the point of closest approach of the corresponding potential curves would occur for low vibrational levels of the $B^3\Pi_g$ state, as is actually observed.

2. A second explanation that has been given for the anomalous behavior of the excited states of some molecules is that ionic forces between the two atoms play a role.[6] It is difficult to decide whether or not this effect would be important in the case of the C_2 molecule.

At the present time no decision can be made as to which of the two explanations given above is the correct one in the case of the $B^3\Pi_g$ state. Such a decision must await the discovery and analysis of bands from much higher vibrational levels of this state and an accurate knowledge of the dissociation energies.

I wish to acknowledge many helpful suggestions made by Dr. G. Herzberg during the course of this study and also his generosity in reading the manuscript.

[5] See, e.g., A. G. Gaydon, *Dissociation Energies and Spectra of Diatomic Molecules* (London: Chapman & Hall, Ltd., 1947).

[6] A. G. Gaydon, *Proc. Phys. Soc.*, **58**, 525, 1946.

THE PROBABLE BEHAVIOR OF THE NEXT SUNSPOT CYCLE

W. GLEISSBERG
Istanbul University Observatory
Received April 18, 1949

ABSTRACT

The probability laws of sunspot variations, which have yielded successful predictions for the present sunspot cycle, lead to the conclusion that, with a high degree of probability, a steep ascent to a very high maximum is to be expected also in the next cycle and that the period of low activity preceding the next cycle probably will be extremely short.

In the September, 1942, issue of this *Journal*[1] I published four probability laws of sunspot variations, which permit us to predict the probable features of a sunspot cycle from the observed features of the preceding ones. From these probability laws I deduced the following three predictions for the then next sunspot cycle, the eighteenth in the Zürich statistics: (1) The probability that the highest smoothed relative number of the coming cycle will exceed 145 is 86 per cent. (2) The probability that in the coming cycle the reduced period of rising will be shorter than 32 months is 91 per cent. (3) It may be expected with a probability of 93 per cent that the period of low activity which will precede the next spot cycle will be shorter than 40 months.

Now the maximum of cycle 18 has passed. It occurred in May, 1947, and the highest smoothed relative number was 151.8. The reduced period of rising, i.e., the time during which the smoothed relative sunspot numbers increase from a quarter of their maximum value to the maximum, began in August, 1945, and ended in May, 1947; it therefore lasted 21 months. And as, in cycle 17, the reduced period of falling had ended[2] in July, 1942, so the period of low activity preceding cycle 18 lasted from July, 1942, to August, 1945, i.e., 37 months.

From these observational data we see that all the above predictions have come true. As far as I know, this is the first time that essential features of a sunspot cycle have been successfully predicted before its beginning. Moreover, the success of these predictions proves that the hypothesis of the occurrence of alternately high and low maxima cannot be maintained; for, according to this hypothesis, one would have expected a low maximum in cycle 18. Actually, a prediction which was based upon this hypothesis[3] has failed.

As the length of the period of low activity, the length of the reduced period of rising, and the height of the maximum now are known for the present sunspot cycle (i.e., cycle 18), we are able to establish predictions concerning the corresponding characteristics of the next cycle (i.e., cycle 19).

When we wish to predict the probable features of a solar cycle, we have first to investigate whether $t_r^{(4)}$, the four-cycle average of the reduced period of rising, is increasing or decreasing. For this purpose let us complete the table of the characteristics of the sunspot cycles published in my earlier paper cited above.[1] By adding, to Table 1 of that paper, the data yielded by the observations in the meantime, we obtain the accompanying Table 1. In this table R_M denotes the highest smoothed relative number, t_l the period of low activity, t_r the reduced period of rising, t_f the reduced period of falling, and the quantities marked with the upper index (4) are the averages for every four consecutive

[1] *Ap. J.*, **96**, 234, 1942.

[2] W. Gleissberg, *Beob.-Zirk.*, **25**, 89, 1943.

[3] A. H. Shapley, *Terr. Mag.*, **49**, 43, 1944.

cycles. The unit of t_l, t_r, and t_f is 1 month. As the arrangement of this table is the same as that of Table 1 in my previous paper,[1] no further explanation of its contents is needed.

When I was making the predictions for cycle 18, the last known value of $t_r^{(4)}$ was 33, and there was no doubt that $t_r^{(4)}$ would continue decreasing. The present situation is

TABLE 1

THE CHARACTERISTICS OF THE SUNSPOT CYCLES AND THEIR FOUR-CYCLE AVERAGES

Cycle No.	R_M	t_l	t_r	t_f	$R_M^{(4)}$	$t_l^{(4)}$	$t_r^{(4)}$	$t_f^{(4)}$
0	92.6	...	...	41				
1	86.5	41	52	48				
					113.4	...	...	49
2	115.8	22	29	58				
					125.5	**33**	**31**	**59**
3	158.5	29	17	48				
					116.2	40	33	54
4	141.2	41	28	81				
					99.4	52	34	53
5	49.2	66	57	27				
					77.7	**59**	**43**	49
6	48.7	73	35	54				
					79.1	56	42	**42**
7	71.7	57	51	35				
					99.7	51	36	52
8	146.9	29	24	52				
					112.0	44	35	56
9	131.6	45	34	68				
					129.2	**37**	**29**	**60**
10	97.9	45	31	70				
					111.2	45	34	56
11	140.5	30	26	51				
					100.2	47	35	53
12	74.6	62	47	34				
					91.8	49	36	49
13	87.9	51	36	57				
					83.0	**55**	**38**	**48**
14	64.2	53	35	54				
					83.9	49	37	49
15	105.4	52	32	46				
					91.7	47	33	51
16	78.1	39	43	40				
					113.6	43	30	
17	119.2	45	23	63				
18	151.8	37	21					

more difficult. Now the last known value of $t_r^{(4)}$ is 30; and, as the two minima of $t_r^{(4)}$ which have been observed hitherto have been 31 and 29, respectively, it seems uncertain whether the next value of $t_r^{(4)}$ will be below 30 or above 30. We can, however, base our judgment upon the course of the values in columns $R_M^{(4)}$ and $t_l^{(4)}$, which are strongly correlated to the values of $t_r^{(4)}$. From these columns we see that the last known values of $R_M^{(4)}$ and $t_l^{(4)}$ still are far from their previous maximum and minimum values, respectively. Thus we may suppose that the increase of $R_M^{(4)}$ and the decrease of $t_l^{(4)}$ will continue and that, therefore, $t_r^{(4)}$ is still decreasing.

On the supposition that $t_r^{(4)}$ is still decreasing, the following equations can be deduced[4] from the probability laws of sunspot variations:

$$\text{prob}\,[t_r < 4t_r^{(4)*} - S_3(t_r) - 1] = 0.95\,, \tag{1}$$

$$\text{prob}\,[R_M > 1080 - 20t_r^{(4)*} - S_3(R_M)] = 0.95\,, \tag{2}$$

$$\text{prob}\,[t_l < 10t_r^{(4)*} - S_3(t_l) - 150] = 0.95\,, \tag{3}$$

where the symbol "prob" denotes the probability that the inequality which follows this symbol in brackets will be fulfilled in the next sunspot cycle; S_3 denotes the sum of the quantity in parentheses for the last three cycles; and $t_r^{(4)*}$ denotes the last known value of $t_r^{(4)}$. From Table 1 we have

$$t_r^{(4)*} = 30\,, \qquad S_3(t_r) = 21 + 23 + 43 = 87\,,$$

$$S_3(R_M) = 151.8 + 119.2 + 78.1 = 349.1\,,$$

$$S_3(t_l) = 37 + 45 + 39 = 121\,.$$

Substituting these values in equations (1), (2), and (3), we obtain

$$\text{prob}\,[t_r < 32] = 0.95\,, \qquad \text{prob}\,[R_M > 130.9] = 0.95\,, \qquad \text{prob}\,[t_l < 29] = 0.95\,.$$

These equations contain the following predictions:

It can be expected with a probability of 0.95 that: (1) in cycle 19 the smoothed relative sunspot numbers will rise from a quarter of their maximum value to the maximum within less than 32 months; (2) the highest smoothed relative number of cycle 19 will be higher than 130; and (3) the period of low activity which will precede cycle 19 will be shorter than 29 months.

Predictions 1 and 2 indicate that in the next sunspot cycle a steep ascent of solar activity to a very high maximum will again occur. Prediction 3 is of special interest, since a period of low activity which was shorter than 29 months has not been observed since cycle 2, i.e., for more than 180 years (see Table 1, column t_l). From this short duration of the period of low activity we can conclude that the coming minimum will not be a deep one.

[4] A detailed proof of these equations will be published in *Pub. Istanbul U. Obs.*, No. 36.

NOTES

THE DIAMETER OF NEPTUNE*

The *American Ephemeris and Nautical Almanac* for 1950 uses 2".44 for the diameter of Neptune at its mean distance, 30.07 a.u. In the revised edition of Russell, Dugan, and Stewart's *Astronomy*, Vol. **1**, the value 2".28, due to W. Rabe,[1] has been adopted. Rabe's value is based on seven series of observations made over a century after personal equations estimated by Rabe were applied to the original measures. All but one series (by Lassell) were based on micrometer measures.

Experiments carried out with the 82-inch telescope have convinced the writer that micrometer measures on small disks are far less trustworthy than measures obtained by either of the following two types of instruments: (1) a disk meter, showing an artificial disk matching the appearance of the planetary disk in diameter, brightness, and color; and (2) a double-image micrometer in which the two images produced are brought into contact. The writer used an instrument of the first type in measuring satellite diameters,[2] following earlier similar work by Camichel; while an instrument of the second type was acquired from Dr. B. Lyot in 1946.

The diameter of Neptune was measured with the 82-inch telescope on four occasions, as shown in the accompanying tabulation. The magnification in all cases was 720 diame-

Date (U.T.)	Instrument	No. of Settings	Seeing	d" (Mean distance)	Weight
March 1, 1948......	Disk meter	2 (1)	1	2.079	0
March 24, 1948......	Disk meter	17 (2)	2+	2.041	2
Feb. 24, 1949......	Double-image	3 (1)	3	2.013	1
Feb. 24, 1949......	Disk meter	20 (3)	3–3+	2.054	4
Weighted average	....	....	....	2.044±0.006 (m.e.)	....

ters. The measures with the double-image micrometer were somewhat difficult because of the light-losses inherent in this instrument and the comparative faintness of Neptune. The disk-meter measures were very easy and were made in series of several settings each, separated by other activities. The number of series is given in the table in parentheses. No pronounced ellipticity of the disk was noted, and the diameter measures refer to the average for the visible disk.

The scale value of the attachments was determined as follows. A preliminary calibration was obtained from the dimensions of the disk meter, from its optics, and from microscopic measurement of the holes producing the artificial disks. This calibration is called the "provisional" one and is attached in tabular form to the instrument. The double-image micrometer was used mounted on the disk meter and tied in with its system through measurement of the largest of the artificial disks by the double-image method.

* *Contributions from the McDonald Observatory, University of Texas*, No. 179.

[1] *A.N.*, **234**, 153, 1928.

[2] *The Atmospheres of the Earth and Planets* (Chicago: University of Chicago Press, 1949), pp. 305–306; *Contr. McDonald Obs.*, No. 161.

This could be done very accurately. Thereupon, three visual binaries, for which good photographic positions were available, were measured with the double-image micrometer (a direct comparison of artificial disks with visual binaries was much less satisfactory, although it had led to a rough verification of the provisional scale). This calibration led to a correction of 0.5 per cent to the provisional scale. The representation of the three binaries is shown in the accompanying tabulation. The average distance is 3″77, and the

Pair	Measured	True	O−C
ADS 13692	3″448	3″408	+0″040
15060	3.741	3.792	− .051
16291	4.122	4.113	+0.009

m.e. of the average of the measured positions ±0″027, or ±0.7 per cent. The correction to the provisional scale is therefore +0.5 ± 0.7 per cent (m.e.), which, while small and uncertain, was applied to all measures quoted.

Combining measuring errors and scale errors we have:

$$d\,(\text{Neptune}) = 2''044 \pm 0''016\ (\text{m.e.})\,.$$

It is believed that systematic errors are negligible. Accordingly, we adopt $d = 2''04 \pm 0''02$; diameter 44,600 ± 400 km = 3.50 ± 0.03 Earth; and density equal to 2.22 cgs. The correction to the density is large and appreciably increases the diversity among the Jovian planets.

The magnitude of Neptune was measured photoelectrically by A. Shatzel on May 3, 1949, who found 7.95 IPv reduced to mean opposition (29.07 a.u.). This value is 0.30 fainter than that previously assumed, but the albedo is changed only slightly, to 0.49, owing to a similar correction to the disk size. However, it has been suggested by W. Becker that Neptune is somewhat variable.

GERARD P. KUIPER

YERKES AND McDONALD OBSERVATORIES
July 12, 1949

NOTE ON THE PHYSICAL SIGNIFICANCE OF STEWART'S SUNSPOT FORMULA

Stewart and his collaborators[1] have given the following mathematical expression for the course of solar activity within a spot cycle:

$$R = F\,\theta^{a}\,e^{-b\theta}\,,$$

where R denotes Wolf's relative sunspot number and θ the time as reckoned from the beginning of the cycle; F, a, and b are constants whose values vary from cycle to cycle. The aim of this note is to show that the above formula, which has been established by Stewart and his collaborators without proof, can be deduced from very simple and reasonable suppositions concerning the rates of formation and disintegration of sunspots.

Since the variation of solar activity arises from the formation of new spots and from the disintegration of existing spots, we can write

$$\frac{dR}{d\theta} = f_1(R,\,\theta) - f_2(R,\,\theta)\,,$$

[1] J. Q. Stewart and H. A. A. Panofsky, *Ap. J.*, **88**, 385, 1938; J. Q. Stewart and F. C. Eggleston, *Ap. J.*, **91**, 72, 1940.

where $f_1(R, \theta)$ and $f_2(R, \theta)$ represent the formation and the disintegration of spots, respectively. The functions $f_1(R, \theta)$ and $f_2(R, \theta)$ must be positive for all possible values of R and θ. The higher the solar activity, the greater the number of new formed and of disintegrating spots. Thus we may suppose that $f_1(R, \theta)$ and $f_2(R, \theta)$ are proportional to R:

$$f_1(R, \theta) = Rf_3(\theta), \qquad f_2(I, \theta) = Rf_4(\theta),$$

where $f_3(\theta)$ and $f_4(\theta)$ again are positive functions. On the other hand, it is obvious that, while the rate of disintegration need not change with time, the intensity of formation of new spots is gradually decreasing during the spot cycle. Thus the most simple supposition will be as follows:

$$f_3(\theta) = \frac{a}{\theta}, \qquad f_4(\theta) = b,$$

where a and b are positive constants. Hence

$$\frac{dR}{d\theta} = \frac{a}{\theta} R - bR.$$

Integration of this differential equation yields

$$R = F\theta^a e^{-b\theta},$$

where F is the constant of integration. This is Stewart's formula. Its physical significance, therefore, can be expressed as follows: The rate of formation of new spots and the rate of disintegration of existing spots both are proportional to the intensity of solar activity; and the rate of formation of new spots, moreover, is inversely proportional to the time from the beginning of the spot cycle.

W. Gleissberg

Istanbul University Observatory
April 9, 1949

AN ULTRAVIOLET LIGHT-CURVE OF V 444 CYGNI*

In the course of photometric observations of Wolf-Rayet spectroscopic binaries with the 82-inch reflector of the McDonald Observatory, a few observations in the ultraviolet were obtained of V 444 Cygni. This system is a Wolf-Rayet eclipsing binary in which the primary minimum (Wolf-Rayet star in front) is appreciably broader than the secondary.[1] The difference in width cannot be explained by eccentricity of the orbit but must have its origin in a tenuous scattering envelope about the Wolf-Rayet star. If this envelope has a high electron density and is responsible for scattering of light from the secondary star at primary minimum,[2] the width of the primary minimum should be independent of wave length. This has been investigated by Kron and Gordon[3] at effective wave lengths λ 4500 and λ 7200. Their observations showed that, after correcting for a slight difference in depth, there was no significant difference between the two wave lengths. The observations presented here give further evidence that the character of the primary minimum is independent of wave length.

The photometer employed was that previously described.[4] A UG2 filter and 1P21

* *Contributions from the McDonald Observatory, University of Texas*, No. 170.

[1] G. E. Kron and Katherine C. Gordon, *Ap. J.*, **97**, 311, 1943.

[2] Zdeněk Kopal and Martha B. Shapley, *Ap. J.*, **104**, 160, 1946.

[3] *A.J.*, **52**, 154, 1947.

[4] *Ap. J.*, **108**, 58, 1948.

photocell were employed for isolating the ultraviolet. The effective wave length was not carefully determined but is estimated to be λ 3550 A from the known transmission of the filter and published spectral sensitivity of the 1P21 photocell.

The individual observations are recorded in Table 1. They are presented in detail in order to facilitate future studies of the time of primary minima. The phases were computed from the formula

$$JD = 2428771.379 + 4.21238 .$$

The individual observations at primary minima have been plotted in Figure 1, along with the light-curves in the blue and infrared as determined by Kron and Gordon, so

TABLE 1

PHOTOMETRIC OBSERVATIONS OF HD 193576 AT λ 3550

JD 2432+	Heliocentric Phase (In Days)	Δm HD 193032 − V 444 Cyg	JD 2432+	Heliocentric Phase (In Days)	Δm HD 193032 − V 444 Cyg
430.693	2.968	+0.006	448.664	4.090	−0.184
430.696	2.971	+ .009	448.673	4.099	− .195
430.698	2.973	+ .005	448.676	4.102	− .201
439.669	3.519	− .002	448.678	4.104	− .203
439.672	3.552	− .006	448.736	4.162	− .269
439.675	3.555	− .001	448.739	4.165	− .276
444.598	0.024	− .305	448.742	4.168	− .265
444.601	0.027	− .303	449.585	0.798	+ .014
444.610	0.036	− .298	449.588	0.801	+ .016
444.612	0.038	− .292	449.590	0.803	+ .013
444.616	0.042	− .297	449.594	0.807	+ .014
444.685	0.111	− .238	449.598	0.811	+ .013
444.689	0.115	− .230	451.578	2.791	+ .012
444.691	0.117	− .227	451.581	2.794	+ .015
444.695	0.121	− .222	451.583	2.796	+ .016
444.777	0.203	− .125	451.587	2.800	+ .004
444.780	0.206	− .121	451.589	2.802	+ .011
444.783	0.209	− .114	452.580	3.793	− .021
444.786	0.212	− .106	452.582	3.795	− .020
445.590	1.016	.000	452.585	3.798	− .021
445.594	1.020	.000	452.588	3.801	− .020
445.597	1.023	.000	452.591	3.804	− .023
445.600	1.026	− .003	452.660	3.873	− .048
445.719	1.145	− .002	452.663	3.876	− .043
445.723	1.149	+ .009	452.666	3.879	− .046
445.726	1.152	+ .005	452.735	3.948	− .083
445.728	1.154	+ .008	452.737	3.950	− .073
445.731	1.157	+ .010	452.740	3.953	− .071
445.734	1.160	+ .011	454.582	1.583	+ .010
445.737	1.163	+ .012	454.585	1.586	+ .009
447.586	3.012	+ .001	454.587	1.588	+ .010
447.589	3.015	− .003	455.581	2.582	+ .009
447.591	3.017	− .002	455.584	2.585	+ .001
447.594	3.020	+ .001	455.587	2.588	+ .006
448.580	4.006	− .115	456.576	3.577	− .018
448.582	4.008	− .116	456.579	3.580	− .011
448.585	4.011	− .114	456.581	3.582	− .014
448.587	4.013	− .119	459.587	2.375	+ .003
448.590	4.016	− .116	459.589	2.377	.000
448.658	4.084	− .178	459.594	2.382	+0.003
448.661	4.087	−0.190			

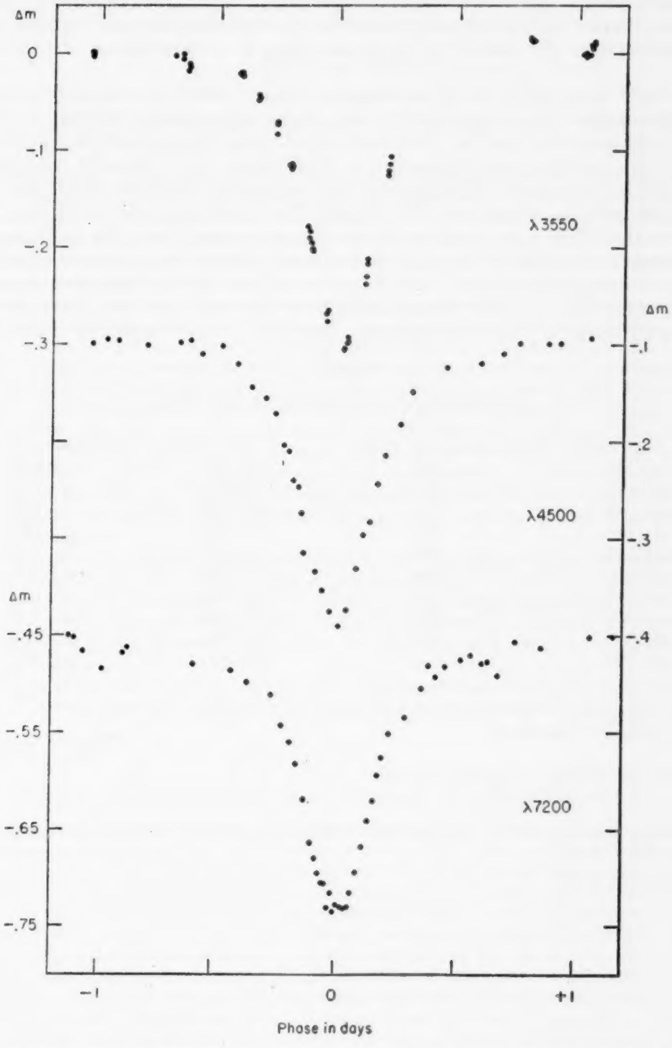

FIG. 1.—Light-curves of V 444 Cygni. The observations at λ 3550 were obtained by Hiltner and those at λ 4500 and λ 7200 by Kron and Gordon.

that comparison of the minimum at the three different wave lengths is facilitated.[5] It is obvious that, after a slight correction for difference in depth, the character of the ultra-violet-curve is essentially identical with the others. Consequently, this further supports the conclusion that the scattering in the envelope is a consequence of high electron density.

It had been observed by Kron and Gordon[3] that V 444 Cygni was subject to night-to-night fluctuations by as much as 0.1 mag. in the infrared and 0.06 mag. in the blue. Similar fluctuations, but smaller, have been noted by the author in CQ Cephei,[6] another eclipsing binary in which one component is a Wolf-Rayet star. This point was given careful attention in the present investigation. The comparison star HD 193032 was checked against a second comparison star, HD 193681. The results are given in Table 2. On the assumption that there is no variation of the two comparison stars, the probable error of a single observation is ± 0.0037 mag., which is not abnormal. It is apparent from Figure 1 and from the unplotted points of Table 1 that the nightly fluctuations were never greater than 0.01 mag. That no large fluctuations were observed here may have one of two explanations. Either the fluctuations are a function of wave length, or, which is more probable, the present observations, which were continued for only one month, were made during a period of inactivity.

TABLE 2

COMPARISON OF HD 193032 AND HD 193681

JD 2432+	Δm HD 193681 − HD 193032	JD 2432+	Δm HD 193681 − HD 193032
430.702	+0.029	449.591	+0.029
439.676	+ .031	449.596	+ .033
444.617	+ .035	449.599	+ .028
444.695	+ .033	451.588	+ .042
444.788	+ .019	452.589	+ .033
445.601	+ .036	452.593	+ .029
445.738	+ .031	452.741	+ .024
447.596	+ .033	455.588	+ .035
448.591	+ .035	456.582	+ .036
448.744	+0.021	459.591	+0.033

W. A. HILTNER

YERKES AND McDONALD OBSERVATORIES
March 23, 1949

[5] The author is grateful to Dr. Kron and Miss Gordon for permission to reproduce their observations in the blue and infrared.

[6] *A.J.*, **53**, 198, 1948.

REVIEWS

Einführung in die Dynamik von Sternsystemen. By E. van der Pahlen. Basel: Verlag Birkhäuser, 1947. Pp. 240. Swiss Fr. 36.

Investigations on the mathematical theory of stellar dynamics have centered largely on two problems. The first relates to stellar encounter, its importance for stellar dynamics and the manner in which it is incorporated into the framework of a general theory. The second relates to the consequences for the dynamical theory which the known kinematics of stellar motions implies. The present book is devoted to summarizing and in part extending the results of known investigations on these two problems.

In the treatment of stellar encounters the author follows an early investigation of Charlier. This method consists in evaluating the energy, ΔE, exchanged between two stars describing hyperbolic orbits about each other and finding the average rate of increase of ΔE^2. But in the treatments which have followed Charlier's, ΔE is first averaged over some of the parameters of the encounter, squared, and then averaged over the remaining parameters. The reviewer cannot see that this procedure gives any meaningful result. It would seem far more rational to analyze the effect of encounters on the motion of a star directly by finding the mean rate of change of the velocity in the direction of motion and at right angles to the direction of motion. When this is done, it is found that the effect of encounters is systematically to reduce the mean *velocity* to zero while at the same time making the mean dispersion tend to a finite limit. Treatments of stellar encounters along these lines appeared during the war, but they were apparently inaccessible to the author.

The treatment of the second major problem in the book is exceptionally complete and satisfactory. As is well known, the central problem here is equivalent to one of defining the potential in a dynamical system which admits an integral (other than the energy integral) which is quadratic in the velocities. Detailed investigations of this problem have appeared in the literature, but Dr. van der Pahlen's treatment is more concise and in certain parts more elegant than the published investigations.

The book is attractively written and is a very useful addition to astronomical literature.

S. Chandrasekhar

Yerkes Observatory

Kinematic Relativity. By E. A. Milne. Oxford: Clarendon Press, 1949. Pp. vi+238. $6.50.

One of the most fully documented alternative theories to the Einstein theory of gravitation which has appeared in recent years is the "kinematic relativity" theory of Professor E. A. Milne, of Oxford University. The book under review is the second written by him on this subject; the first, entitled *Relativity, Gravitation, and World-Structure,* was reviewed in an earlier issue of this *Journal.*[1] The basic formulation of the theory remains unchanged, but a considerable extension has been made in the discussion of the gravitational problem and in the extension to electrodynamics. The exposition of the preliminary kinematical part of the theory has been materially altered from that of the earlier book by the introduction of a group theoretical discussion along the lines of the paper by Milne and Whitrow.[2] The reader will find it profitable to refer also to the general treatment by Robertson[3] in this *Journal,* to which, strangely enough, no reference is made in this book. In consideration of the extensive discussion of the kinematical aspects[4] of

[1] *Ap. J.,* **83,** 61, 1936 (reviewed by H. P. Robertson).

[2] *Zs. f. Ap.,* **15,** 263, 1938.

[3] *Ap. J.,* **82,** 284, 1935; **83,** 187 and 257, 1936.

[4] The reader may be interested to refer to the older discussion by G. D. Birkhoff in his book, *Relativity and Modern Physics* (Cambridge, Mass.: Harvard University Press, 1927), which proceeds from arguments very similar to those developed by Milne.

Milne's theory which has already appeared in the literature, we shall not undertake to summarize it again here but will aim rather at giving the reader unfamiliar with Milne's ideas some notion of their scope and intent in relation to the more general corpus of present-day theoretical physics.

It is perhaps not unfair to say that in Milne's view the most fundamental fact about the universe is that it is "expanding" and that this fact is of such transcendent importance that we must build all our theories of physics to be conformable with it rather than consider the expansion to be derivable from other more prosaic laws of physics. We are challenged to develop all our theories of dynamics, gravitation, electrodynamics, cosmic rays, electron spin, etc., on the fixed pattern provided by the theory. It is this contention which makes of Milne's theory much more than just a model for the expanding universe and which requires that its fundamental postulates be subjected to full exploration from all angles before assent is accorded to them. In a word, Milne proposes to give us a theory comparable in scope to that originally proposed for Einstein's general theory of relativity as a comprehensive theory of the physical universe, with the as yet missing correlation with quantum mechanics presumably to be filled in later.

The basic element of Milne's universe, which is called by him the *substratum*, consists of a distribution of moving points, or "fundamental observers," concerning which three basic assumptions are made: (*a*) each fundamental observer moves with constant velocity in a radial direction directly away from any other fundamental observer, as observed in the reference system of the latter; (*b*) the Hubble speed-distance law of nebular recession, giving a linear homogeneous relation between the recession speed and the distance between any two observers, is exactly correct out to the confines of the observable universe, which is then bounded by observers having a recession speed c (velocity of light); and (*c*) the distribution of the fundamental observers in space is preserved under the only continuous group of symmetry transformations between fundamental observers which is allowed in the theory, which is the 6-parameter *homogeneous* Lorentz group of transformations (i.e., not including changes of origin of the space and time co-ordinates). The theory necessarily exhibits a singular epoch of "creation," which on the time scale of this expanding universe is at $t = 0$, the same for every fundamental observer; at this instant the particles of this model universe began to pour out from the common point of creation $x = y = z = 0$. Milne shows that these conditions can be satisfied in just one way.

The manner in which the concept of gravitation comes into the theory can be indicated briefly by a consideration of the argument used by Milne for the establishment of the equation of motion for a free test particle in the presence of the substratum. The equation itself is

$$\frac{d\boldsymbol{v}}{dt} + (\boldsymbol{r} - \boldsymbol{v}t)\,\frac{c^2 - v^2}{c^2t^2 - r^2} = 0\,, \tag{1}$$

where $\boldsymbol{r} = x\boldsymbol{i} + y\boldsymbol{j} + z\boldsymbol{k}$ is the space co-ordinate vector of the particle and $\boldsymbol{v} = d\boldsymbol{r}/dt$ is its velocity vector. The singularity associated with the epoch of creation requires that the solutions of equation (1) satisfy the conditions

$$|\,\boldsymbol{r}\,| \leqslant ct\,, \qquad |\,\boldsymbol{v}\,| \leqslant c\,, \qquad \boldsymbol{r}(t) \to 0 \quad \text{as} \quad t \to 0\,.$$

Equation (1) is actually established by Milne with no thought of gravitational action between the test particle and the substratum in mind, but simply from the requirement that it shall be as similar as possible to Newton's equation of motion of a free particle and that it shall be form-invariant under the allowed group of symmetry transformations between equivalent fundamental observers. In fact, Milne regards his arguments as a derivation of the dynamical equation of motion (1) from purely kinematical principles. But if we now regard equation (1) as a Newtonian equation of motion for the particle, then the second member would be considered as being of the nature of a force exerted by the substratum on the particle; and we therefore attribute it to the *gravitational action* of the substratum on the particle! It must be said in fairness that Milne makes a much more extended analysis of the analytical character of this assumption by the consideration of more general statistical distributions of fundamental observers and of the corresponding equations of motion for a particle; but the reviewer believes that the statement given above is a fair summary of the essential physical argument by which Milne converts his kinematic assumptions into a theory of gravitation. It constitutes Milne's substitute for Einstein's "principle of equivalence."

One can but be struck at once by the fact that, since in Milne's argument the test particle

and the substratum (or more general statistical system) form an indissoluble entity and since there would presumably never arise the concept of a particle moving freely in the presence of *nothing else*, we should be at a loss to know what the Newtonian equation $d\boldsymbol{v}/dt = 0$ could possibly mean, despite the fact that it is evidently being used as the basis for the interpretation of the second member of equation (1) as a gravitational force. It would seem to be much more consonant with the logic of Milne's argument to regard equation (1) as the natural equation of motion of the particle under *no* forces; but then the whole connection between kinematics and gravitation would appear to be dissolved, or at least pushed onto some other plane. In any event the reviewer will readily admit that Milne's arguments on this point seem to him to be very precarious as a physical basis for such an important element of the theory.

One of the further points in Milne's theory which has been much discussed is the introduction of a second time scale (τ-scale). If one makes the following transformation of variables on the equations of motion of a particle as given by Milne

$$\begin{aligned} \boldsymbol{r} &= \boldsymbol{R}_1 c t_0 \cdot e^{(\tau - t_0)/t_0} \cdot \sinh \frac{R}{c t_0}, \\ t &= t_0 \cdot e^{(\tau - t_0)/t_0} \cdot \cosh \frac{R}{c t_0}, \end{aligned} \qquad (2)$$

where $\boldsymbol{R} = x'\boldsymbol{j} + y'\boldsymbol{i} + z'\boldsymbol{k}$ and $\boldsymbol{R}_1 = \boldsymbol{R}/R$, then to a first approximation for low velocities these equations can be reduced to Newtonian form (sec. 79). From this Milne contends that we must consider two time scales—(*a*) the *t*-scale appropriate to the description of "expanding universe" phenomena and (*b*) the τ-scale appropriate to comparisons with Newtonian dynamics. In this view the time variables appearing in Newton's equations and in the Maxwell-Lorentz equations of the electromagnetic field are of quite different natures. This is perhaps not a question to which there is a quick and easy answer, but the following remark seems to be in order. Since the structure of the underlying symmetry group of the theory cannot be altered merely by making a transformation of co-ordinates, it hardly appears feasible to argue that the 6-parameter homogeneous Lorentz group of the *t*-scale theory is transformable in this manner into the 10-parameter symmetry group of the Newtonian theory. The proposed reduction to Newtonian mechanics would therefore be expected to be incomplete in the sense that, to maintain the correlation with the *t*-scale theory, we could not expect to make use of the full symmetry group of Newton's equations in the *t*-scale theory.

Turning to the introduction of a theory of the electromagnetic field within the framework of Milne's ideas, one might anticipate that, since the (homogeneous) Lorentz group is a part of the theory from the beginning, there would be no particular difficulty until he tried to establish contact with dynamics through the expression for the ponderomotive forces of the fields on the charges and currents, with the resultant determination of the physical meaning of the field vectors. This seems to be the case, in fact; but, unfortunately, the argument is too detailed to summarize here in an intelligible manner, and the reader must refer to Milne's treatment.

One's reaction to Milne's theory as a whole is almost certain to be determined by his reaction to Milne's fundamental philosophy. It is the reviewer's opinion that we may willingly allow the logical possibility of constructing a self-consistent model universe along the lines assumed and may even grant that features will arise in it which may be made to correspond with more or less exactitude to such familiar ideas as gravitation, electricity, etc. But it is clear from the mathematical structure of the theory that these correspondences must be forced in nature, owing to the restricted character of the underlying symmetry group allowed in the theory. It does not seem at all surprising, for instance, that the attempt to formulate the dynamical equations in Lagrangian and Hamiltonian form remains incomplete. Quite apart from the comparison of Milne's and Einstein's theories, there remains the far more important fact that *neither* of these theories seems to offer a very hopeful basis as a framework for a generalized formulation of quantum mechanics. The entirely different mathematical structure of modern quantum theory makes it more likely that they will prove to be incompatible, except in some limiting sense. If this view is correct, then it is probable that Milne's theory has been introduced too late into the scheme of modern physics to be of much influence on the development of quantum-mechanical theory. Its influence in other directions remains to be determined.

E. L. HILL

Department of Physics
University of Minnesota

The Atmospheres of the Earth and Planets: Papers Presented at the Fiftieth Anniversary Symposium of the Yerkes Observatory, September, 1947. Edited by GERARD P. KUIPER. Chicago: University of Chicago Press, 1949. Pp. vii+366. $7.50.

This volume is an impressive illustration of the extent to which modern physical methods of study have expanded our knowledge of what, not so many years ago, seemed to be small regions of study. It is confined to those branches of the field which are definitely of astronomical interest — and therefore deals only incidentally, as required for its purpose, with the main mass of studies of the ionosphere. Nevertheless, it contains so much important material that a full study, especially of the admirable research surveys included in it, would occupy a large part of a year's work for an energetic graduate student.

The strongest impression produced by reading it is of the extreme complexity of most of the problems. This is astrophysics at room temperature— or at least at laboratory temperature— where the properties of matter are complicated by chemical combination, condensation of liquid, and solid particles, etc., and the physical conditions undergo large diurnal and seasonal variations. Eddington wrote wisely of the hope of understanding "so simple a thing as a star."

No one reviewer could speak with authority upon all the problems discussed in this volume. The writer's qualification is that he was unable to attend the symposium, and so can at least view the work from the outside— so far outside that Rossby's important meteorological paper can only be mentioned.

The thorough discussion of atmospheric scattering by van de Hulst is a full-dress research survey. He regards photometric observations during twilight as the most promising method for future study of scattering in the earth's atmosphere and calls for more observations upon the planets.

The observations of the ultraviolet solar spectrum from rockets— doubtless the most striking feature of the original symposium— are now familiar, but Greenstein's estimate of the intensity to be anticipated in the "continuous" background, though published in 1943,[1] is less so than it should be. The rapid drop in this occurs at a longer wave length than he then anticipated, probably owing to absorption by O_2 in the solar atmosphere, as he later suggested.[2] Beyond λ 900, "a direct photograph would show the corona and not the sun." In chapter v, Whipple, Jacchia, and Kopal present evidence for seasonal variations as the density of the upper atmosphere, derived from Harvard observations of meteors; but they wisely refrain from theoretical explanation.

Chapter vi contains a second research survey by Swings on the spectra of the night sky and the aurora. Previously proposed identifications are critically examined. Those accepted for the night sky are the first positive and Vegard-Kaplan bands of N_2 and the Herzberg system of O_2 and the familiar lines of [O I] and Na. The conditions of their appearance and the evidence for other possible bands are discussed in detail, and also the twilight phenomena, which include the appearance of bands of N_2^+. All these appear in the auroral spectrum as well as lines of [N I] and at times the Balmer lines and lines of He I or even He II. A thorough discussion of the conditions for excitation of both spectra ends with the sentence: "We are on the opening stages of the exploration of one of the most fascinating fields in geophysics." In the following chapter Spitzer treats of the extreme upper part of the earth's atmosphere. The "exosphere," where the free path is so long that upward-moving molecules are brought back by gravity rather than by collision, is reached at a density not far from 10^{-12} that at the surface. For the corresponding altitude "a value between 500 and 1000 km seems likely." The uncertain factor is the temperature at the high levels, which depends upon the intensity of solar radiation beyond 900 A. A new calculation of the rate of escape of gases from an atmosphere much hotter at the top than lower down indicates that a steady temperature of about 1500° C is required to dissipate helium into space as fast as it is released by the weathering of igneous rocks, but one as low as 500° is possible if the escape takes place at intervals when the temperature of the critical layers is raised to 2000° or more by the strong radiation of solar flares.

The late R. T. Chamberlin, in a short and lucid presentation of the geological evidence, leaves open the question whether the earth was originally a single molten mass or was formed by accretion, and he presents the evidence that the changes in climate and atmospheric conditions since early geologic time have been small and fluctuating.

Next, Harrison Brown presents strong evidence that the inert "rare" gases are very much

[1] *Pub. A.A.S.*, **10**, 307, 1943.

[2] At the meeting of the A.A.S., December, 1947.

rarer on earth than cosmically, which may be explained if the earth's atmosphere is almost entirely of secondary origin—the result of chemical processes that took place since the formation of the planet. It may well be, as he suggests, that much of the terrestrial argon A^{40} may have been produced during geologic time by the radioactive decay of K^{40}. But this decay is a cosmic process which would increase the absolute abundance of argon, but not its relative abundance in different systems unless the initial abundance of K^{40} in these were different. Indeed, since free potassium atoms exist in interstellar space, while most of those on earth are locked up deep in the crust, the change might well increase the ratio of observable argon in the nebulae as compared with the earth.

Three following papers deal with spectroscopic observations. Adel presents bolometric results, including the first evidence for telluric N_2O and HDO; Migeotte the discovery of telluric CH_4; and Dunham gives an admirable summary of the well-known photographic work at Mount Wilson.

Kuiper's "Survey of Planetary Atmospheres" is the most striking chapter in a notable book. Once more it exhibits its author's remarkable flair for studying a problem thoroughly, predicting what new phenomena may be expected to be observable, and then observing and finding them!

The study begins with insolation and escape-velocity and with estimates of the "deficiency factor" representing the ratio of the relative abundance on the given body to the general "cosmical" values. (The known values for the earth range from unity for the metals to 10^{-10} for Ne and 10^{-14} for He.) With the resulting composition for the "atmophile" portion of the body, the probable abundance of all plausible compounds is studied, with allowance for the chemical and photochemical reactions to which they may be exposed.

The observations extend from λ 3000 to λ 27,000 (with a PbS cell). The resulting discoveries of CH_4 on Titan and CO_2 on Mars are well known, as is also the evidence that the polar caps of Mars are "composed of H_2O frost at temperatures much below 0° C," while the rings of Saturn are also probably frost-covered, and that the green areas of Mars differ greatly in their reflecting power in the infrared from the higher plants but not from lichens.

The reflecting power of the "desert" areas of Mars was found to differ widely from that of terrestrial red soil and rock but was closely matched by a "brownish, fine-grained felsite." The conclusions that the higher regions of Mars are composed of similar rocks is somewhat startling. But the traditional "red" color of Mars is measured on the stellar scale in which sunlight is yellow. It might be interesting to set up some device whereby rock samples illuminated by a "daylight" lamp giving a distribution similar to sunlight in the visible region could be viewed at night at such a distance that they appeared as points about as bright as Mars and compared for color.

New and better estimates of the amounts of gases in planetary atmospheres are given. The greatest values (in kilometers at S.P.T.) are 1.0 for CO_2 on Venus, and 1.5 and 2.5 for CH^4 on Uranus and Neptune—the last two much smaller than the early estimates.

On the assumption that the surface temperature is that of a "gray" body exposed to solar radiation, it is impossible to explain how so much CH_4 can be observable in Uranus and Neptune, or NH_3 in Jupiter and Saturn. Kuiper, discussing Neptune, rejects, for good reasons, the hypothesis of a methane ocean and accepts that of an atmosphere of almost pure hydrogen, in which the "dewpoint" for formation of clouds of methane is reached at a depth exceeding 120 km and at a temperature which may be 40° K higher than that at the outer limit. Opacity of the atmosphere for long waves may diminish the observed radiometric temperature almost to the boundary value.

It may be added that, on all four planets, the clouds are composed of frozen gas and that the possibility of influence of internal planetary heat still deserves investigation.[3]

The relation between gravity and pressure leads to a small point which even Kuiper has missed. Surface-gravity on Titan is one-seventh that on Saturn. Hence, for an atmosphere of pure methane, seven times the "thickness" could exist without condensation on Titan—other things being equal. The actual amount is less than on Saturn and could not condense on the sunlit side even if no hydrogen were present—though there may be condensation on the dark side.

Some problems, such as the composition of the cloud-layer on Venus, remain unsolved. The laboratory absorption spectra, next described by Herzberg, were obtained with paths up to 5 km in length, using multiple reflections in long tubes and low gas pressures, and provided funda-

[3] Compare the discussion of the older data (Russell, Dugan, and Stewart, *Astronomy*, **1** (rev. ed.; Boston: Ginn & Co., 1945), 367, 383, 401.

mental data for Kuiper's work. Forbidden (quadrupole) absorption lines of H_2 should appear in high-dispersion spectra of Uranus and Neptune if these atmospheres are deep enough.

A short note by Franck on the possibility of photosynthesis on Mars—leaving the question open for the present—concludes a volume of remarkably high and varied interest.

HENRY NORRIS RUSSELL

Princeton University Observatory

ERRATA

In Volume **107**, page 287, 1948 (Babcock, Moore, and Coffeen, "The Ultraviolet Solar Spectrum, λλ 2935–3060," *Mt. W. Contr.*, No. 745), the undersigned introduced an error by applying +0.001 A for reducing to standard atmospheric conditions. The correction should have been −0.001 A. All wave lengths in Tables 1 and 3 should be diminished by 0.002 A.

In Table 2 the first line reads:

2995–3133 A........................ +0.0008;

it should read:

2995–3133 A........................ −0.0012.

A new second line should be added, reading:

3133–3370 A...................... (−0.0010)†,

and the footnote concerning λλ 3133–3370 should be deleted.

HAROLD D. BABCOCK

The legend for Figure 1 of Nassau and van Albada, "A Study of M-Type Stars in Cygnus" (*Ap. J.*, **109**, 393, 1949) is defective; it should read as follows:

FIG. 1.—Principal features in infrared spectra of M stars. *a*, φ Ser (K4); *b*, 83 UMa (M2); *c*, α Her A (M5); *d*, BD+49°2999 (M7); *e*, U Her, April 7, 1947 (M7) shows band near λ 7900; *f*, S UMa, April 8, 1947 (S2e) shows *LaO* band; *g*, Y CVn, April 8, 1947 (N3 or $C5_4$).

The following paragraph should be added to the note by Miller and van Dien, "A Large New Planetary Nebula" (*Ap. J.*, **109**, 537, 1949):

"We are indebted to Dr. Minkowski for informing us that he learned of this object by letter from the Harvard College Observatory in 1941, that it was found on the Metcalf plate by Miss Rebecca Jones, and that no description of it has been published. The data presented above may therefore be of some interest."